Structural Dynamic Systems
Computational Techniques
and Optimization

Finite Element Analysis (FEA)
Techniques

Edited by
Cornelius T. Leondes
Professor Emeritus
University of California
at Los Angeles

1998

Gordon and Breach Science Publishers

1 FINITE ELEMENT TECHNIQUES FOR NONLINEAR POSTBUCKLING AND COLLAPSE OF ELASTIC STRUCTURES

NORMAN F. KNIGHT, JR.

Aerospace Engineering Department, Old Dominion University, Norfolk, VA 23529-0247

1.1. INTRODUCTION

The design of structures for automotive, naval, aircraft, and space applications exploits the finite element modeling and analysis techniques to ensure reliability and robustness in a given design. More and more often, the use of nonlinear structural analyses are required in order to simulate the complex physical response to extreme loading conditions and to utilize the structural design and material to its fullest extent. Ideally structural collapse should not occur under normal operating conditions; however, an understanding of the collapse phenomena can lead to increased structural integrity and confidence in residual strength predictions.

The finite element method is an approximation method for solving differential equations of mathematical physics. Starting from the differential equations and boundary conditions, a weak form of the problem is developed in a variational sense. This variational statement is used to define elemental properties that may be written as matrices and vectors as well as to identify primary and secondary variables and all possible boundary conditions. Specific equilibrium problems are solved by first discretizing the spatial domain of the problem, evaluating the elemental matrices and vectors, assembling elemental terms to form the global system of algebraic equations, applying boundary conditions, and solving the resulting system

f algebraic equations. This system of equations is often nonlinear. In solid ıechanics, the types of nonlinearity include geometric nonlinearity (typiılly from the strain-displacement relations), material nonlinearity (typiılly from the stress-strain relations), and boundary condition nonlinearity ypically from contact or friction).

Nonlinear finite element analyses are readily performed using any one of :veral commercially available finite element software systems such as ISC/NASTRAN, HKS/ABAQUS, or ANSYS. Today's analyst can easily ıodel the spatial geometry of large complex systems and generate finite ement models which easily exceed one million active degrees of freedom. oupling these two facts with the availability of high-performance comput-ıg systems provides analysts with simulation capabilities that far exceed ıe capabilities available less than a decade ago. Several aspects of such ɔmputations are described by Hibbitt (1986, 1993).

Common to all of the nonlinear solution techniques is the need to trace ıt the entire load-displacement response curve. As such, the computational ɔst of including such a nonlinear analysis approach within a design optiızation loop will be high. This feature provides the impetus for the develɔment of robust and efficient nonlinear analysis methods for designing ructures. If the structure is designed to exploit its postbuckling stiffness, ıen effective design methodologies need to be developed and incorporated to the structural optimization procedure. Within the design optimization ;quence, the values of the design parameters may vary, and in composite ructural design, the number of possible design parameters increases draatically (e.g., Stroud, 1982). Each change in a design variable typically quires at least one additional nonlinear analysis if gradient-based optimiıtion methods are used. The use of traditional nonlinear analysis methods ithin such a design optimization sequence is unattractive, or more presely uneconomical, from a computational standpoint and also from the :signer's standpoint in that only limited design configurations can be ;sessed in a given amount of computational time.

The objectives of this paper are to present a brief overview of the finite ement method, to review selected finite element analysis techniques as ɔplied to determining the nonlinear postbuckling and collapse response of astic structures, and to describe selected application problems. First, some the fundamental concepts associated with finite element approximations e described. Second, the basic equations of nonlinear solid mechanics are ven for the case of small strain, large elastic deformations including a brief scussion of lamination theory for composite structures. Third, different ıriational formulations are presented along with their finite element mods. Then solution techniques for nonlinear systems (both static and dyımic) are discussed. The traditional approach of nonlinear finite element

analysis using a Newton-Raphson approach is reviewed. Reduction methods for nonlinear problems such as the global function approach and the reduced basis approach are summarized. Next selected applications are described, and finally some concluding remarks are made.

1.2. FINITE ELEMENT FUNDAMENTALS

Finite element fundamentals are reviewed in this section. First, an overview of the method is given, followed by classification of finite element techniques, and concluded by a discussion of finite element approximation functions. Only selected aspects of the finite element method are presented and described herein. The interested reader is encouraged to look further into the finite element method by studying one of the many available books on the topic (e.g., Bathe, 1996; Cook, 1995; Cook, Malkus, and Plesha, 1989; Crisfield, 1992; MacNeal, 1994; Reddy, 1993; Szabo and Babuska, 1991; Zienkiewicz and Taylor, 1989, 1991).

1.2.1. Overview of the Finite Element Method

The finite element method is a technique for solving differential equations which eliminates the major difficulty associated with finite difference techniques, perturbation methods, variational methods, and the method of weighted residuals — the representation of complicated domains and their boundary conditions. An operational definition of the finite element method is one that gives a description of the fundamentals of the method; namely, "the principle of going from the part to the whole." The finite element method was initially conceived as an extension of variational methods to handle arbitrary domains. Early finite element methods were associated with the direct stiffness method from structural analysis. Later it was discovered that the finite element method was an extension of the method of weighted residuals which could handle any differential equation. Further discussion of the historical developments of the finite element method is given by Zienkiewicz (1970, 1983).

The finite element method is a general discretization technique in which a given domain is decomposed into a finite number of subdomains or "finite elements" where families of fields (e.g., displacements, stresses, temperatures), which may have different analytical expressions within each subdomain, are considered. An element may be isolated from the assemblage of elements and its properties studied independently regardless of its ultimate location within the domain (i.e., within the assemblage of elements).

1.2.2. Classification of Finite Element Techniques

Finite element techniques many be classified in many ways: dimensionality, shape, element parameters, fundamental unknowns, formulation, and discipline. Dimensionality refers to two possible aspects of how the differential equation being treated and its associated finite element. It usually refers to the spatial domain of the differential equation governing the response such as a one-dimensional problem for a beam or a two-dimensional problem for plane elasticity. It may also refer to the spatial domain in which the element is able to react such as a one-dimensional beam element deforming in a plane or in three-dimensional space (i.e., planar beam or spatial beam).

Shape refers to the geometry of the element. One-dimensional elements may be straight or curved and may be planar or spatial elements. Two-dimensional elements may be triangles or quadrilaterals with either straight or curved edges and with either flat or curved surfaces. Three-dimensional elements may be tetrahedrals, wedges, or hexahedrals with flat or curved faces.

Element parameters refer to the types of unknowns of the element and typically include either nodal values, unknown coefficients, or averaged values over the element. Nodal methods express the field variables in terms of values of the field variable, and possibly their derivatives, at the nodes of the element. This is the most common class of elements employed in commercial finite element codes. Coefficient methods are a carry over from the classical Rayleigh-Ritz approximation approach and is sometimes referred to as the *a*-basis approach. In this method, the field variables are expressed as a polynomial or as a Fourier series with unknown coefficients. The unknowns are coefficients and post-processing is necessary to obtain the solution. This method is most common in *p*-version finite element codes which feature edge modes and bubble modes in a hierarchical manner (see Szabo and Babuska, 1991). Cell methods have element parameters that are selected to be averaged (or representative) values of the fundamental unknowns in a small volume element or over a surface element. This method is mainly used in fluid flow problems. In some cases, these methods are combined in order to enhance element performance.

One such case is the addition of incompatible modes to the 4-node quadrilateral membrane element (e.g., Taylor, Beresford and Wilson, 1976). Four incompatible modes are added to the shape functions of the 4-node bilinear quadrilateral membrane element, and their unknown coefficients are statically condensed out at the element level. For the general quadrilateral shape, a modified integration scheme is also employed. This modification significantly improves the element's performance and, in the limit as the mesh is refined, the displacement field incompatibility dies out and a constant strain state is approached.

Fundamental unknowns refer to the type of element parameters considered for the element. Single-field methods have only a single field (e.g., displacements or temperature) as unknown. Multi-field methods have multiple field variables (e.g., displacements and stresses) as unknowns. In solid mechanics, these multi-field methods are referred to as mixed finite element methods. In addition, hybrid finite element methods have different approximations within the element and along the element boundary. For example, the stress field may be approximated within the element but interelement continuity of the stresses is not required; only compatibility of the nodal displacements (e.g., Pian, 1964). Another example involves having the displacement approximated in one manner along the boundary of the element and a different approximation within the element. This approach gives rise to "enriched elements" where specific analytic solutions are embedded within the element (e.g., Tong, 1984; Krawczuk, 1994; Chen, 1995).

Formulation refers to the procedure used to develop elemental properties such as the element stiffness matrices, element force vectors, and element mass matrices. In the beginning days of finite element analysis, element properties were derived using the direct stiffness method, often based on physical insight and intuition, and limited to a simple set of elements. Since it was recognized that the finite element method is essentially a piecewise-continuous version of the Rayleigh-Ritz procedure, formulations based on variational principles in mechanics began to appear. However, not all problems have an associated natural variational principle like the principle of minimum potential energy in solid mechanics. As the finite element method matured, it was recognized that the method of weighted-residuals, such as the Bubnov-Galerkin method, could be used with the differential equations themselves to establish a weak-form statement rather than a solid mechanics energy principle to form a variational statement. This approach placed the finite element method on a strong mathematical foundation for extensions into other disciplines.

Discipline refers to the type of engineering problem being solved: solid and structural mechanics, fluid mechanics, heat transfer, biomechanics, electromagnetics, and so forth. For the most part, finite elements have been more widely used in solid and structural mechanics and dynamics than in other engineering disciplines. However, with the exception of computational fluid dynamics, the finite element method is perhaps the more popular approximate solution method for heat transfer problems, electromagnetic problems and coupled field problems. A good resource for background information and formulation aspects of different disciplines is given in the *Finite Element Handbook* (Kardestuncer and Norrie, 1987).

1.2.3. Finite Element Approximation Functions

In the finite element method, two basic approximations are made: one for the geometry of the problem (e.g., shape or domain) and one for the response variables or fields of the problem (e.g., displacements, temperature). These approximations are made using interpolation or shape functions over each element. For example, the field variable approximations in one-dimension can be written as

$$\phi(\xi) = \sum_{i=1}^{NNPE} N_i(\xi)\, \bar{\phi}_i \tag{1}$$

where $\phi(\xi)$ is the field being approximated, $\bar{\phi}_i$ are the nodal values of the field, $N_i(\xi)$ are the shape functions for the field, ξ is the natural coordinate of the one-dimensional element, and NNPE is the number of nodes per element. Generally, natural coordinates range from $-1 \le \xi \le 1$ which facilitates the use of common numerical integration procedures in the evaluation of elemental matrices and vectors as well as to facilitate the generation of shape functions.

Shape functions are required to satisfy certain requirements within the element as well as at interelement boundaries. First, the approximation functions need to exhibit nonzero derivatives up through those appearing in the weak-form statement; that is they must be sufficiently differentiable. Second, the nodal interpolants need to produce nodal values when evaluated at a node. Third, the approximation must be able to represent constant values of the primary variables. Finally, the minimum continuity requirement on the approximation functions is defined by the highest derivative of each field variable appearing in the weak-form statement of the problem. If the first derivative with respect to the spatial variables is the highest derivative appearing in the weak-form statement, then only the field variable itself is required to be continuous across interelement boundaries which defines C^0 continuity (e.g., rods, Timoshenko beams, plane elasticity, three-dimensional elasticity, solids of revolution Mindlin plates/shells). If the second derivative with respect to the spatial variables is the highest derivative appearing in the weak-form statement, then the field variable and its first derivative are required to be continuous across interelement boundaries which defines C^1 continuity (e.g., Bernoulli-Euler beams, Kirchhoff plates/shells).

For C^0 problems, the approximation functions for 1-D and for 2-D quadrilaterals are typically based on the one-dimensional Lagrange interpolation functions determined using the product rule. This approach can be used to generate a p^{th} order, one-dimensional Lagrange interpolation function $L_K^p(\xi)$ using

$$L_K^p(\xi) = \prod_{\substack{i=1 \\ i \neq K}}^{p+1} \left(\frac{\xi_i - \xi}{\xi_i - \xi_K} \right) \tag{2}$$

These one-dimensional functions are readily carried over to two- and three-dimensional elements and the generation of their shape functions. For C^1 problems, the approximation functions for 1-D are based on the Hermite interpolation functions and are generally restricted to the first order which are cubic spline functions. For the 2-D problems, these approximation functions are developed by examining the continuity requirements along the edges of the element (e.g., Melosh, 1963).

In a manner similar to the approximation of the field variable, the geometry of the element may also vary over the element by using nodal values of the coordinates and shape functions in terms of the natural coordinates of the element. That is, a one-dimensional curve can be described by

$$x(\xi) = \sum_{i=1}^{NNPE} \tilde{N}_i(\xi)\, \bar{x}_i \tag{3}$$

where $x(\xi)$ is the coordinate being approximated, $\bar{x}_i$ are the nodal values of the coordinate, $\tilde{N}_i(\xi)$ are the shape functions for the coordinate, and ξ is the natural coordinate of the one-dimensional element. If the shape functions for the field variables $N_i(\xi)$ are the same as the shape functions for the geometry of the element $\tilde{N}_i(\xi)$, then an **isoparametric** formulation is obtained (the field variables and the geometry are approximated in the same manner). If the field variable approximations $N_i(\xi)$ are of lower order than the geometry approximation $\tilde{N}_i(\xi)$, then a **superparametric** formulation is obtained (geometry approximation is higher order than the field variable approximation). If the field variable approximations $N_i(\xi)$ are of higher order than the geometry approximation $\tilde{N}_i(\xi)$, then a **subparametric** formulation is obtained (geometry approximation is lower order than the field variable approximation).

While these traditional techniques of generating the element shape functions and element characteristic matrices and vectors are commonly taught in a first-course in finite element analysis, they are frequently not used in their academic form by the commercial software developers of finite element codes. Some developers incorporate internal incompatible modes (see Taylor *et al.*, 1976), others include "drilling" freedoms (see Allman, 1984), and most have proprietary "tuning parameters" that are adjusted to improve

the performance and reliability of their elements. In additional, the development of hierarchical shape functions and hierarchical elements (i.e., *p*-version finite element method, see Szabo and Babuska, 1991) has matured sufficiently and is now appearing in commercial codes (e.g., Rasna/Mechanica and MSC/NASTRAN Version 69) rather than just appearing in research-oriented codes.

1.3. BASIC EQUATIONS OF NONLINEAR SOLID MECHANICS

The basic equations of nonlinear solid mechanics for small-strain, elastic behavior are reviewed in this section. The basic equilibrium equations are described first, followed by a discussion of the constitutive equations, then the strain-displacement relations, and finally the compatibility relations. The purpose of this section is to establish a common basis from which to proceed for the subsequent sections.

1.3.1. Equilibrium Equations

The basic equations for small-strain, elastic nonlinear deformations are described. The first set of equations is the equilibrium equations. These partial differential equations are normally derived by considering a differential element of the material subjected to a three-dimensional stress state. Summing forces in each of the three coordinate directions gives

$$\begin{aligned}
\frac{\partial \sigma_{xx}}{\partial x}+\frac{\partial \sigma_{xy}}{\partial y}+\frac{\partial \sigma_{xz}}{\partial z}+f_x &= \rho \frac{\partial^2 u_x}{\partial t^2} \\
\frac{\partial \sigma_{yx}}{\partial x}+\frac{\partial \sigma_{yy}}{\partial y}+\frac{\partial \sigma_{yz}}{\partial z}+f_y &= \rho \frac{\partial^2 u_y}{\partial t^2} \\
\frac{\partial \sigma_{zx}}{\partial x}+\frac{\partial \sigma_{zy}}{\partial y}+\frac{\partial \sigma_{zz}}{\partial z}+f_z &= \rho \frac{\partial^2 u_z}{\partial t^2}
\end{aligned} \tag{4}$$

where σ_{ij} is the second-order stress tensor, f_i are the body forces, ρ is the mass density, and u_i is the displacement field. Summation of moments about a point in each direction gives the symmetry of the stress tensor for most engineering materials (see Reissner (1944) for an exception). Most plate and shell formulations assume inextensibility in the thickness direction, thereby reducing the three-dimensional problem to that of a two-dimensional problem with assumed kinematics in the thickness coordinate direction.

1.3.2. Constitutive Equations

The constitutive equations relate stresses to the strains. In general, a potential function is postulated such that for an adiabatic process, a strain energy density function $\mathcal{U}$ exists from which the stress-strain relations can be developed

$$\sigma_{ij} = \frac{\partial \mathcal{U}}{\partial \varepsilon_{ij}} \tag{5}$$

where ε_{ij} is the second-order strain tensor. For generalized Hookean materials, the constitutive relations are defined in terms of the stiffness coefficients C_{ijkl} which are dependent only on position within the structure and the corresponding stress-strain relations are

$$\sigma_{ij} = C_{ijkl}\, \varepsilon_{kl} \tag{6}$$

The fourth-order tensor C_{ijkl} has 81 terms. Due to the symmetry nature of the stress and strain tensors, only 21 independent terms are needed to describe an anisotropic, homogeneous material. For an orthotropic material, only 9 independent terms are required. If there is one plane where all properties are equal in all directions, the material is termed transversely isotropic giving only 9 independent terms. If there is an infinite number of planes of material property symmetry, then only 2 independent terms occur (usually taken as Young's modulus E and Poisson's ratio ν; the modulus of rigidity G can be computed from these two terms as $G = E/(2(1 + \nu))$).

For a laminated composite structure, a state of plane stress is typically assumed, and some researchers include the transverse shear effects. Each lamina is treated as an orthotropic layer as indicated in Figure 1. Within each layer, the stress-strain relations for an orthotropic material are written in the

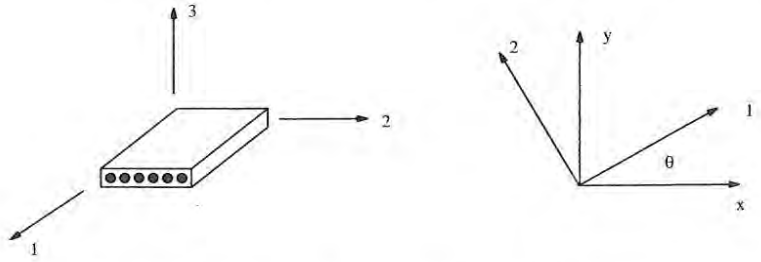

Figure 1. Material coordinate system as related to global x–y system.

principal material directions where direction 1 denotes the fiber direction and direction 2 denotes a direction transverse to the fiber

$$\begin{Bmatrix}\sigma_{11}\\ \sigma_{22}\\ \sigma_{12}\\ \sigma_{23}\\ \sigma_{13}\end{Bmatrix}=\begin{bmatrix}Q_{11} & Q_{12} & 0 & 0 & 0\\ Q_{12} & Q_{22} & 0 & 0 & 0\\ 0 & 0 & Q_{66} & 0 & 0\\ 0 & 0 & 0 & Q_{44} & 0\\ 0 & 0 & 0 & 0 & Q_{55}\end{bmatrix}\begin{Bmatrix}\varepsilon_{11}\\ \varepsilon_{22}\\ 2\varepsilon_{12}\\ 2\varepsilon_{23}\\ 2\varepsilon_{13}\end{Bmatrix} \tag{7}$$

where the Q_{ij} terms denote the reduced stiffness terms written in compact form.

These reduced stiffness coefficients are related to the engineering material properties by

$$\begin{aligned}Q_{11} &= \frac{E_1}{1-\nu_{12}\nu_{21}}\\ Q_{12} &= \frac{\nu_{12}E_2}{1-\nu_{12}\nu_{21}} = \frac{\nu_{21}E_1}{1-\nu_{12}\nu_{21}}\\ Q_{22} &= \frac{E_2}{1-\nu_{12}\nu_{21}}\\ Q_{66} &= G_{12}\\ Q_{44} &= G_{23}\\ Q_{55} &= G_{13}\end{aligned} \tag{8}$$

where E_1 is the longitudinal elastic modulus, E_2 is the transverse elastic modulus, ν_{12} is the major Poisson ratio, G_{12} is the inplane shear elastic modulus, and G_{13} and G_{23} are the transverse shear elastic moduli. Then for the given fiber orientation of each layer relative to the x-axis, the transformed reduced stiffnesses are $\overline{Q}_{ij}$ obtained in the form:

$$\overline{Q}_{11} = Q_{11}\cos^4\theta + 2(Q_{12}+2Q_{66})\sin^2\theta\cos^2\theta + Q_{22}\sin^4\theta$$

$$\overline{Q}_{22} = Q_{11}\sin^4\theta + 2(Q_{12}+2Q_{66})\sin^2\theta\cos^2\theta + Q_{22}\cos^4\theta$$

$$\overline{Q}_{12} = (Q_{11}+Q_{22}-4Q_{66})\sin^2\theta\cos^2\theta + Q_{12}(\sin^4\theta+\cos^4\theta)$$

$$\overline{Q}_{16} = (Q_{11}-Q_{12}-2Q_{66})\sin\theta\cos^3\theta + (Q_{12}-Q_{22}+2Q_{66})\sin^3\theta\cos\theta$$

$$\overline{Q}_{26} = (Q_{11}-Q_{12}-2Q_{66})\sin^3\theta\cos\theta + (Q_{12}-Q_{22}+2Q_{66})\sin\theta\cos^3\theta$$

$$\overline{Q}_{66} = (Q_{11}+Q_{22}-2Q_{12}-2Q_{66})\sin^2\theta\cos^2\theta + Q_{66}(\sin^4\theta+\cos^4\theta)$$

$$\overline{Q}_{44} = Q_{44}\cos^2\theta + Q_{55}\sin^2\theta \tag{9}$$

$$\overline{Q}_{55} = Q_{44}\sin^2\theta + Q_{55}\cos^2\theta$$

$$\overline{Q}_{45} = Q_{44}\sin\theta\cos\theta + Q_{55}\sin\theta\cos\theta$$

Hence, the stress-strain relations including the transverse shear terms are obtained in the x–y coordinate system using the transformed reduced stiffnesses:

$$\begin{Bmatrix}\sigma_{xx}\\ \sigma_{yy}\\ \sigma_{xy}\\ \sigma_{yz}\\ \sigma_{xz}\end{Bmatrix}=\begin{bmatrix}\overline{Q}_{11} & \overline{Q}_{12} & \overline{Q}_{16} & 0 & 0\\ \overline{Q}_{12} & \overline{Q}_{22} & \overline{Q}_{26} & 0 & 0\\ \overline{Q}_{16} & \overline{Q}_{26} & \overline{Q}_{66} & 0 & 0\\ 0 & 0 & 0 & \overline{Q}_{44} & \overline{Q}_{45}\\ 0 & 0 & 0 & \overline{Q}_{45} & \overline{Q}_{55}\end{bmatrix}\begin{Bmatrix}\varepsilon_{xx}\\ \varepsilon_{yy}\\ 2\varepsilon_{xy}\\ 2\varepsilon_{yz}\\ 2\varepsilon_{xz}\end{Bmatrix} \tag{10}$$

For two-dimensional problems wherein one dimension is significantly smaller than the other two (i.e., plane stress membrane or plate bending), kinematic assumptions are imposed on the displacement field. First-order assumptions allow the in-plane displacement field components to vary linearly through the thickness. For example,

$$\begin{aligned}u_x(x,y,z) &= u^0(x,y) + z\theta_x(x,y)\\ u_y(x,y,z) &= v^0(x,y) + z\theta_y(x,y)\\ u_z(x,y,z) &= w^0(x,y)\end{aligned} \tag{11}$$

Furthermore these bending rotations (θ_x and θ_y) can be related to the derivatives of the out-of-plane displacement if transverse shear effects are neglected. In two-dimensional problems, stress resultants are usually defined since the mechanical behavior through the thickness is assumed *a priori*. For plate and shell formulations, three sets of stress resultants are defined based on the assumed kinematics of the displacement field. Then the stress resultants can be defined as

$$\begin{Bmatrix} N_x \\ N_y \\ N_{xy} \end{Bmatrix} = \int_{-\frac{h}{2}}^{+\frac{h}{2}} \begin{Bmatrix} \sigma_{xx} \\ \sigma_{yy} \\ \sigma_{xy} \end{Bmatrix} dz \quad \begin{Bmatrix} M_x \\ M_y \\ M_{xy} \end{Bmatrix} = \int_{-\frac{h}{2}}^{+\frac{h}{2}} \begin{Bmatrix} \sigma_{xx} \\ \sigma_{yy} \\ \sigma_{xy} \end{Bmatrix} z\, dz \quad \begin{Bmatrix} Q_y \\ Q_x \end{Bmatrix} = \int_{-\frac{h}{2}}^{+\frac{h}{2}} \begin{Bmatrix} \sigma_{yz} \\ \sigma_{xz} \end{Bmatrix} dz \tag{12}$$

where N_x, N_y, and N_{xy} are the in-plane membrane stress resultants, M_x, M_y, and M_{xy} are the bending stress resultants, and Q_x, and Q_y are the transverse shear stress resultants. Then by substitution of the kinematics given by Equation 11 into the strain-displacement relations (see Section 1.3.3) and grouping the terms by powers of the thickness coordinate z gives the point strains at any point through the thickness of the laminate:

$$\begin{Bmatrix} \varepsilon_{xx} \\ \varepsilon_{yy} \\ 2\varepsilon_{xy} \end{Bmatrix} = \begin{Bmatrix} \varepsilon^0_{xx} \\ \varepsilon^0_{yy} \\ 2\varepsilon^0_{xy} \end{Bmatrix} + z \begin{Bmatrix} \varkappa_x \\ \varkappa_y \\ 2\varkappa_{xy} \end{Bmatrix}$$

$$\begin{Bmatrix} \gamma_{yz} \\ \gamma_{xz} \end{Bmatrix} = \begin{Bmatrix} \gamma^0_{yz} \\ \gamma^0_{xz} \end{Bmatrix} \tag{13}$$

where the superscript zero indicates that these terms are constant through the thickness based on the assumed kinematics. Integrating these expressions through the thickness of the laminate gives the constitutive relations in terms of stress resultants and strain measures (midplane strains and changes in curvatures);

$$\begin{Bmatrix} N_x \\ N_y \\ N_{xy} \\ M_x \\ M_y \\ M_{xy} \\ Q_y \\ Q_x \end{Bmatrix} = \begin{bmatrix} A_{11} & A_{12} & A_{16} & B_{11} & B_{12} & B_{16} & 0 & 0 \\ A_{12} & A_{22} & A_{26} & B_{12} & B_{22} & B_{26} & 0 & 0 \\ A_{16} & A_{26} & A_{66} & B_{16} & B_{26} & B_{66} & 0 & 0 \\ B_{11} & B_{12} & B_{16} & D_{11} & D_{12} & D_{16} & 0 & 0 \\ B_{12} & B_{22} & B_{26} & D_{12} & D_{22} & D_{26} & 0 & 0 \\ B_{16} & B_{26} & B_{66} & D_{16} & D_{26} & D_{66} & 0 & 0 \\ 0 & 0 & 0 & 0 & 0 & 0 & S_{44} & S_{45} \\ 0 & 0 & 0 & 0 & 0 & 0 & S_{45} & S_{55} \end{bmatrix} \begin{Bmatrix} \varepsilon^0_{xx} \\ \varepsilon^0_{yy} \\ \gamma^0_{xy} \\ \varkappa_x \\ \varkappa_y \\ \varkappa_{xy} \\ \gamma^0_{yz} \\ \gamma^0_{zx} \end{Bmatrix} \tag{14}$$

where the A_{ij} coefficients represent the extensional or membrane stiffness terms, the B_{ij} coefficients represent the bending-extensional coupling stiffness terms, the D_{ij} coefficients represent the bending stiffness terms, and the S_{ij} coefficients represent the transverse shear stiffness terms based on first-order, shear-deformation theory (FSDT). In classical laminated plate theory (CLPT), the S_{ij} terms are neglected, and the transverse shear strains are treated as zero. This change in kinematics affects the finite element formulation in that the continuity requirement is increased from C^0 for FSDT to C^1 for CLPT since the bending rotations are equated to the slopes of the out-of-plane deflection. Both the CLPT and FSDT formulations convert the multi-layer laminate into an equivalent anisotropic single-layer system using classical lamination theory as described by Jones (1975). Other computational models for composite laminates have been proposed and have been reviewed by Reddy (1989), Noor and Burton (1989, 1990), Noor (1992), and Reddy and Robbins (1994). Stiffness coefficients for equivalent single-layer theories are computed using the transformed reduced stiffnesses and integrating through the thickness of the laminate to obtain:

$$\begin{aligned} A_{ij} &= \sum_{k=1}^{NLAYERS} \overline{Q}_{ij}^{(k)} (z_k - z_{k-1}) \quad i, j = 1, 2, 6 \\ B_{ij} &= \frac{1}{2} \sum_{k=1}^{NLAYERS} \overline{Q}_{ij}^{(k)} (z_k^2 - z_{k-1}^2) \quad i, j = 1, 2, 6 \\ D_{ij} &= \frac{1}{3} \sum_{k=1}^{NLAYERS} \overline{Q}_{ij}^{(k)} (z_k^3 - z_{k-1}^3) \quad i, j = 1, 2, 6 \\ S_{ij} &= \sum_{k=1}^{NLAYERS} \overline{Q}_{ij}^{(k)} (z_k - z_{k-1}) \quad i, j = 4, 5 \end{aligned} \tag{15}$$

It should be noted that while transverse shear flexibility is included in the element formulation, the resulting transverse shear strains based on the assumed kinematic field are *constant* through the thickness, and the transverse shear stresses recovered from the constitutive relations are *discontinuous* at layer interfaces in the laminate. Post-processing of the solution by integrating the equilibrium equations through the thickness and imposing transverse shear stress continuity at layer interfaces is needed in order to obtain accurate interlaminar stresses. Procedures for accurate recovery of interlaminar stresses by integrating the equilibrium equations have been described by Engblom and Ochoa (1985), Govindarajan *et al.* (1993) and Canisius and Foschi (1993) among others. Englestad *et al.* (1992) is the only paper that compares interlaminar stresses recovered by integrating the equilibrium equations with those obtained from the interlaminar constitutive relations for a postbuckled composite panel.

1.3.3. Strain-Displacement Equations

Various forms of the strain-displacement relations are widely used in finite element codes. For problems associated with postbuckling and collapse of elastic structures considered herein, a Lagrangian formulation is used wherein the deformations are referenced to the original configuration and differentiation and integration is performed relative to the original configuration. These strain-displacement relations are defined using the Green-Lagrange strains and are given by

$$\varepsilon_{xx} = \frac{\partial u_x}{\partial x} + \frac{1}{2}\left[\left(\frac{\partial u_x}{\partial x}\right)^2 + \left(\frac{\partial u_y}{\partial x}\right)^2 + \left(\frac{\partial u_z}{\partial x}\right)^2\right] \tag{16a}$$

$$\varepsilon_{yy} = \frac{\partial u_y}{\partial y} + \frac{1}{2}\left[\left(\frac{\partial u_x}{\partial y}\right)^2 + \left(\frac{\partial u_y}{\partial y}\right)^2 + \left(\frac{\partial u_z}{\partial y}\right)^2\right] \tag{16b}$$

$$\varepsilon_{zz} = \frac{\partial u_z}{\partial z} + \frac{1}{2}\left[\left(\frac{\partial u_x}{\partial z}\right)^2 + \left(\frac{\partial u_y}{\partial z}\right)^2 + \left(\frac{\partial u_z}{\partial z}\right)^2\right] \tag{16c}$$

$$\gamma_{xy} = \frac{\partial u_x}{\partial y} + \frac{\partial u_y}{\partial x} + \left[\frac{\partial u_x}{\partial x}\frac{\partial u_x}{\partial y} + \frac{\partial u_y}{\partial x}\frac{\partial u_y}{\partial y} + \frac{\partial u_z}{\partial x}\frac{\partial u_z}{\partial y}\right] \tag{16d}$$

$$\gamma_{xz} = \frac{\partial u_x}{\partial z} + \frac{\partial u_z}{\partial x} + \left[\frac{\partial u_x}{\partial x}\frac{\partial u_x}{\partial z} + \frac{\partial u_y}{\partial x}\frac{\partial u_y}{\partial z} + \frac{\partial u_z}{\partial x}\frac{\partial u_z}{\partial z}\right] \tag{16e}$$

$$\gamma_{yz} = \frac{\partial u_y}{\partial z} + \frac{\partial u_z}{\partial y} + \left[\frac{\partial u_x}{\partial y}\frac{\partial u_x}{\partial z} + \frac{\partial u_y}{\partial y}\frac{\partial u_y}{\partial z} + \frac{\partial u_z}{\partial y}\frac{\partial u_z}{\partial z}\right] \tag{16f}$$

where ε_{xx}, ε_{yy}, ε_{zz} are the normal strains and γ_{xy}, γ_{yz}, γ_{xz} are the shearing strains.

For plates and shells, the transverse normal strain is neglected based on the transverse inextensibility assumption. As such, only the nonlinear terms associated with the in-plane strain terms are retained. That is,

$$\varepsilon_{xx} = \frac{\partial u_x}{\partial x} + \frac{1}{2}\left[\left(\frac{\partial u_x}{\partial x}\right)^2 + \left(\frac{\partial u_y}{\partial x}\right)^2 + \left(\frac{\partial u_z}{\partial x}\right)^2\right] \tag{17a}$$

$$\varepsilon_{yy} = \frac{\partial u_y}{\partial y} + \frac{1}{2}\left[\left(\frac{\partial u_x}{\partial y}\right)^2 + \left(\frac{\partial u_y}{\partial y}\right)^2 + \left(\frac{\partial u_z}{\partial y}\right)^2\right] \tag{17b}$$

$$\gamma_{xy} = \frac{\partial u_x}{\partial y} + \frac{\partial u_y}{\partial x} + \left[\frac{\partial u_x}{\partial x}\frac{\partial u_x}{\partial y} + \frac{\partial u_y}{\partial x}\frac{\partial u_y}{\partial y} + \frac{\partial u_z}{\partial x}\frac{\partial u_z}{\partial y}\right] \tag{17c}$$

$$\gamma_{xz} = \frac{\partial u_x}{\partial z} + \frac{\partial u_z}{\partial x} \tag{17d}$$

$$\gamma_{yz} = \frac{\partial u_y}{\partial z} + \frac{\partial u_z}{\partial y} \tag{17e}$$

Furthermore, some researchers only include the nonlinear terms associated with the out-of-plane or transverse deflection w which gives the so-called von Karman strains:

$$\varepsilon_{xx} = \frac{\partial u_x}{\partial x} + \frac{1}{2}\left(\frac{\partial u_z}{\partial x}\right)^2 \tag{18a}$$

$$\varepsilon_{yy} = \frac{\partial u_y}{\partial y} + \frac{1}{2}\left(\frac{\partial u_z}{\partial y}\right)^2 \tag{18b}$$

$$\gamma_x = \frac{\partial u_x}{\partial y} + \frac{\partial u_y}{\partial x} + \frac{\partial u_z}{\partial x}\frac{\partial u_z}{\partial y} \tag{18c}$$

$$\gamma_{xz} = \frac{\partial u_x}{\partial z} + \frac{\partial u_z}{\partial x} \tag{18d}$$

$$\gamma_{yz} = \frac{\partial u_y}{\partial z} + \frac{\partial u_z}{\partial y} \tag{18e}$$

The von Karman nonlinear strains work well for many plate and shell problems provided no plate or shell junctures occur such as for finite element models of built-up structures. When modeling a stiffened panel, if a stiffener is modeled using shell elements and attached to the panel skin and the structural response involves global buckling mode shapes, then the

out-of-plane deflections of the skin are related to the inplane deflections of the stiffeners. In such cases, all nonlinear terms, at least for the inplane strains, are necessary. In addition, solutions predicted using the von Karman nonlinear strains are reported by Kim and Chaudhuri (1995) to over estimate deflections in the advanced postbuckling regime for transversely loaded, laminated curved panels.

1.3.4. Compatibility Equations

The six strain components can be completely defined at a point provided the displacement field in terms of u, v, and w is known. However, if the strains are given, the six partial differential equations given by the linear terms of Equation 16 must be solved and cannot be taken as arbitrary functions of x, y, and z. The strains are subject to conditions of compatibility such that a unique, single-valued displacement field is obtained. These compatibility equations are developed by examining derivatives of the normal and shearing strains in order to obtain common forms of derivatives of the displacement field variables on both sides of the equations. A unique single-valued displacement is ensured by satisfying the six strain compatibility equations for three-dimensional elasticity:

$$\begin{aligned}
&\frac{\partial^2\varepsilon_{xx}}{\partial y^2}+\frac{\partial^2\varepsilon_{yy}}{\partial x^2}=\frac{\partial^2\gamma_{xy}}{\partial x\partial y} \qquad 2\frac{\partial^2\varepsilon_{xx}}{\partial y\partial z}=\frac{\partial}{\partial x}\left(-\frac{\partial\gamma_{yz}}{\partial x}+\frac{\partial\gamma_{xz}}{\partial y}+\frac{\partial\gamma_{xy}}{\partial z}\right)\\
&\frac{\partial^2\varepsilon_{yy}}{\partial z^2}+\frac{\partial^2\varepsilon_{zz}}{\partial y^2}=\frac{\partial^2\gamma_{yz}}{\partial y\partial z} \qquad 2\frac{\partial^2\varepsilon_{yy}}{\partial x\partial z}=\frac{\partial}{\partial y}\left(+\frac{\partial\gamma_{yz}}{\partial x}-\frac{\partial\gamma_{xz}}{\partial y}+\frac{\partial\gamma_{xy}}{\partial z}\right)\\
&\frac{\partial^2\varepsilon_{zz}}{\partial x^2}+\frac{\partial^2\varepsilon_{xx}}{\partial z^2}=\frac{\partial^2\gamma_{xz}}{\partial x\partial z} \qquad 2\frac{\partial^2\varepsilon_{zz}}{\partial x\partial y}=\frac{\partial}{\partial z}\left(+\frac{\partial\gamma_{yz}}{\partial x}+\frac{\partial\gamma_{xz}}{\partial y}-\frac{\partial\gamma_{xy}}{\partial z}\right)
\end{aligned} \tag{19}$$

For two-dimensional plane elasticity, there is only a single compatibility equation; namely,

$$\frac{\partial^2\varepsilon_{xx}}{\partial y^2}+\frac{\partial^2\varepsilon_{yy}}{\partial x^2}=\frac{\partial^2\gamma_{xy}}{\partial x\partial y} \tag{20}$$

For displacement-based finite element models, these compatibility equations are guaranteed to be satisfied since the displacement field is assumed rather than either the stress or strain field.

1.4. VARIATIONAL FORMULATIONS AND THEIR FINITE ELEMENT MODELS

Variational formulations and their associated finite element models are described in this section. First, an overview of variational principles in solid mechanics is presented as a road map for the different principles. Then the single-field displacement finite element model is presented, followed by the assumed-stress hybrid model, and finally the mixed finite element model is presented.

1.4.1. Overview of Variational Principles in Solid Mechanics

The field of solid mechanics is richly blessed with variational statements from mathematical physics. These variational statements range from single-field statements in terms of displacements only or stresses only to four-field statements involving displacements, strains, stresses, and tractions. These principles can be readily derived by starting with the basic equations of nonlinear solid mechanics, and conversely, the basic equations of nonlinear solid mechanics can be derived as subsidiary conditions for the stationary values of the variational principles. Traditionally the principle of virtual work has been used in the development of most finite element codes. This principle is a single-field principle wherein the nodal displacements are the primary unknowns, and strains and stresses are secondary or derived quantities from the displacements.

By imposing or relaxing various assumptions, alternate variational principles are easily derived as indicated in the flow diagram presented in Figure 2. This type of flow diagram was first proposed by Washizu (1968) and later modified by Pian and Tong (1969) and Pian (1973). The principle of of virtual work assumes only that a kinematically consistent set of displacements and strains exists and makes no assumption as to the constitutive relations. If an elastic material is assumed and if the displacement boundary conditions are satisfied, the principle of minimum total potential energy results. If the assumption of a kinematically consistent set of displacements and strains is relaxed as well as relaxing the assumption on the displacement boundary conditions, then the four-field generalized variational principle is obtained. Next if Cauchy's formula is used to relate tractions to the stress tensor, the Hu-Washizu three-field variational principle is obtained. Then by again enforcing the assumption that the displacements and strains form a kinematically consistent set and also by defining the strain energy in terms of the stresses, strains, and complementary strain energy as

$$U=\sigma_{ij}\,\varepsilon_{ij}-U^C \tag{21}$$

the functional form of the Hellinger-Reissner two-field variational principle

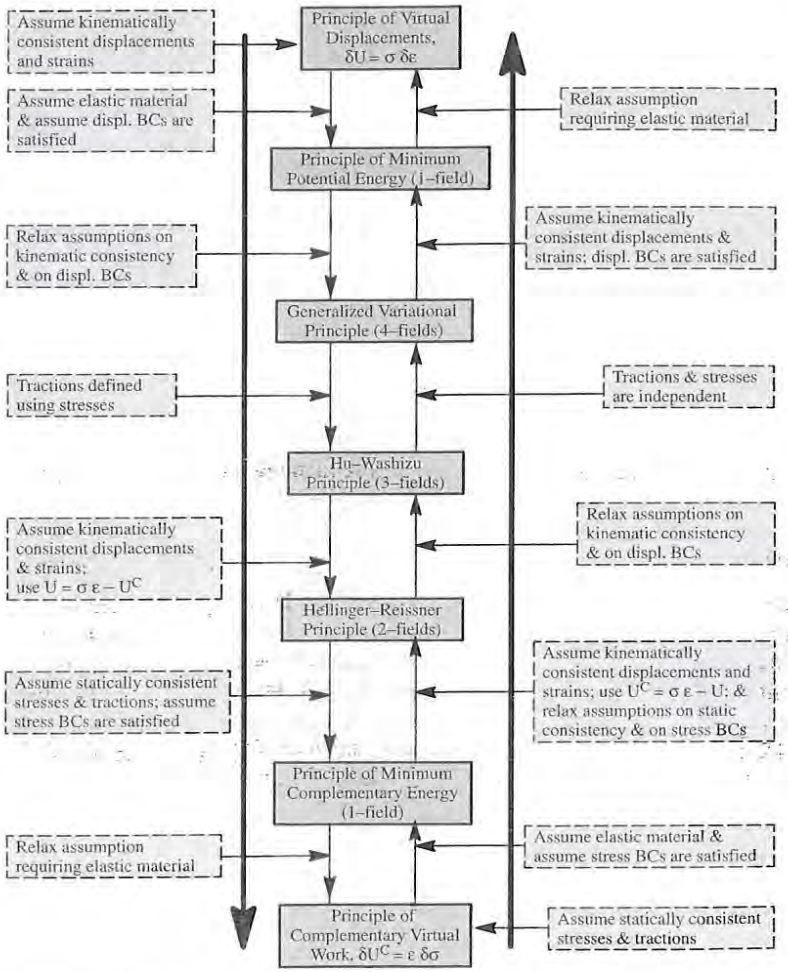

Figure 2. Flow diagram of variational principles from solid mechanics.

1.4.2. Single-Field Displacement Finite Element Models

Single-field displacement finite element models are nearly always developed from either the principle of virtual work or the principle of minimum total potential energy wherein the unknown field is the displacement field. In such models, the element equations are developed by substituting the finite element approximations for each component of the displacement field into the variational statement of the problem and then extremizing the resulting expression with respect to each nodal variable. For the principle of minimum total potential energy, the resulting expression for the total potential energy of a linear elastic system has the form:

$$\pi = \frac{1}{2} \boldsymbol{d}_e{}^T \boldsymbol{k}^e \boldsymbol{d}_e - \boldsymbol{d}_e{}^T \boldsymbol{f}_e \tag{22}$$

where $\boldsymbol{d}_e$ is the vector of element nodal degrees of freedom, $\boldsymbol{k}_e$ is the element stiffness matrix, and $\boldsymbol{f}_e$ is the vector of element nodal loads. Extremizing this expression gives the elemental equations as:

$$\frac{\partial \pi}{\partial \boldsymbol{d}_e} = \boldsymbol{k}^e \boldsymbol{d}_e - \boldsymbol{f}_e = \boldsymbol{0} \tag{23}$$

The element stiffness matrix is computed as followed:

$$\boldsymbol{k}_e = \int_{V_e} \boldsymbol{D}_N{}^T \Gamma^T \boldsymbol{H}^T \boldsymbol{C} \boldsymbol{H} \Gamma \boldsymbol{D}_N \, dV = \int_{V_e} \boldsymbol{B}^T \boldsymbol{C} \boldsymbol{B} \, dV \tag{24}$$

where $\boldsymbol{H}$ relates the deformation gradient vector to the strains, Γ is a block-diagonal matrix wherein each block corresponds to a component of the displacement field and represents the inverse of the Jacobian matrix for the element, $\boldsymbol{C}$ is the matrix of constitutive relations for the element; and $\boldsymbol{D}_N$ is a matrix of derivatives of the shape functions for the element. For some simple elements, the integration required in Equation 24 can be performed exactly; however, for the general case, such integrals are evaluated using Gaussian quadrature or perhaps symbolically. The use of symbolic manipulation tools and software are becoming more and more a part of the development process for new finite element formulations (e.g., Korncoff and Fenves, 1979; Noor and Andersen, 1979, 1981; Tan, Chang and Zheng, 1991; Rengarajan, Knight and Aminpour, 1995).

Numerical integration or quadrature replaces the integrals with weighted sums of the integrand evaluated at selected points. Typically quadrature rules are used based either on an interval of zero to one (Lobatto quadrature) or over the range negative one to positive one (Gauss quadrature). The integration can be shown to be exact if the integrand is a polynomial of order $p = 2\,NQP + 1$ where NQP means the number of quadrature points rounded to the next highest integer. In finite element analysis, three terms appear in relation to this numerical integration process. *Full integration* refers to the number of integration points required to evaluate the integral exactly if the edges of the element are straight, the nodes are evenly spaced, and the

element has uniform thickness. *Reduced integration* refers to any order of numerical integration lower than that defined by *full integration.* It is bounded on the lower end by the number of integration points required to exactly integrate the volume of the element regardless of the element's shape. This is usually one order lower than that required for *full integration. Selectively reduced integration* refers to using *full integration* for some terms of the element stiffness matrix and *reduced integration* for other terms (e.g., *full integration* for the membrane and bending terms and *reduced integration* for the transverse shear terms). While reduced integration does generally soften the element and reduces the amount of computational work at the element level, it also generates zero-energy modes within the element that can corrupt a solution. Such problems are described in many finite element books such as Cook *et al.* (1989) and Cook (1995).

Assembly of the element equations gives a global or assembled system of equations in the form

$$\boldsymbol{K}\ \boldsymbol{D} = \boldsymbol{P} \tag{25}$$

where $\boldsymbol{K}$ is a positive-definite, symmetric, sparse matrix. The solution to this system of linear algebraic equations is usually obtained by using a direct method based on Cholesky LU-decomposition. This process involves three steps: the decomposition of $\boldsymbol{K}$ into the product $\boldsymbol{LU}$; the forward-reduction step which solves $\boldsymbol{LX} = \boldsymbol{P}$; and the back-substitution step which solves $\boldsymbol{UD} = \boldsymbol{X}$. Evaluations of advanced equation solvers, both direct and iterative, have been reported by many researchers including Agarwal, Storaasli and Nguyen (1990), Poole (1991), Poole, Knight and Davis (1992), and Bathe, Walczak and Zhang (1993).

Recovery of secondary variables such as the element strains and stresses is done after the global displacement solution vector is obtained. Extraction of the nodal displacements associated with each element is based on the connectivity array of the element, and the elemental strains and stresses at selected points within the element are computed from

$$\begin{aligned} \varepsilon_e &= \boldsymbol{H}\ \Gamma\ \boldsymbol{D}_N\ \boldsymbol{d}_e = \boldsymbol{B}\ \boldsymbol{d}_e \\ \sigma_e &= \boldsymbol{C}\ \varepsilon_e \end{aligned} \tag{26}$$

where in most cases Γ and $\boldsymbol{D}_N$ are functions of location within the element. Usually finite element developers compute these secondary quantities at the so-called Barlow points (see Barlow, 1976) which correspond to Gauss quadrature points one order less than required for full integration of the element stiffness matrix. However, various post-processing codes require either nodal values or a single value per element. To obtain nodal values,

some global smoothing algorithm can be used such as nodal averaging, topological interpolation, or even a projected least-squares interpolation. If only a single value per element is needed, the value at the element centroid is typically computed.

These single-field displacement models are the most commonly used models in finite element software. Their formulation is straight-forward. Recovery of secondary solution variables such as strains and stresses involve element level computations and differentiation of element shape functions. This results in discontinuous strains and stresses across interelement boundaries. Often post-processing techniques are used to obtain *smoothed solutions* for these secondary variables, but smoothing can mask true discontinuities in the model so the analyst must proceed carefully. Smoothing element stresses, for example, over a two-dimensional domain with thickness variations is improper.

1.4.3. Hybrid Finite Element Models

Hybrid finite element models may be developed from different perspectives; several of which are described by Atluri *et al.* (1983). One approach is to assume one set of displacement approximation along the element boundaries and a different set of displacement approximations within the element. This approach is called the assumed-displacement hybrid method and gives rise to the so called *enriched* elements which may feature a closed-form exact solution for some discontinuity (e.g., Tong, 1984; Kaya and Nied, 1993; Krawczuk, 1994). Another approach is to assume similar approximations for more than one field (i.e., displacements and stresses) but only impose interelement continuity on one field (i.e., displacements). This approach is called the assumed-stress hybrid method and was first proposed by Pian (1964).

In the assumed-stress hybrid method, approximations are assumed for the stresses and displacements of the form:

$$\begin{aligned} \sigma &= \boldsymbol{P}\ \beta_e \\ \boldsymbol{u} &= \boldsymbol{N}\ \boldsymbol{d}_e \end{aligned} \tag{27}$$

where P represents a matrix of polynomial expressions for the stress field, β_e is a vector of stress parameters for the element, $\boldsymbol{N}$ is a matrix of shape functions for the displacement field, and d_e is the vector of nodal displacement unknowns. Typically the stress field is assumed such that the equilibrium equations are satisfied within the element. These approximations are then substituted into a multi-field variational statement such as the Hellinger-Reissner principle

$$\pi = \sum_{e=1}^{NELEM} \int_{V_e} \sigma^T \partial \boldsymbol{u}\, dV - \frac{1}{2}\int_{V_e} \sigma^T \boldsymbol{C}^{-1} \sigma\, dV - \int_{S_\sigma} \boldsymbol{u}^T \overline{\boldsymbol{T}}\, dS - \sum_{I=1}^{NCONC} u|_{x_I} F|_{x_I} \quad (28)$$

where the finite element approximations are made for $\boldsymbol{u}$ and σ, ∂ represents a matrix of differential operators that relate the displacement field to the strain components, and $\boldsymbol{C}$ is the constitutive matrix. The last term in the functional given by Equation 28 involves the work done by concentrated point forces and/or moments acting at x_I and I ranges from 1 to NCONC. Substituting the finite element approximations given by Equation 27 into this functional and then imposing the stationary condition ($\delta\pi = 0$) with respect to the nodal displacement degrees of freedom and the unknown stress parameters yields the elemental linear stress analysis equations of

$$\boldsymbol{k}_e\, \boldsymbol{d}_e = \boldsymbol{r}_e \quad (29)$$

where the linear stiffness matrix is computed from

$$\boldsymbol{k}_e = \boldsymbol{T}^T\, \boldsymbol{H}^{-1}\, \boldsymbol{T} \quad (30)$$

$$\boldsymbol{H} = \int_{V_e} \boldsymbol{P}^T\, \boldsymbol{C}^{-1}\, \boldsymbol{P}\, dV \quad (31)$$

$$\boldsymbol{T} = \int_{V_e} \boldsymbol{P}^T\, \partial\, \boldsymbol{N}\, dV \quad (32)$$

where $\boldsymbol{P}$ is a matrix of polynomial approximation functions for the stress field and $\boldsymbol{N}$ is a matrix of shape functions for the displacement field. These element expressions are derived using the linear strain-displacement relations at the element level and are evaluated using symbolic computations (see Rengarajan *et al.*, 1995). Assembly of the element equations gives a global or assembled system of equations having the same form as the single-field displacement model even though more computational work has been performed at the element level in evaluating the matrices $\boldsymbol{H}$ and $\boldsymbol{T}$.

By using the nonlinear strain-displacement relations and then linearizing the equations, the geometric stiffness matrix can be derived. The element internal force vector for the hybrid stress element is readily computed using the low-order corotational approach and is given by

$$f_{int} = \boldsymbol{T}^T\, \beta \quad (33)$$

In the low-order corotational approach, the deformation process is decomposed into a rigid-body-motion component and a strain-producing component wherein the linear strain-displacement relations are used at the element level. The high-order corotational approach is similar except that the nonlinear strain-displacement relations are used at the element level. For a geometrically nonlinear problem, this internal force vector represents the local internal force vector which must be projected to the global system using the corotational utilities described by Stanley and Nour-Omid (1990).

1.4.4. Mixed Finite Element Models

Mixed finite element models are defined as finite element models with nodal variables belonging to more than one field (e.g., Noor, 1980; Atluri *et al.* 1983). Mixed finite element models are somewhat related to the assumed-stress hybrid elements in that the formulation of mixed elements also start with a multi-field variational principle; however, no assumption is made between equilibrium and the nature of the stress field approximations. The stress field is assumed in terms of unknown nodal variables just as the displacement field is assumed. That is,

$$\begin{aligned} \sigma &= \mathcal{N}\, \sigma_e \\ \boldsymbol{u} &= \boldsymbol{N}\, \boldsymbol{d}_e \end{aligned} \quad (34)$$

As such, the primary variables of the mixed finite element formulation include both displacement and stress nodal values, and interelement continuity of the displacements and stresses is now inherent in the formulation. In this formulation, the stresses are computed directly and not recovered by differentiation of the displacement field. Two sets of element equations are obtained at the element level

$$\begin{aligned} -\boldsymbol{F}_e\, \sigma_e + \boldsymbol{S}_e\, \boldsymbol{d}_e &= 0 \\ \boldsymbol{S}_e^T\, \sigma_e &= \boldsymbol{P} \end{aligned} \quad (35)$$

The first set of equations represents the inverse of the constitutive relations (i.e., strain-stress relations), while the second set of equations represents equilibrium conditions. The element matrices $\boldsymbol{F}_e$ and $\boldsymbol{S}_e$ are defined as

$$\boldsymbol{F}_e = \int_{V_e} \mathcal{N}^T\, \boldsymbol{C}^{-1}\, \mathcal{N}\, dV \quad (36)$$

$$\boldsymbol{S}_e = \int_{V_e} \mathcal{N}^T\, \partial\, \boldsymbol{N}\, dV \quad (37)$$

These element equations are then assembled into a global generalized stiffness matrix of the form

$$\begin{bmatrix} -\boldsymbol{F} & \boldsymbol{S} \\ \boldsymbol{S}^T & \boldsymbol{0} \end{bmatrix} \begin{Bmatrix} \sigma \\ \boldsymbol{D} \end{Bmatrix} = \begin{Bmatrix} \boldsymbol{0} \\ \boldsymbol{P} \end{Bmatrix} \tag{38}$$

where σ is the global vector of nodal stress unknowns, $\boldsymbol{D}$ is the global vector of nodal displacement unknowns. The solution of this system of equations involves the decomposition of a negative semi-definite global generalized stiffness matrix (see Johnsen, 1972).

Mixed finite element models involve substantially more nodal unknowns than displacement-based models or even assumed-stress hybrid models. For example, a shell element based on first-order shear deformation theory will have five nodal displacement degrees of freedom (six if the drilling freedom is included) and eight nodal stress resultant degrees of freedom. Thus a 4-node shell element will involve a total of 52 degrees of freedom for the mixed approach while only 20 degrees of freedom for the displacement-based approach. However, the solution obtained using the mixed finite element model does impose interelement continuity of the element stresses. This requirement may be relaxed and the stresses computed in terms of the displacement degrees of freedom before assembly so that the global assembled equations retain only displacements as nodal unknowns. In this case, the computational work per element is similar to that of an assumed-stress hybrid element. The potential of mixed formulations has been described by Noor and Peters (1990).

1.5. SOLUTION TECHNIQUES FOR NONLINEAR SYSTEMS

1.5.1. Historical Perspective

Nonlinear finite element analysis procedures have been under development for more than three decades with tremendous strides being taken and yet still tremendous challenges are still being faced. Some of the fundamental work has been presented by Hartung (1973) and Hinton, Owen and Taylor (1982). For these nonlinear problems, the interplay between various aspects of the problem and the analysis (such as structural response, problem formulation, approximations, numerical solvers, iteration convergence, interpretation of results, boundary conditions, loading) can become entangled causing analysts great difficulties in obtaining and verifying robust accurate solutions. Shell analysis has always challenged analysts with spatial modeling issues, response complexities, and formulation aspects (e.g., Almroth and Starnes, 1975; Hartung, 1971; Noor, Belytschko and Simo, 1989; Palazotto and Dennis, 1992; Stanley and Felippa, 1986; Stein, Wagner and Wriggers,

1988; Wempner, 1992). While many issues have been resolved, new issues have emerged as the computing technology and our understanding have evolved.

Solution techniques for systems of nonlinear algebraic equations evolved from the simple methods used to find the zeroes (or roots) of a single nonlinear equation. Early researchers in nonlinear finite element analysis attempted to exploit the solvers available for first-order ordinary differential equations by re-casting the algebraic equations in that form (see Stricklin and Haisler, 1977). These methods provided ways to exploit certain features of the problem and were computationally simple and fast; however, like most techniques for initial-value problems, they were also susceptible to solution drift and numerical errors. Because of these issues, most researchers turned to an incremental-iterative procedure based on the Newton-Raphson method. This method has been widely used as a root-finding method of a single nonlinear equation, and various aspects of the method are readily explained from a geometric point-of-view using a single degree-of-freedom system. In addition, this method can be readily extended to a *system* of nonlinear equations and represents the most widely used method for solving a nonlinear system of algebraic equations.

There are many variants of this method available that are mostly associated with trying to reduce the computational effort required to solve a particular problem — i.e., related to the frequency of updating the tangent stiffness matrix and the solution-marching control strategy. Numerous papers and books are available that describe solution procedures, outline computational algorithms, and describe structural simulations (e.g., Almroth and Brogan, 1977; Bathe, 1996; Bergan, 1980; Crisfield, 1992; Felippa, 1976; Hinton, Owen and Taylor, 1982; Stricklin and Haisler, 1977). Solution procedures based on the Newton-Raphson method require the evaluation of the residual vector and the tangent stiffness matrix, the solution of a linearized system of equations, and the updating of the solution vector based on the obtained incremental values. Some researchers modify the method so that the tangent stiffness matrix is re-evaluated only periodically based on some criterion such as slow convergence, while others update the tangent stiffness matrix only at the beginning of each load step. When this update is performed, the element tangent stiffness matrices must be evaluated and then assembled, followed by the imposition of boundary conditions and decomposition of this updated tangent stiffness matrix. This step is perhaps the most time consuming part of the computation.

These days, most finite element codes provide a nonlinear analysis capability for both static and transient dynamic problems. In most cases, the Newton-Raphson procedure is available and used as the default solution algorithm. In addition, some codes use the *full* Newton-Raphson method as

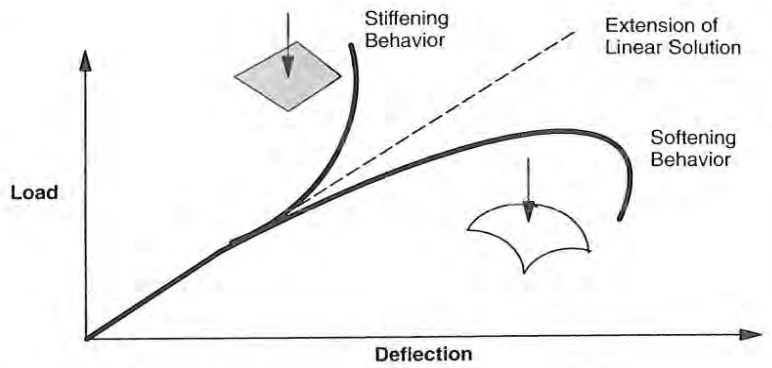

Figure 3. Typical types of nonlinear structural behavior.

their default method in order to provide robustness for novice users of their code. As an alterative, quasi-Newton methods such as the Broyden-Fletcher-Goldfarb-Shanno (BFGS) method as described by Matthies and Strang (1979) and Bathe (1996) are often used. Other quasi-Newton methods are reviewed by Dennis and Moore (1977). Nonlinear problems are very difficult and it is nearly impossible to anticipate all possible solution combinations that users may attempt. Users of nonlinear codes need to be especially cognizant of the structural problem being solved, options and defaults provided by the code developers, and should thoroughly interrogate the computed results of the simulation. In the subsequent sections, various aspects of some of the more common solution procedures are discussed.

1.5.2. Solution Techniques for Nonlinear Static Analysis

The nonlinear structural response considered herein is typically one of two types as indicated in Figure 3. If the structure tends to increase in stiffness as the load level increases, then the response is referred to as a stiffening behavior. One example would be a beam or plate with a transverse load. If the structure tends to decrease in stiffness as the load level increases, then the response is referred to as a softening behavior. One example would be an arch or shell with a transverse load acting towards its center of curvature. Using a linear analysis method tends to give conservative solutions for structures exhibiting a stiffening behavior and unconservative solutions for structures exhibiting a softening behavior.

Stiffening behavior is generally straightforward to obtain; although in some cases, very small load increments are required. As the load is increased, the structure stiffens typically due to membrane stretching. For example, a trampoline surface will exhibit a stiffening behavior as the surface is deflected. As the membrane strains increase, their nonlinear terms become increasingly important and add stiffness to the structure. As this nonlinear stiffness increases, large load increments produce only small deflections until a vertical tangent is reached. In all cases, the tangent stiffness matrix remains positive definite and its determinant increases in value.

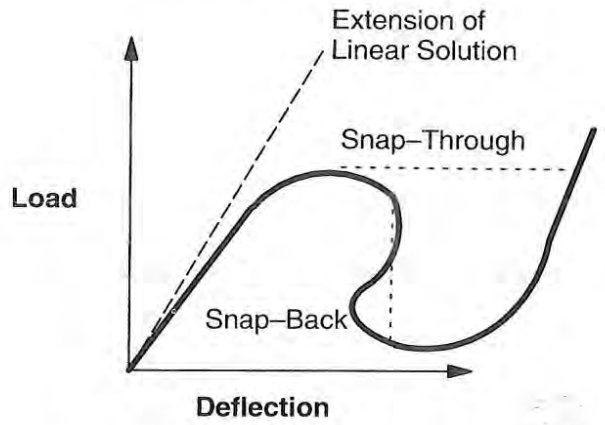

Figure 4. Typical softening behavior exhibiting limit points with snap-through and snap-back behavior.

Softening behavior leads to overall structural collapse, snap-through and/or snap-back conditions as part of the nonlinear solution as illustrated in Figure 4. This type of behavior is associated with the loss of positive-definiteness of the tangent stiffness matrix and hence causes numerical difficulties for the analyst. In most finite element codes, the equation solver assumes that the tangent stiffness matrix remains positive definite through the analysis, and when limit points are encountered, the equation solver often fails. For example in Figure 4, as the load is increased from zero (load control), the response softens until a point is reached which corresponds to a horizontal tangent (i.e., zero determinant of tangent stiffness matrix) and if the load is increased further the structure snaps-through. On the other hand, if a key deflection variable is incremented (displacement control), a vertical tangent is reached and a snap-back behavior may be present.

Softening behavior is also related to another type of structural response which depends on the applied loading. This response is associated with buckling of structures due to in-plane loads and is generally related to a

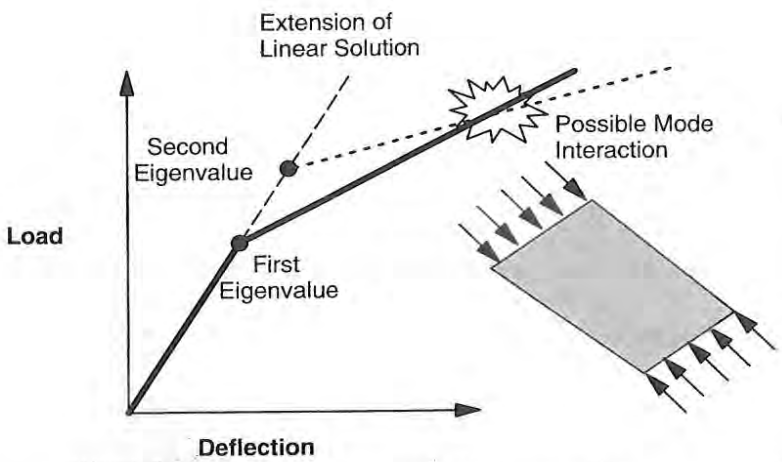

Figure 5. Typical softening behavior exhibiting isolated critical points.

reduction in stiffness without the response exhibiting a limit point as shown in Figure 5. Buckling is associated with transitioning from one deformation mode to another (or adjacent equilibrium configuration) at a common load level. That is, a perfect column loaded in compression will respond as a rod until the applied load reaches a critical value (the buckling load) at which time the lowest energy state now becomes a beam bending mode. In this case, there exists a load level with two adjacent equilibrium configurations: one with a rod or membrane behavior and another with a beam or bending behavior. These critical values correspond to the eigenvalues of the structure based on a given stress state. Often times these eigenvalues are isolated or spaced from one another. For example, the eigenvalues of a simply supported column of length L with an axial load P are given by $P_n = n^2\pi^2 \dfrac{EI}{L^2}$ and are widely spaced from each other and hence called isolated bifurcation points. Such problems are difficult to solve even though the load-deflection curve generally does not exhibit a horizontal tangent. However, the buckling load does correspond to a critical value or eigenvalue which corresponds to a point where the determinant to the tangent stiffness matrix is zero. As such, the nonlinear terms must be *triggered* in order to *jump* onto the adjacent equilibrium path. This is usually done by incorporating the actual imperfect geometry of the structure (initial geometric imperfections) or by imposing a small lateral or eccentric load. The solution process usually continues

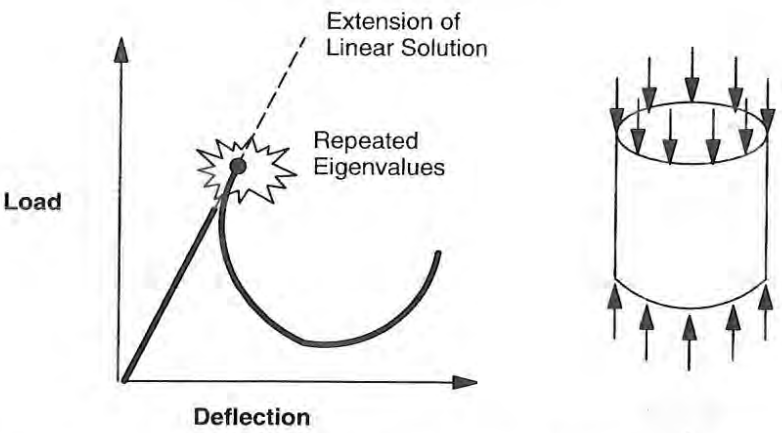

Figure 6. Typical softening behavior exhibiting repeated eigenvalues and structural collapse.

smoothly in the postbuckled regime as the eigenvalues of the tangent stiffness matrix generally remain isolated.

If a secondary critical point is reached, then mode interaction may occur, and multiple negative roots are present in the tangent stiffness matrix. Such problems are generally referred to as "drop dead problems" since the nonlinear static solution procedure stops dead in its tracks. In such cases, the most likely cause of the numerical difficulties is the "mode switching" or "mode jumping" phenomena that would lead to a new equilibrium configuration for the structure. To pass such critical points in the response curve numerically, an equivalence transformation may be performed as described by Thurston (1980) and Thurston *et al.* (1986). Alternatively, a transient dynamic analysis may be started at the critical point until a new "stable" equilibrium configuration is obtained (see Riks *et al.*, 1996).

Softening behavior which exhibits a rapid reduction in load carrying capacity is generally associated with structural collapse and in shell structures occurs due to multiple or repeated eigenvalues. One example is a circular cylindrical shell subjected to axial compression as shown in Figure 6. In this case, multiple repeated eigenvalues or closely spaced eigenvalues cause difficulty in predicting the nonlinear structural response. In most cases, the nonlinear solutions along the unstable equilibrium path are not observable in the laboratory as they represent a dynamic event. However, analytically tracing this unstable branch may provide insight into the overall failure scenario and provide information useful for improving the design.

In this region, often structural material failures occur and the problem becomes even more complex since geometry changes due to large deflections and rotations as well as material constitutive law changes due to local failures and/or inelastic behavior both occur.

1.5.2.1. Load Control

Starting with the variational statement of the problem, the elemental properties are defined by imposing the stationary conditions on the variational statement of the problem. The stationary condition requires a balance of the internal and external forces. That is,

$$f^{int}(\mathbf{u}, \lambda) = f^{ext}(\lambda) \tag{39}$$

where the internal forces, at a given load level λ, are related to the linear and nonlinear stiffnesses of the structure due either to geometric, material, or contact nonlinearities or to a combination of these sources. These equations are often written in an alternate form as

$$\boldsymbol{K}_0\boldsymbol{u} + \boldsymbol{Q}_{NL}(\mathbf{u}, \lambda) = f^{ext}(\lambda) = \lambda f^{ext} \tag{40}$$

where $\boldsymbol{u}$ is a vector of nodal generalized displacements, $\boldsymbol{K}_0$ is the linear stiffness matrix, $\boldsymbol{Q}_{NL}$ is the vector of nonlinear terms, f^{ext} is the vector of externally applied loads, and λ is the load factor for assumed proportional loading. A linear stress analysis problem corresponds to the case when the vector of nonlinear terms $\boldsymbol{Q}_{NL}$ is neglected.

Traditionally, the nonlinear algebraic equations given by Equation 40 are solved using the Newton-Raphson approach (e.g., Bushnell, 1985) using load control. In this approach, the load factor λ is incremented and a nonlinear solution is determined using the Newton-Raphson iterative approach. At a load level defined by λ_{n+1} where n denotes the previous load level (or load step), the tangent stiffness matrix $(\boldsymbol{K}_T)^{(i)}_{n+1}$ derived from the second variation of the variational statement and the residual force vector (or force imbalance vector) $(\boldsymbol{R})^{(i)}_{n+1}$ derived from the linearization of a Taylor-series expansion about the solution $(\boldsymbol{u})^{(i)}_{n+1}$ are formed for the ith iteration. That is,

$$(\boldsymbol{K}_T)^{(i)}_{n+1}\,\Delta\boldsymbol{u}^{(i+1)} = (\boldsymbol{R})^{(i)}_{n+1} \tag{41}$$

where

$$(\boldsymbol{K}_T)^{(i)}_{n+1} = \frac{\partial f^{int}(\boldsymbol{u}^{(i)}_{n+1}, \lambda_{n+1})}{\partial \boldsymbol{u}} \tag{42}$$

$$(\boldsymbol{R})^{(i)}_{n+1} = f^{ext}(\lambda_{n+1}) - f^{int}(\boldsymbol{u}^{(i)}_{n+1}, \lambda_{n+1}) \tag{43}$$

$$\boldsymbol{u}^{(i+1)}_{n+1} = \boldsymbol{u}^{(i)}_{n+1} + \Delta\boldsymbol{u}^{(i+1)} \tag{44}$$

Using this algorithm, the nonlinear static structural response is determined in an iterative manner for a fixed load level wherein Equation 41 is used to determine the iterative change in the generalized displacements $\Delta\boldsymbol{u}^{(i+1)}$ and to update the solution vector giving $\boldsymbol{u}^{(i+1)}_{n+1}$. Next the residual force vector for the $i+1^{st}$ iteration is evaluated. Then convergence criteria are evaluated and compared to a specified error tolerance. Common stopping criteria include a maximum number of iterations, a maximum amount of CPU time, and a modified Euclidean norm of the residual force vector given by

$$\frac{1}{N}\sqrt{\left((\boldsymbol{R})^{(i+1)}_{n+1}\right)^T\left((\boldsymbol{R})^{(i+1)}_{n+1}\right)} \le \varepsilon_{tol} \tag{45}$$

or a modified Euclidean norm of the iterative change in the generalized displacements given by

$$\frac{1}{N}\sqrt{\frac{(\Delta\boldsymbol{u}^{(i+1)})^T(\Delta\boldsymbol{u}^{(i)+1})}{\left(\boldsymbol{u}^{(i+1)}_{n+1}\right)^T\left(\boldsymbol{u}^{(i+1)}_{n+1}\right)}} \le \varepsilon_{tol} \tag{46}$$

where N is the number of degrees of freedom and ε_{tol} is a specified convergence tolerance. The use of these error norms results in combining translational and rotational degrees of freedom together in forming the inner product. Nour-Omid *et al.* (1983) defined an *energy norm* that provides natural scaling of both translational and rotational freedoms. The energy norm is defined by

$$\varepsilon_{energy} = \sqrt{\frac{\left(\boldsymbol{R}^{(i+1)}_{n+1}\right)^T(\Delta\boldsymbol{u}^{(i)+1})}{\left(\boldsymbol{R}^{(1)}_{n+1}\right)^T\left(\boldsymbol{u}^{(1)}_{n+1}\right)}} \le \varepsilon_{tol} \tag{47}$$

Bergan and Clough (1972) found that different error norms (maximum norm or Euclidean norm) closely follow each other and give essentially the same behavior. If convergence is not achieved, then the tangent stiffness matrix (Equation 42) and residual force vector (Equation 43) are re-evaluated using $\boldsymbol{u}^{(i+1)}_{n+1}$, and Equation 41 is solved again. Once convergence is achieved, the load level is incremented (e.g., $\lambda_{n+2} = \lambda_{n+1} + \Delta\lambda$) and the solution process is started for the new load level. The size of the load increment $\Delta\lambda$ may

be fixed during the analysis or it may be adjusted depending on the performance of the solution procedure (i.e., desired number of iterations per load step). However, the load level at each load step is held constant during the iterative process at that load level (i.e., fixed at λ_{n+1}).

Various forms of the Newton-Raphson algorithm are commonly used. The two most common being the full Newton-Raphson method and the modified Newton-Raphson method. In the full Newton-Raphson method, the tangent stiffness matrix given by Equation 42 is formed and factored on every iteration and the residual force vector given by Equation 43 is formed on every iteration as part of the iterative solution procedure given by Equation 41. As such, convergence is rapid but the computational cost per iteration is significant. In the modified Newton-Raphson method, only the residual force vector is formed on every iteration — the tangent stiffness matrix is not updated on every iteration. Instead the tangent stiffness matrix is updated only at the beginning of each load step or perhaps only when convergence has not been attained after a specified maximum number of iterations. This method is very common, provides accurate solutions to many problems, and does alleviate some of the computational cost of performing nonlinear finite element analysis for many structural mechanics problems without sacrificing accuracy or robustness.

1.5.2.2. Displacement Control

In the displacement-control procedures (Zienkiewicz, 1971; Batoz and Dhatt, 1979; Ramm, 1981, 1982), a specific generalized displacement degree of freedom is identified as the primary degree of freedom that drives the solution algorithm. Examples include the transverse displacement component at the crown of a spherical shell or arch subjected to external pressure loading and the end shortening of a panel subjected to inplane compression causing a postbuckling response. Hence, such a degree of freedom is selected to be known or specified and incremented during the solution process. As this variable is incremented, the remaining degrees of freedom and the load parameter then make up the nonlinear system to be solved. Ramm (1981, 1982) has described the displacement control procedure in detail. It has been commonly used for snap-through problems and problems with a limit point; however, for structures which exhibit a snap-back behavior this procedure will fail. The success of the displacement control procedure also rests in the selection of which degree of freedom to use as a control variable. Fujii *et al.* (1992) have presented an automated procedure for the selection of the "best-suited" control parameter. Ramm (1982) points out that this solution procedure is essentially a special case of the arc-length control procedures which are discussed next.

1.5.2.3. Arc-Length Control

In the arc-length control procedures (Riks, 1970, 1987, 1992; Wempner, 1971; Crisfield, 1981, 1982; Ramm, 1982), the load level is considered as an additional variable within each iteration so that the solution follows some specified path until convergence is attained. For a single degree-of-freedom system, this path may be in a plane normal to the tangent line at the beginning of the load step or the path may be on an arc of a circle of given radius (i.e., constant arc length). Since the load level is now a variable, an additional equation is needed. This equation is referred to as a constraint equation and has a form amenable to computation given by

$$C(\boldsymbol{u},\lambda)=\left(\overline{\Delta \boldsymbol{u}}^{(i)}\right)^T\left(\overline{\Delta \boldsymbol{u}}^{(i)}\right)+(\Delta\lambda)^2\alpha^2\left(\bar{f}_{ext}\right)^T\left(\bar{f}_{ext}\right)-(\Delta l)^2=0 \quad (48)$$

where Δl is the arc-length parameter, $\bar{f}_{ext}$ is the external base load vector assuming proportional loading, $\Delta\lambda$ is the increment in load, α is a units scaling parameter, and $\overline{\Delta \boldsymbol{u}}^{(i)}$ is the incremental displacement change given by

$$\overline{\Delta \boldsymbol{u}}^{(i)}=\boldsymbol{u}_{n+1}^{(i)}-\boldsymbol{u}_n^{converged}=\boldsymbol{u}_{n+1}^{(i)}-\boldsymbol{u}_n^{(I_n)} \quad (49)$$

That is, the incremental displacement change represents the difference between the converged solution for the nth step and the solution obtained for the ith iteration of the $n+1$ step. Furthermore, it is assumed that the loading is independent of the displacements and that the arc-length parameter is independent of the loading. This reduces the constraint equation to

$$C(\boldsymbol{u})=\left(\overline{\Delta \boldsymbol{u}}^{(i)}\right)^T\left(\overline{\Delta \boldsymbol{u}}^{(i)}\right)-(\Delta l)^2=0 \quad (50)$$

The solution to the original nonlinear system of equations, Equation 40, with the constraint equation, Equation 50, requires both equations to be linearized by considering the leading terms of a Taylor-series expansions about the last converged solution.

Implementation details of the arc-length control solution procedure are illustrated in Figures 7 to 12 which are discussed next. Each step in the computational procedure is given in a flowchart and graphically depicted using a single degree-of-freedom system. The procedure is divided into three parts. Part 1 represents the basic operations required at the beginning of each step. Part 2 describes the basic operations performed during each iteration. Part 3 describes the basic operations performed to test for convergence. The discussion begins by assuming that a solution for the nth step has already been obtained. Note that superscripts in parenthesis denote iteration number, and subscripts denote step number.

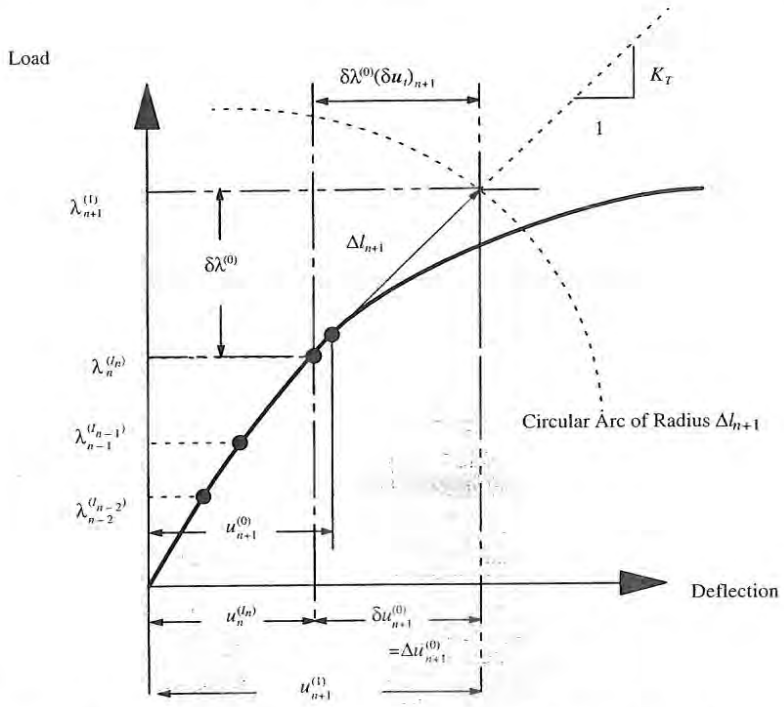

Figure 7. Graphical view of arc-length control solution strategy — part 1.

Part 1 represents the initialization process as indicated in Figures 7 and 8. At the beginning of the nth step, the converged displacement solution and the corresponding stress and strain states have been obtained. It is assumed that the number of iterations required to obtain converged solutions for the past several steps is denoted by I_{n-2} for the $n-2$ step, I_n for the $n-1$ step, and I_n for the nth step. The beginning of the subsequent steps involve the tasks outlined in Figures 7 and 8 which comprise Part 1 of the algorithm. The first task is to obtain an initial estimate or "guess" of the solution for the next step $\boldsymbol{u}_{n+1}^{(0)}$. This may be the last converged solution or it may be computed using an extrapolation procedure. Herein a quadratic extrapolation procedure is used based on three previous converged solutions as indicated on Figure 7 and given by

$$\boldsymbol{u}_{n+1}^{(0)} = c_n \boldsymbol{u}_n^{(I_n)} + c_{n-1} \boldsymbol{u}_{n-1}^{(I_{n-1})} + c_{n-2} \boldsymbol{u}_{n-2}^{(I_{n-2})} \tag{51}$$

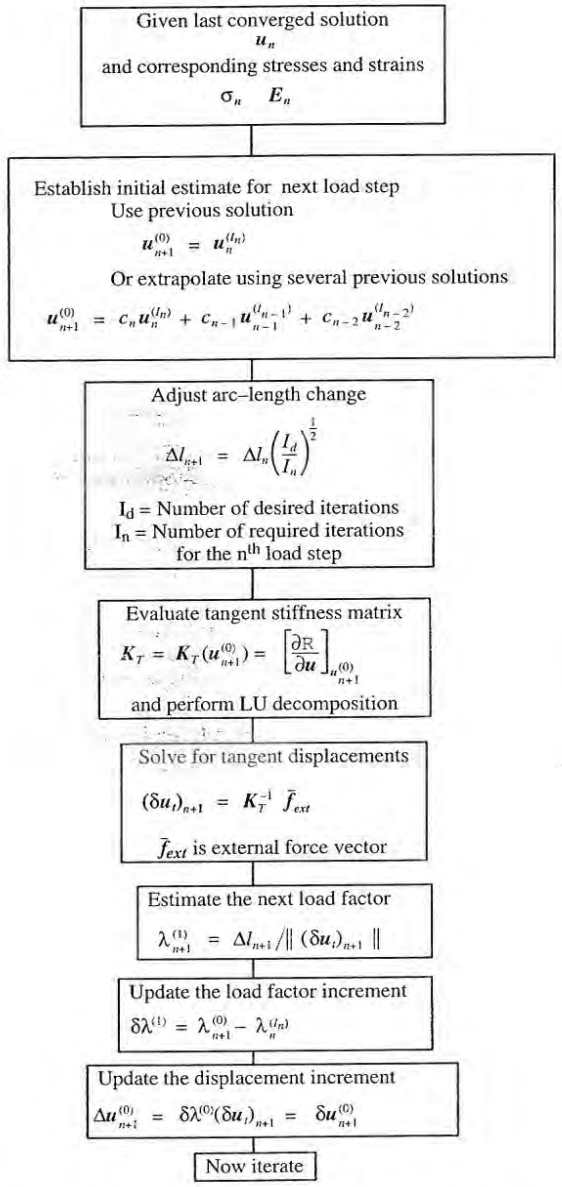

Figure 8. Flowchart of arc-length control solution strategy — part 1.

The values of the coefficients for the extrapolation can be shown to be equal to

$$\begin{aligned} c_n &= \frac{l_{n+1}\,\Delta l_{TOTAL}}{l_n\,\Delta l_n} \\ c_{n-1} &= -\frac{l_{n+1}\,\Delta l_{n+1}}{l_{n-1}\,\Delta l_n} \\ c_{n-2} &= \frac{\Delta l_{TOTAL}\,\Delta l_{n+1}}{l_{n-1}\,l_n} \end{aligned} \tag{52}$$

where l is the arc-length parameter for the previous steps or

$$\begin{aligned} l_{n-1} &= \Delta l_{n-1} \\ \Delta l_n &= l_n - l_{n-1} \\ \Delta l_{n+1} &= l_{n+1} - l_n \\ \Delta l_{TOTAL} &= l_{n+1} - l_{n-1} \end{aligned} \tag{53}$$

Using these coefficients, the predicted starting solution for the solution vector is computed. Next, the arc-length parameter Δl is adjusted based on the extrapolation procedure just described or it may be updated based on the convergence behavior of the problem according to:

$$\Delta l_{n+1} = \Delta l_n \left(\frac{I_d}{I_n} \right)^B \tag{54}$$

If the number of iterations required for convergence for the nth step (I_n) is fewer than the user-specified number of *desired* iterations per step (I_d), then the arc-length parameter is increased. Some analysts use a value for the exponent β of unity rather than the value of one-half indicated in the flowchart, Figure 8. However, the value of one-half, as suggested by Ramm (1981, 1982), leads to an overall saving in computational effort because of a reduced probability of *thrashing* caused by successively increasing and then decreasing the value of the arc-length parameter. Next, the tangent stiffness matrix is updated using the new estimate for the solution and the tangent displacement vector is computed for the given external force vector. Solving for the updated tangent displacements must be repeated each time the tangent stiffness matrix is updated. Using this solution, the value of the next load factor $\lambda_{n+1}^{(1)}$ is computed as well as the initial displacement increment $\Delta \boldsymbol{u}_{n=1}^{(0)}$. At this point, the iteration process given in Part 2 is begun.

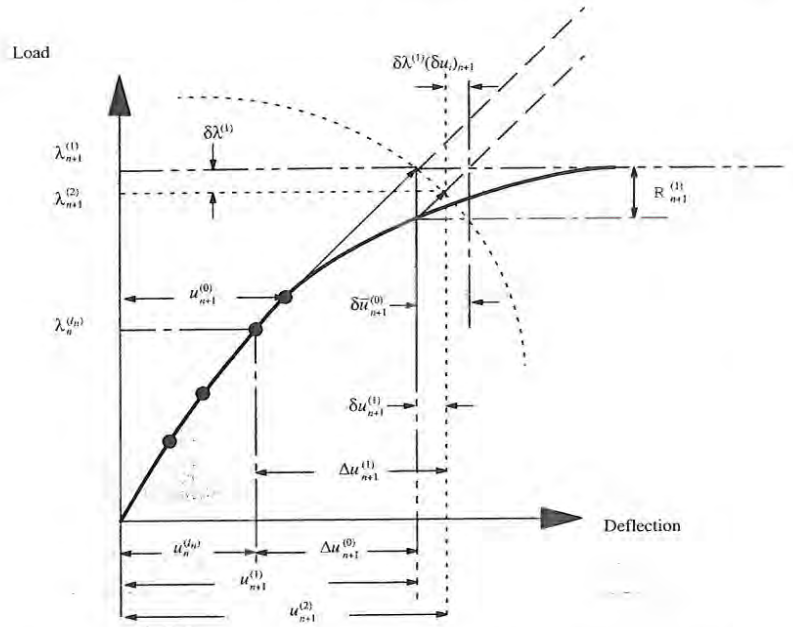

Figure 9. Graphical view of arc-length control solution strategy — part 2.

Part 2 represents the iteration process as indicated in Figures 9 and 10. This iteration process is rather straightforward although somewhat tedious. First the internal force vector is computed using the initial estimate of the solution, and then a new residual vector is formed for the current iteration. Using the present tangent stiffness matrix (which has already been factored), the iterative change in displacements $\delta\bar{\boldsymbol{u}}_{n+1}^{(i)}$ is computed. At this point, the corresponding change in load factor is computed. In the present case as indicated in Figure 9, a cylindrical constraint equation is used, and the arc-length equation is solved using consistent linearization based on a Taylor-series expansion in order to compute $\delta\lambda^{(i)}$. Having this value, the load factor is updated, and the total displacement change for the ith iteration at the $n+1$ step $\delta\boldsymbol{u}_{n+1}^{(i)}$ is obtained using the iterative change in displacements, the change in load, and the tangent displacements. Finally, the total accumulated iterative displacement change is determined and the displacement solution updated to give $\boldsymbol{u}_{n+1}^{(i+1)}$. At this point, convergence of the iteration process is examined.

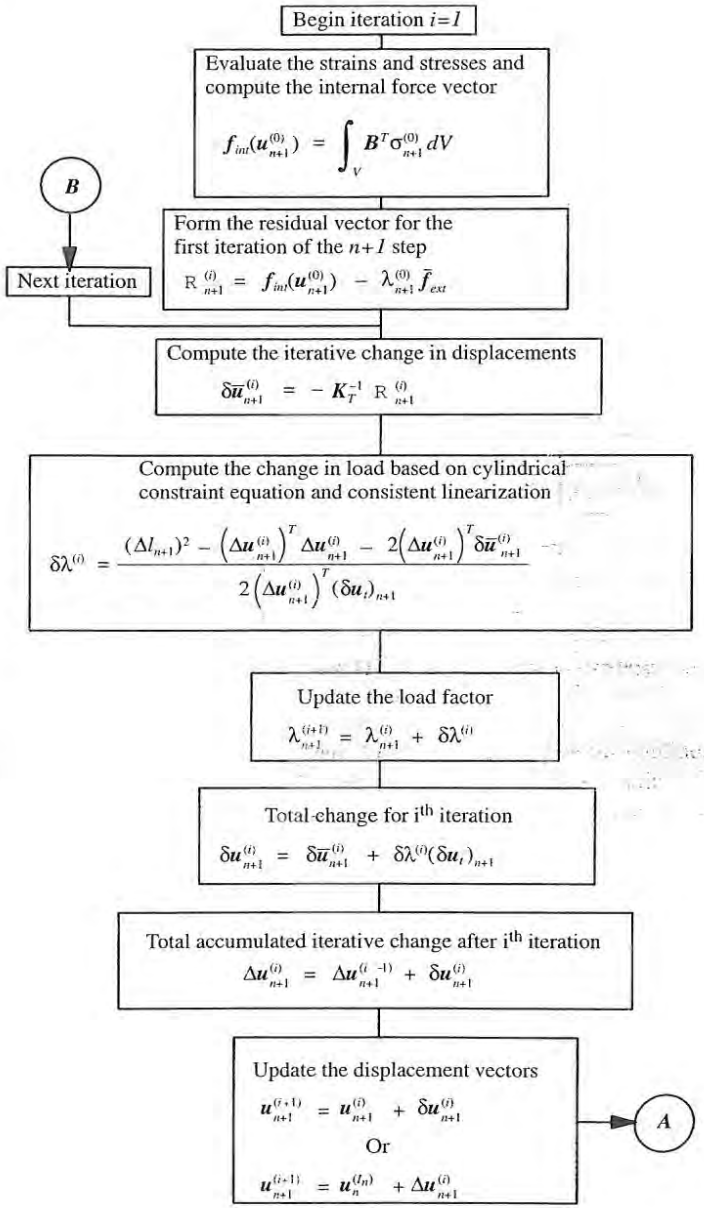

igure 10. Flowchart of arc-length control solution strategy — part 2.

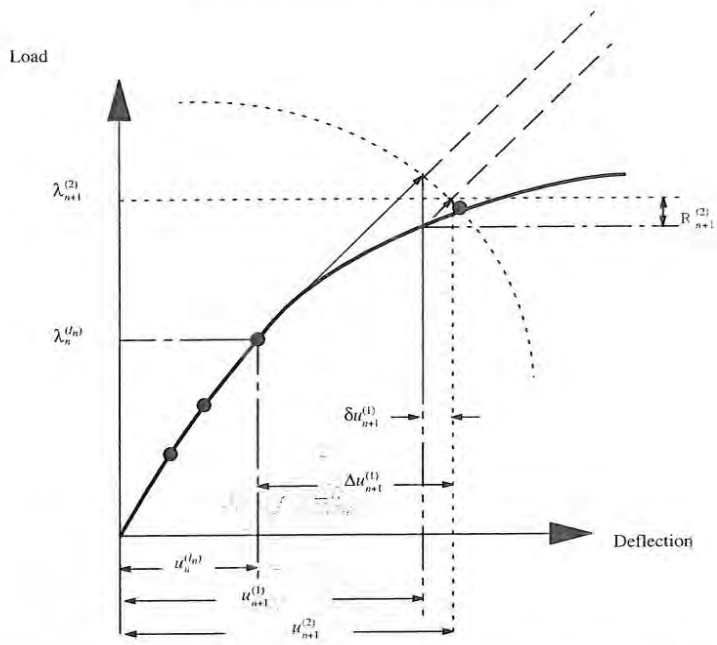

Figure 11. Graphical view of arc-length control solution strategy — part 3.

Part 3 of the iteration process continues as indicated in Figures 11 and 12. This part of the process essentially prepares for the next iteration by computing an updated internal force vector and residual vector. Then various convergence or stopping criteria are assessed with suitable action taken. In these figures, it is assumed that the tangent stiffness matrix is held constant during the iteration process at each step and is updated after a convergence solution is obtained. Strictly speaking, it is only at a converged displacement solution that the tangent stiffness matrix is truly the *tangent* stiffness matrix.

1.5.2.4 Reduction Methods

Reduction methods are a class of methods that use a change of variables to transform the nonlinear finite element equations given in Equation 40 from the generalized displacement degrees of freedom $\boldsymbol{u}$ to a much smaller or reduced set of unknowns $\boldsymbol{q}$. This change of variables generally takes the form

$$\boldsymbol{u}_{N\times 1} = \Gamma_{N\times r}\, \boldsymbol{q}_{r\times 1} \tag{55}$$

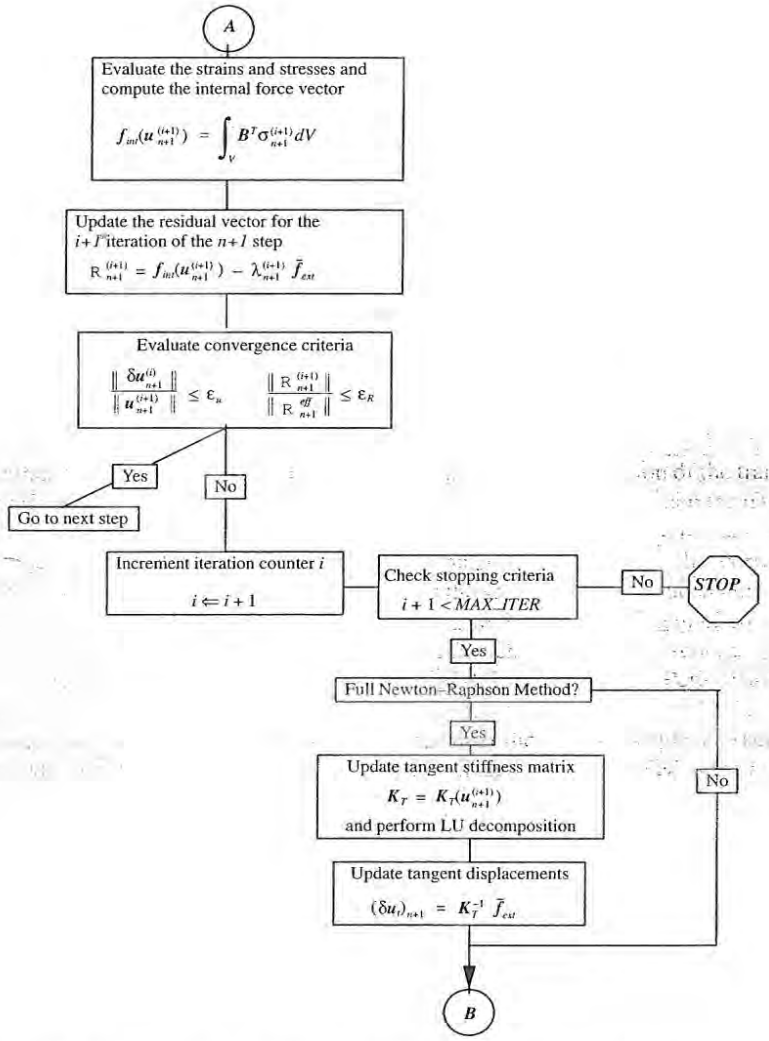

Figure 12. Flowchart of arc-length control solution strategy — part 3.

where $\boldsymbol{q}$ is the vector of undetermined coefficients of the reduced system of equations, Γ is the transformation matrix of vectors used in the change of variables, N is the number of unknowns in the original or full system, and r is the number of unknowns in the reduced system with $r << N$. These

methods are similar to modal methods used in structural dynamics problems in that a smaller set of unknowns needs to be determined, and these unknowns are the participation weights for each column in the transformation matrix. In effect, these reduction methods represent a form of Rayleigh-Ritz method applied to the discrete system (i.e., two-stage Rayleigh-Ritz methods, see Noor, Peters and Andersen, 1980). The columns of the transformation matrix Γ are vectors in terms of the global degrees of freedom of the original system of nonlinear equations. Some reduction methods require physical insight in selecting columns of the transformation matrix and adapting the method to specific problems. Generally, reduction methods work well for problems which exhibit a small change in the spatial characteristics of the structural response over a large range of load levels. Reduction methods for nonlinear problems include the global function approach and the reduced basis approach.

The success of reduction methods in solving nonlinear structural mechanics problems depends strongly on the definition of the transformation matrix Γ, on the definition of error sensors to detect when (or if) the transformation matrix needs to be updated, and on an effective implementation scheme for the generation of the transformation matrix, the corresponding reduced system of equations, and the solution of the reduced nonlinear system. Once the problem is transformed to the reduced system of equations, the solution process continues wherein each solution represents a "predicted" solution based on the specific transformation matrix. Periodically, the "predicted" solution for the original or full system is recovered using the transformation matrix. For example, consider the solution sequence sketched in Figure 13. Suppose a transformation matrix Γ_n was formed at the nth load step and the solution marched forward using the reduced system until reaching the $n+10^{th}$ load step. Then the "predicted" solution for the full system at the $n+10^{th}$ load step will be given by

$$(\boldsymbol{u}_{n+10})^{Predicted} = \Gamma_n \, \boldsymbol{q}_{n+10} \tag{56}$$

This "predicted" solution for the global degrees of freedom is then used as an initial guess for the Newton-Raphson iteration procedure (Equations 41–44) in order to recover the true or "corrected" solution $\boldsymbol{u}_{n+10}^{corrected}$. Once a converged solution is obtained (i.e., the "corrected" solution), the transformation matrix of global functions Γ_{n+10} is updated — perhaps adding new columns and/or deleting previous columns. Then an updated reduced system of equations is generated, and the nonlinear analysis continues using the updated reduced system of equations.

The global function approach of Almroth and colleagues (1978, 1981) chooses the columns of the transformation matrix Γ to be a subset of the previous nonlinear solutions. The solution process begins by solving the

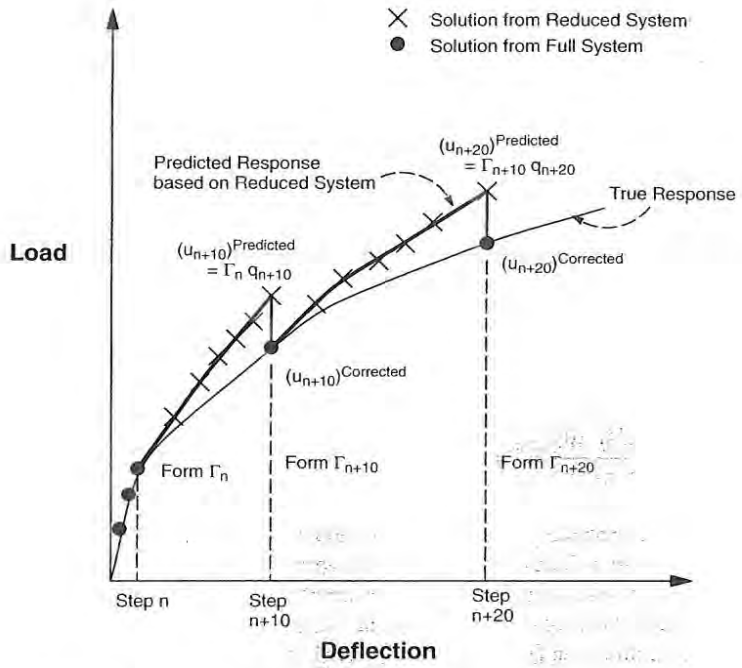

Figure 13. Schematic of reduction method solution process.

nonlinear system for several load steps and then uses these solution vectors to form the columns of the transformation matrix. That is,

$$(\Gamma_{N\times r})_n = [\bar{u}_1\ \bar{u}_2 \cdots \bar{u}_r]_n \tag{57}$$

where each column or global function is related to a nonlinear solution for a previous load level and $r \le n << N$. Since these global functions are converged nonlinear solutions obtained by solving Equation 40 using the traditional approach directly, the computational cost of generating the transformation matrix is not small. For example, if three global functions are to be used and if a modified Newton-Raphson method which updates the tangent stiffness matrix only on the first iteration at each load step is used, then the tangent stiffness matrix will need to be formed and factored at least three times plus perhaps three to five iterations per load step. However, if

the nonlinear solution for subsequent load levels is self-similar to these early nonlinear solutions (i.e., same overall deformation pattern), then many subsequent load steps may be taken without requiring an update to the transformation matrix. If the solution does change substantially from the earlier solutions (e.g., limit point problems or problems with localized instabilities), frequent updating of the transformation matrix may be required and thereby possibly negate any computational savings accrued by solving the reduced system of equations. Strategies for the selection and modification of the global functions are reported by Stehlin and Brogan (1984).

The reduced basis approach of Noor and colleagues (1979, 1980, 1981) chooses the columns of the transformation matrix to be path derivatives of the generalized displacement degrees of freedom with respect to a generalized parameter s. That is, for load step n,

$$(\Gamma_{N\times r})_n = \left[\bar{u}\ \frac{\partial \bar{u}}{\partial s}\ \frac{\partial^2 \bar{u}}{\partial s^2} \cdots \frac{\partial^{r-1} \bar{u}}{\partial s^{r-1}}\right]_n \tag{58}$$

where each column is related to a path derivative of the generalized displacement degrees of freedom. The choice of the generalized parameter was originally the load parameter λ; however, a more effective choice was later found to be the arc-length parameter associated with the nonlinear solution algorithm. These path derivatives are computed by successive differentiation of Equation 40 and is reported to only require a single decomposition of the linear stiffness matrix for the generation of the initial set of basis vectors. The solution procedure continues in a manner similar to that described for the global function approach.

1.5.3. Solution Techniques for Nonlinear Transient Dynamic Analysis

Nonlinear transient structural dynamic analysis methods have been evolving since the early development work in the finite element method (see Belytschko, 1974, 1975; Tillerson, 1975; Belytschko and Hughes, 1983; Lee and Belytschko, 1995). Transient structural dynamics problems are generally classified by the frequency of the applied loading. If the frequency of the applied loading is less than approximately one third of the natural frequency of the structure, then often only a quasi-static analysis is performed and the inertial effects are neglected. Above this frequency value, the time-dependent nature of the problem should be accounted for in any assessment of the structural behavior. Some loading conditions result in a

forced vibration type of response wherein overall structural response characteristics are to be determined. For these cases, the transient behavior is often obtained using either a reduction method (e.g., mode displacement method) if the behavior is linear or at most only mildly nonlinear. As an alternative, direct numerical time integration procedures based on implicit methods (e.g., Newmark β methods) are usually applied because of their unconditional numerical stability for linear transient analysis; however, the user must assume the responsibility for establishing the accuracy of the transient dynamic simulation (i.e., re-run the simulation with a smaller time step and compare the two solutions). When the loading is a very short dynamic event, such as impact or accident conditions, wave propagation aspects need to be considered. In these problems, direct numerical time integration procedures based on explicit methods (e.g., central difference method) are usually applied. These methods generally only exhibit conditional numerical stability for linear transient analysis and require a very small time step. Most general-purpose finite element structural analysis computer codes offer one or both of these methods and frequently multiple time-integration algorithms are also available.

Solving the equations of motion for the structure involves two main steps. First, the structure is discretized in the spatial domain usually by the finite element method and sometimes by using finite difference approximations for the spatial derivatives. This results in a system of semi-discrete equations (a system of algebraic equations in the spatial domain and ordinary differential equations in the time domain) as given by:

$$\boldsymbol{M}\ddot{\boldsymbol{u}}_{t+\Delta t} + \boldsymbol{C}\dot{\boldsymbol{u}}_{t+\Delta t} + \boldsymbol{f}^{int}(\boldsymbol{u}_{t+\Delta t}) = \boldsymbol{f}^{ext}_{t+\Delta t} \tag{59}$$

where

$$\boldsymbol{f}^{int}(\boldsymbol{u})_{t+\Delta t} = \boldsymbol{K}_0\boldsymbol{u}_{t+\Delta t} + \boldsymbol{Q}_{nl}(\boldsymbol{u}_{t+\Delta t}) \tag{60}$$

represents the internal force vector which is usually calculated directly by integrating over each element and the indicated matrix operations at the global level are never performed. The second step is to solve these differential equations in time by using a direct time integration method (implicit or explicit) to march the solution forward in the time domain.

1.5.3.1. Explicit Methods

Explicit time integration methods determine the current equilibrium configuration in terms of the previous equilibrium configuration and in a sense only involve a linear combination of vectors. The equilibrium configuration

of the structure at time $t + \Delta t$ is computed from the equilibrium configurations prior to that time. The computational algorithm for an explicit method based on central difference operators involves replacing the time derivatives in the semi-discrete equations of motion written at time t with the following approximations:

$$\dot{\boldsymbol{u}}_t = \frac{1}{\Delta t}(\boldsymbol{u}_{t+\Delta t} - \boldsymbol{u}_{t-\Delta t}) \tag{61a}$$

$$\ddot{\boldsymbol{u}}_t = \frac{1}{(\Delta t)^2}(\boldsymbol{u}_{t+\Delta t} - 2\boldsymbol{u}_t + \boldsymbol{u}_{t-\Delta t}) \tag{61b}$$

After making these substitutions and gathering like terms, the equations to be solved at each time step are:

$$\left(\frac{1}{(\Delta t)^2}\boldsymbol{M} + \frac{1}{2\Delta t}\boldsymbol{C}\right)\boldsymbol{u}_{t+\Delta t} = \boldsymbol{f}^{ext}_t - \boldsymbol{f}^{int}(\boldsymbol{u})_t + \frac{2}{(\Delta t)^2}\boldsymbol{M}\boldsymbol{u}_t - \left(\frac{1}{(\Delta t)^2}\boldsymbol{M} - \frac{1}{2\Delta t}\boldsymbol{C}\right)\boldsymbol{u}_{t-\Delta t} \tag{62}$$

Close examination of this system of equations reveals that at most the decomposition of the left-hand-side matrix would only be necessary initially and then again whenever the time step size is changed if the mass and damping matrices were not diagonal matrices. However, as is often the case, a diagonal mass matrix and mass-proportional damping matrix are used in nonlinear transient dynamic simulations. Hence the solution of these equations is a trivial process without resorting to any equation solver (e.g., LU decomposition, Gaussian elimination, or preconditioned conjugate gradient (PCG) methods; e.g., see Poole, 1991). They require minimal computer storage, low memory requirements, and the computational effort per time step is minimal. However, being only conditionally stable even for linear problems, explicit schemes require the size of the time step to be smaller than the shortest period of vibration of the structure (i.e., time steps of the order of microseconds). The use of a conditionally stable time integrator is somewhat of a contradiction to the basic philosophy of the finite element method. The modeling flexibility offered by the finite element method allows the use of small elements in regions where a stress gradient is large or where other local events occur (e.g., contact, sliding between two surfaces). However, the largest allowable time step that may be used for most explicit schemes is inversely proportional to the highest modeled vibration frequency of the discretized structure. By using smaller and smaller elements, the highest modeled frequency increases and hence the size of the largest allowable time step decreases.

1.5.3.2. *Implicit Methods*

Implicit time integration methods determine the current equilibrium configuration iteratively for nonlinear systems. The equilibrium configuration of the structure at time $t + \Delta t$ is computed iteratively using a Newton-Raphson technique and may include solutions from previous time steps (historical solutions) for multi-step methods. The computational consequence of these schemes is that a system of nonlinear algebraic equations needs to be solved at each time step. In most cases, implicit schemes are unconditionally stable even for nonlinear systems and generally include a procedure to adaptively change the time step size during the simulation. Implicit schemes require additional computer storage, memory utilization, and computational effort per time step since the tangent stiffness matrix is frequently re-evaluated and a matrix decomposition is then required along with the evaluation of the right-hand-side vectors which include the evaluation of the internal force vector. However, the size of the time step for implicit methods is usually much larger than the size of the time step permitted by an explicit scheme. The size of the time step for an implicit scheme is strongly coupled to the temporal variation of the applied load and the duration of the dynamic event being simulated, and it should be selected such that the frequency content of the loading system and excited structural frequencies are accurately represented. For example, simulations of impact and crash events require detailed modeling and the inclusion of contact, friction, material nonlinearities (large strains, elasto-plastic response, composite laminate failure detection and propagation). Furthermore, short duration loading events often necessitate a very small time step just to capture the nonlinear mechanics without any consideration for the direct time integration scheme. The computational algorithm for an implicit method based on the Newmark algorithm involves replacing the time derivatives in the semi-discrete equations of motion with the following approximations:

$$\dot{\boldsymbol{u}}_{t+\Delta t} = \frac{\gamma}{\beta \Delta t}(\boldsymbol{u}_{t+\Delta t} - \boldsymbol{u}_t) - \left(\frac{\gamma}{\beta} - 1\right)\dot{\boldsymbol{u}}_t - \Delta t\left(\frac{\gamma}{2\beta} - 1\right)\ddot{\boldsymbol{u}}_t \tag{63a}$$

$$\ddot{\boldsymbol{u}}_{t+\Delta t} = \frac{\gamma}{\beta(\Delta t)^2}(\boldsymbol{u}_{t+\Delta t} - \boldsymbol{u}_t) - \frac{1}{\beta \Delta t}\dot{\boldsymbol{u}}_t - \left(\frac{1}{2\beta} - 1\right)\ddot{\boldsymbol{u}}_t \tag{63b}$$

where the coefficients α and β are related to the Newmark family of operators. After making these substitutions and gathering like terms, the equations to be solved at each time step are:

$$\boldsymbol{f}^{int}(\boldsymbol{u})_{t+\Delta t} + \left(\frac{1}{\beta(\Delta t)^2}\boldsymbol{M} + \frac{\gamma}{\beta \Delta t}\boldsymbol{C}\right)\boldsymbol{u}_{t+\Delta t} = \boldsymbol{f}^{ext}{}_{t+\Delta t}$$
$$+\boldsymbol{M}\left(\frac{1}{\beta(\Delta t)^2}\boldsymbol{u}_t + \frac{1}{\beta \Delta t}\dot{\boldsymbol{u}}_t + \left(\frac{1}{2\beta} - 1\right)\ddot{\boldsymbol{u}}_t\right) \tag{64}$$
$$+\boldsymbol{C}\left(\frac{\gamma}{\beta \Delta t}\boldsymbol{u}_t + \left(\frac{\gamma}{\beta} - 1\right)\dot{\boldsymbol{u}}_t + \left(\frac{\gamma}{2\beta} - 1\right)\Delta t\,\ddot{\boldsymbol{u}}_t\right)$$

This system is a system of nonlinear algebraic equations that must be solved in an iterative manner at each time step. This solution process based on the full Newton-Raphson approach is summarized as follows. For iteration $i + 1$, the tangent stiffness matrix and residual or force imbalance vector are evaluated using the solution from the ith iteration and then the incremental change in the solution vector is computed. That is,

$$\overline{\boldsymbol{K}^{eff}}^{(i)}\,\Delta \boldsymbol{u}^{(i+1)} = -\boldsymbol{R}^{(i)} \tag{65}$$

where the effective tangent stiffness matrix is given by

$$\overline{\boldsymbol{K}^{eff}}^{(i)} = \left[\frac{\partial \boldsymbol{f}_i^{int}}{\partial \boldsymbol{u}_j}\right]^{(i)} + \left(\frac{1}{\beta(\Delta t)^2}\boldsymbol{M} + \frac{\alpha}{\beta \Delta t}\boldsymbol{C}\right) \tag{66}$$

and the residual vector is given by

$$\boldsymbol{R}^{(i)}_{t+\Delta t} = \boldsymbol{f}^{int}(\boldsymbol{u})^{(i)}_{t+\Delta t} + \left(\frac{1}{\beta(\Delta t)^2}\boldsymbol{M} + \frac{\gamma}{\beta \Delta t}\boldsymbol{C}\right)\boldsymbol{u}_{t+\Delta t} - \boldsymbol{R}^{eff}{}_{t+\Delta t} \tag{67}$$

and the effective force vector including the historical terms is given by

$$\boldsymbol{R}^{eff}{}_{t+\Delta t} = \boldsymbol{f}^{ext}{}_{t+\Delta t} + \boldsymbol{H}_t \tag{68}$$

$$\boldsymbol{H}_t = \boldsymbol{M}\left(\frac{1}{\beta(\Delta t)^2}\boldsymbol{u}_t + \frac{1}{\beta \Delta t}\dot{\boldsymbol{u}}_t + \left(\frac{1}{2\beta} - 1\right)\ddot{\boldsymbol{u}}_t\right)$$
$$+\boldsymbol{C}\left(\frac{\gamma}{\beta \Delta t}\boldsymbol{u}_t + \left(\frac{\gamma}{\beta} - 1\right)\ddot{\boldsymbol{u}}_t + \left(\frac{\gamma}{2\beta} - 1\right)\Delta t\,\ddot{\boldsymbol{u}}_t\right) \tag{69}$$

Then for each iteration during a fixed time step, the solution vector is updated and convergence of the iterative procedure is checked. That is,

$$\boldsymbol{u}_{t+\Delta t}^{(i+1)} = \boldsymbol{u}_{t+\Delta t}^{(i)} + \Delta(\boldsymbol{u})^{(i+1)} \tag{70}$$

and

$$\frac{\left\|\Delta \boldsymbol{u}^{(i+1)}\right\|}{\left\|\boldsymbol{u}^{(i+1)}\right\|} \leq \varepsilon_u \tag{71}$$

Thus each time step involves the solution of a nonlinear system of equations which is typically done using the Newton-Raphson method. Special cases of the Newmark family include the constant average acceleration method or trapezoidal rule (when $\gamma = 1/2$ and $\beta = 1/4$) and the linear acceleration method (when $\gamma = 1/2$ and $\beta = 1/6$). These methods are unconditionally stable when γ and β satisfy the relation

$$2\beta \geq \gamma \geq \frac{1}{2} \tag{72}$$

Also when $\gamma = 1/2$, there is no numerical damping and the algorithm is second-order accurate in time.

A variation of this family of implicit time integrators has been developed by Hilber, Hughes, and Taylor (1977) called the α-methods. This approach introduces algorithmic damping (or numerical damping) without reducing the accuracy of the solution. It is based on the Newmark family of operators given by Equation 63 as applied to a modified set of equations of motion. That is, instead of using Equation 59, this approach uses

$$\begin{aligned} \boldsymbol{M}\,\ddot{\boldsymbol{u}}_{t+\Delta t} + (1+\alpha)\,\boldsymbol{C}\,\dot{\boldsymbol{u}}_{t+\Delta t} + (1+\alpha)\,f^{int}(\boldsymbol{u}_{t+\Delta t}) - \alpha\,\boldsymbol{C}\,\dot{\boldsymbol{u}}_t \\ -\alpha\,f^{int}(\boldsymbol{u}_t) = (1+\alpha)\,f^{ext}{}_{t+\Delta t} - \alpha\,f^{ext}{}_t \end{aligned} \tag{73}$$

where α, β, and γ are selected such that

$$-\frac{1}{3} \leq \alpha \leq 0 \qquad \gamma = \frac{1-2\alpha}{2} \qquad \beta = \frac{1-\alpha^2}{4} \tag{74}$$

This results in a second-order accurate, implicit scheme that is unconditionally stable. As α changes, the algorithmic or numerical damping is increased.

1.5.3.3. Reduction Methods

Reduction methods as applied to transient dynamics problems generally fall into two categories: mode-displacement methods and mode-acceleration methods (e.g., see Bathe, 1996; Craig, 1981; Cook *et al.*, 1989). These reduction methods are similar to the reduction methods used in static problems in that a smaller set of unknowns needs to be determined, and these unknowns are the participation weights for each column in the transformation matrix. These two categories of methods are briefly described next.

In the mode-displacement category, there is a change of variables performed such that

$$\boldsymbol{u}_{N\times 1} = \Gamma_{N\times r}\,\boldsymbol{q}_{r\times 1} \tag{75}$$

where $\boldsymbol{q}$ is the vector of undetermined coefficients of the reduced system of equations, Γ is the transformation matrix of vectors used in the change of variables, and r is the number of unknowns in the reduced system, with $r << N$. In the traditional mode displacement method, the columns of the transformation matrix are taken as a combination of the eigen-mode shapes computed using either the linear stiffness matrix, the current tangent stiffness matrix or a combination of both. As an alternative, Ritz vectors may be used instead of eigen-mode shapes and more accurate solutions are generally obtained for the same number of basis functions used (Wilson *et al.*, 1982). The use of Ritz vectors also avoids the computation of an eigenvalue solution. However, the eigenvalue solution for vibration mode shapes and frequencies provides insight into the dynamic behavior of the structure and justifies their computation in any event.

In the mode-acceleration category, there is also a change of variables performed. However, in this case, the static solution for the base load on the structure is used as the first column of the transformation matrix and additional columns are comprised of the eigen-mode shapes. This approach generally has improved convergence properties when compared with the mode-displacement method. However, all reduction methods are sensitive to the number of modes or reduced basis vectors used, what these vectors represent, the spatial distribution of the loading, and the frequency content of the loading.

1.6. NUMERICAL SIMULATIONS

To provide a nearly level playing field to assess different aspects of finite element technology, the NASA Langley Research Center's structural ana-

lysis software framework COMET or COmputational MEchanics Testbed (Knight, Lotts and Gillian, 1990 and Stewart, 1990, 1991) was developed as a testbed and framework for computational structural mechanics research. COMET's development is directed towards developing advanced structural analysis software within a computational framework so as to aid in the definition of the requirements for a next generation structural analysis system and to serve as a "proving ground" or "obstacle course" for new methods and finite elements. COMET was developed jointly between NASA Langley Research Center and Lockheed Palo Alto Research Laboratory. COMET is a modular, extendible, machine-independent, multi-level software system enabling researchers to implement their formulations, their elements, or their solution algorithms as generically as possible. COMET utilizes a high-level command language and data manager that allows the coupling of independent FORTRAN or C processors together such that specific structural analysis functions may be performed independently or concurrently. It features different libraries of utilities for matrix and vector operations as well as a set of element-independent corotational utilities. Standardized interfaces are also provided for element developers through the generic element processor (or GEP) as described by Stanley and Nour-Omid (1990) and for materials researchers through the generic constitutive processor (or GCP) as described by Hurlbut and Stehlin (1991). It's capabilities include linear and nonlinear stress analysis, transient dynamic analysis, and eigenvalue analyses associated with linear buckling and free vibration of isotropic, orthotropic, anisotropic and laminated composite structures.

One of the significant features of COMET is the ease of which new element formulations can be implemented and evaluated. This evaluation is possible through the use of COMET's generic element processor feature (Stanley and Nour-Omid, 1990), and the commonality of other aspects of the analysis (assembler, solver, etc.). Some of the elements included in COMET's element library are briefly summarized in Table 1. Of the shell elements, only the 4STG element (Rankin and Brogan, 1991) and 3DKT element (Garnet and Pifko, 1983) neglect transverse shear, while 4ANS, 9ANS, 4LAG, 9LAG, AQ4, and MIN3 account for transverse shear deformation. The ANS and LAG elements are described by Park and Stanley (1986), Stanley, Park and Hughes (1986) and Stanley (1991). The AQ4 element (Rengarajan *et al.*, 1995) includes the drilling freedoms in the finite element approximations for in-plane displacement field. The MIN3 element (Tessler, 1985) uses a penalty approach to eliminate the drilling freedoms. Both solid elements (8HEX and 8HYB) have 8 nodes; however, the 8HYB element is an assumed-stress hybrid element which is quite good in bending (Aminpour, 1989).

Table 1. Elements considered in this study.

Element Label	COMET Element Name	Element Description	Ref.
4ANS	ES1/EX47	4-node, flat C^0 shell element based on the assumed natural-coordinate strain formulation	98
9ANS	ES1/EX97	9-node, curved C^0 shell element based on the assumed natural-coordinate strain formulation	98
4LAG	ES1/EX41	4-node, flat C^0 shell element based on the standard Lagrangian formulation with uniformly reduced (1-point) integration	98
9LAG	ES1/EX91	9-node, curved C^0 shell element based on the standard Lagrangian formulation with uniformly reduced (2×2) integration	98
4STG	ES5/E410	4-node flat C^1 shell element based on displacement formulation from STAGS	84
AQ4	ES24/A4S1	4-node flat C^0 shell element based on assumed-stress hybrid formulation and includes drilling freedoms	90
MIN3	ES36/MIN3	3-node flat C^0 shell element based on displacement formulation; automatically artificial drilling stiffness is added at every node.	112
3DKT	ES31/TP2L	3-node flat shell element based on displacement formulation and the discrete Kirchhoff approximations.	34
8HEX	ES10/BR08	8-node brick element based on displacement formulation and using full integration.	103
8HYB	ES3/EX08	8-node brick element based on assumed-stress hybrid formulation.	8, 103

The solution algorithms available in COMET are implemented using its high-level language constructs in the form of callable procedures (see Stewart, 1991). The static nonlinear solution procedure includes options for load control, displacement control, and arc-length control. In addition, a set of corotational utilities (see Stanley and Nour-Omid, 1990; Rankin and Brogan, 1986; Rankin and Nour-Omid, 1988) are available to the element developer. In the corotational formulation, the displacement solution is decomposed into a rigid-body component and a strain-producing component. Local

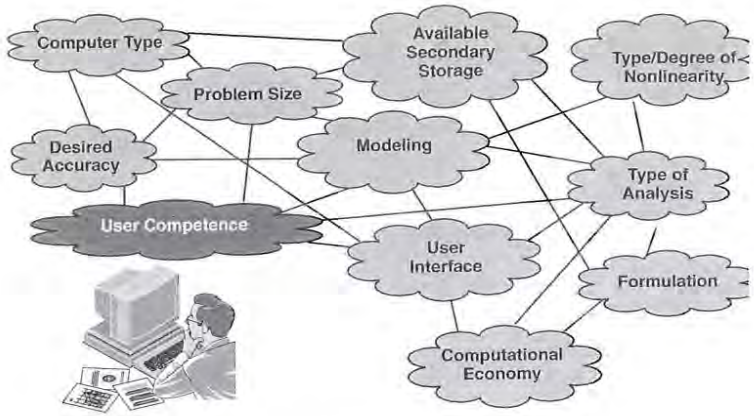

Figure 14. Factors affecting the choice of a solution algorithm.

reference frames are introduced within each element, and these are relat to one another. As an element is displaced, the local coordinate co-rotat with the element and also locally exhibits deformations or straining. If t strain-displacement relations within the element include only the line terms, then the approach is called *a low-order corotational approa* (NLGEOM = 1). If the strain-displacement relations within the eleme include the nonlinear terms, then the approach is called *a high-ora corotational approach* (NLGEOM = 2). If corotation is not used, then t nonlinear strain-displacement relations are needed, and the deformations a referenced to the original undeformed configuration (i.e., a total Lagrangi formulation).

The application problems considered herein are representative of differe plate and shell problems and different analysis tasks. Choosing a soluti algorithm for a specific analysis task can be quite difficult and involv many interrelated factors as indicated on Figure 14. These factors inclu not only mechanics issues and finite element aspects, but also computi issues and hardware needs. All of these factors are continually increasi the level of user competence required to use and understand nonlinear fin element analysis software tools and the advanced computing systems which these tools execute. In addition, if the goal of the analysis is perform test-analysis correlation, then additional factors as identified Knight (1994) need to be addressed in the models and solution process. this section, problems related to the buckling, vibration, postbuckling a collapse of plate and shell structures are given and described. Selec

problems featuring laminated composites and stiffened construction are included in the discussion as well. One large shell analysis problem with local stiffness discontinuities which was studied during the Challenger investigation is discussed in closing.

1.6.1. Buckling and Vibration of a Circular Cylindrical Shell

To assess the eigenvalue analysis capability of shell elements, linear buckling and vibration analyses are carried out on an elastic isotropic thin circular cylinder. The cylinder is simply supported at both ends and has an R/t ratio of 100. The geometric stiffness matrix and the consistent mass matrix are used in these computations. In the analysis, a one-eighth symmetric model is used; however, for visualizing the eigen-mode shapes, a full cylinder model is shown.

Comparison of buckling results, using the 4-node shell elements in COMET, is given by Rengarajan *et al.* (1995). The buckling mode shape is shown in Figure 15a. These finite element results are compared with the theoretical solution and indicate that the ES24/A4S1 or AQ4 element produces significantly better results than the other elements for the same discretization due, in part, to the assumed-stress field features of the element. For the coarse mesh, the use of the STAGS 410 element (ES5/E410) resulted in triggering a "mechanism" in the mode shape.

Comparison of vibration results, using the 4-node shell elements, is also given by Rengarajan *et al.* (1995). These results indicate that the AQ4 element produces better results than the other shear-flexible elements due, in part, to the higher-order assumed-displacement field by including the drilling freedoms. The AQ4 assumed-displacement field is still of lower order than the STAGS element which neglects transverse shear effects. The vibration mode shape corresponding to the lowest vibration frequency is shown in Figure 15b.

The eigen-mode shapes shown in Figure 15 for buckling and vibration pose two different modeling challenges for the analyst. For the free vibration problem, many modes and frequencies exist that are dependent on the resolution of the finite element model. For the buckling problem, there exist repeated (or nearly repeated) eigen-mode shapes near the critical buckling load. It is this density of eigenvalues that causes difficulties in traversing the nonlinear structural response curve. Often times, an analyst develops a particular finite element model for only one case of mode shapes rather than considering both. The danger in such an approach is that once a finite element model has been developed and verified for one purpose, it is frequently passed on to others and used without further checks for different analysis types.

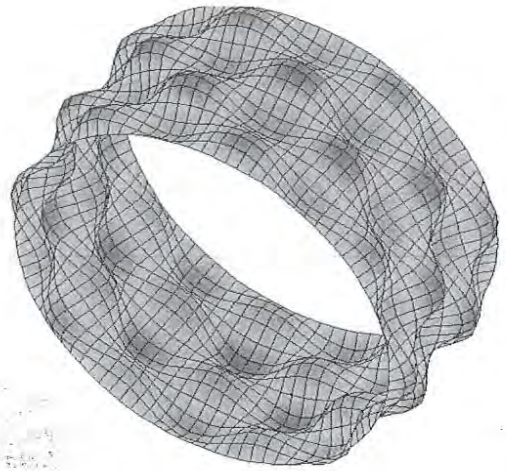

(a) Buckling mode shape

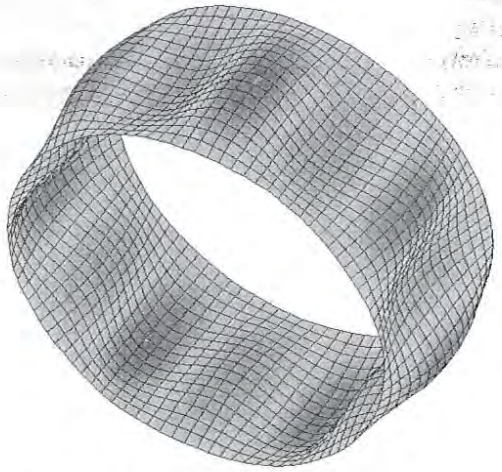

(b) Vibration Mode Shape

Figure 15. Eigen mode shapes for circular cylindrical shell.

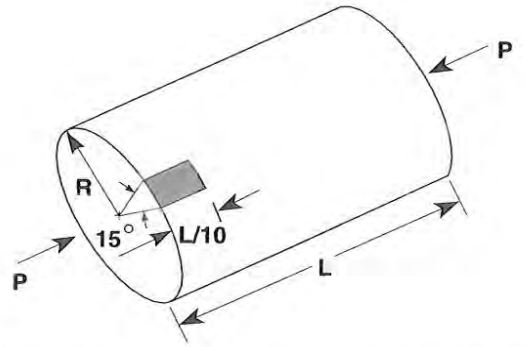

Material Properties:
$E = 10^7$ psi (68.950 GPa)
$\nu = .3$

Geometric parameters:
R = 36.0 in. (914.40 mm)
t = .125 in. (3.175 mm)
L = 100.0 in. (2540.0 mm)

Figure 16. Circular cylinder — geometry, properties, and loading (from Knight *et al.*, 1995).

1.6.2. Collapse of a Cylindrical Shell

This application problem involves the static buckling and postbuckling analysis of a thin circular cylinder ($R/t = 288$ and $L/R = 2.8$) simply supported along its edges, and subjected to uniform axial compression (see Figure 16). The critical buckling load P_{cr} for a simply supported thin circular cylinder is given by

$$P_{cr} = \frac{2\pi}{\sqrt{3(1-\nu^2)}} Et^2 \tag{76}$$

For materials with a Poisson's ratio ν equal to 0.3, Equation 73 gives a critical axial stress of

$$\sigma_{cr} = 0.605 \frac{Et}{R} \tag{77}$$

This problem is a particularly important classical problem for testing the linear and nonlinear performance of shell elements, as well as for testing solution algorithms capable of traversing non-monotonic load-displacement curves (see Hoff, 1966; Anon, 1962). The buckling eigenvalues of the

cylinder are very closely spaced, even though the mode shapes are radically different. This characteristic can pose a challenge for both eigensolvers and nonlinear solution algorithms. In addition, this structure is imperfection sensitive, and hence a small initial geometric imperfection can cause a substantial reduction in the shell's load-carrying capacity, compared with the classical critical buckling load corresponding to a perfect cylinder (see Donnell and Wan, 1950). "Knockdown factors" have traditionally been used to account for the differences between the linear bifurcation buckling load and the experimentally observed behavior. These knockdown factors were developed based on numerous tests. For the shell geometry given in Figure 16, a knockdown factor of 0.41 should be used based on the data in the NASA Space Vehicle Design Criteria for the buckling of thin-walled circular cylinders (Weingarten *et al.*, 1965). One consequence of imperfection sensitivity on the shell finite element analysis is that the finite element model must be refined enough to represent the initial imperfect configuration, as well as the final deformed configuration. Also numerical difficulties associated with possible mode interaction may be caused by the use of a chessboard-pattern initial geometric imperfection shape obtained from the linear buckling analysis when the actual buckling mode shape is axisymmetric.

The finite element model used herein represents a partial ($L/10 \times 15°$) shell-element-based model of the cylindrical shell to represent both linear and nonlinear response. The mesh is rectangular in topology, and restricted to quadrilateral shell elements of either 4- or 9-node variety. The mesh definition is specified as a $n_{ne} \times m_{ne}$ mesh where n_{ne} is equal to m_{ne}. Symmetry conditions on all but the one edge that is simply supported enable the model to represent the lowest buckling mode with a relatively small number of elements. The axial force is distributed along the simply supported edge and is scaled so that the magnitude corresponds to the classical buckling load P_{cr} given by Equation 76.

First, linear buckling analyses from a specified prestress state (i.e., $N_x^0 = \dfrac{P_{cr}}{2\pi R}$, $N_\theta^0 = 0$, and $N_{x\theta}^0 = 0$) are performed. Due to the selected magnitude of the applied load, the lowest eigenvalue should be close to unity. For the geometry and boundary conditions considered herein, classical theory predicts two different buckling mode shapes that correspond to the critical buckling load given by Equation 73; namely, an axisymmetric mode shape and a "chessboard-pattern" mode shape. This particular "chessboard-pattern" mode shape consists of 5 axial half-waves and 12 circumferential whole waves over the entire cylinder or in classical terminology: $m = 5$, $n = 12$. Thus, the partial model will represent one circumferential half-wave and one axial quarter-wave, and should require less than ten shell elements

in each direction to obtain an accurate solution. Buckling analysis results are presented by Knight *et al.* (1995) for a variety of finite element models using the shell elements described in Table 1. These results indicate that nearly all of the finite element models considered herein accurately predict the linear bifurcation buckling solution.

Next, nonlinear analyses are performed wherein the initial geometric imperfection shape for all models is taken as the chessboard-pattern mode shape corresponding to $m = 5$ and $n = 12$. The perturbed geometry is calculated by adding the scaled radial components of this mode shape to the initial finite element nodal coordinates. The scale factor is selected so that the maximum radial perturbation from a circular cylindrical surface is 10% of the cylinder thickness. This initial imperfection is necessary to trigger a realistic postbuckling response in the nonlinear analysis. Without any imperfection, the nonlinear analysis will have significant numerical difficulties as the collapse load is approached due to the mode interaction as a result of the closely spaced eigenvalues. The load-displacement history was obtained for 40 load steps, from a starting load of one-tenth of the classical buckling load and using a convergence criterion of 0.001 on the "energy norm." On the figures showing the nonlinear response curves, the symbols denote converged solutions for each load step — closely spaced symbols mean small changes in load. The applied axial load P normalized by the critical (buckling) load P_{cr} is shown as a function of the end shortening. The converged solution corresponds to the postbuckling response obtained using a 13×13 mesh of 9-node ANS C^0 shell elements (denoted 9ANS) with the high-order corotational approach. Using a nonlinear analysis approach, the collapse load for the converged solution corresponds to a knockdown factor of 0.73. The use of a nonlinear analysis approach increases the "predicted" load-carrying capability compared with that obtained using the traditional "knockdown factor" approach. Several parametric studies have been performed to assess the effect of shell element formulation, shell geometry representation, and formulations for large deflection, large rotation problems on predicting the postbuckling response of a circular cylinder loaded in axial compression.

The effect of shell geometry representation on the postbuckling response is considered by examining the use of isoparametric shell elements wherein both the shell geometry and the displacement field are approximated using the same functions — for example, bilinear shape functions for 4-node isoparametric elements and biquadratic shape functions for 9-node isoparametric elements. Results obtained using the high-order corotational approach and two element types (namely, the standard Lagrangian element type with uniformly reduced integration and the assumed natural-coordinate

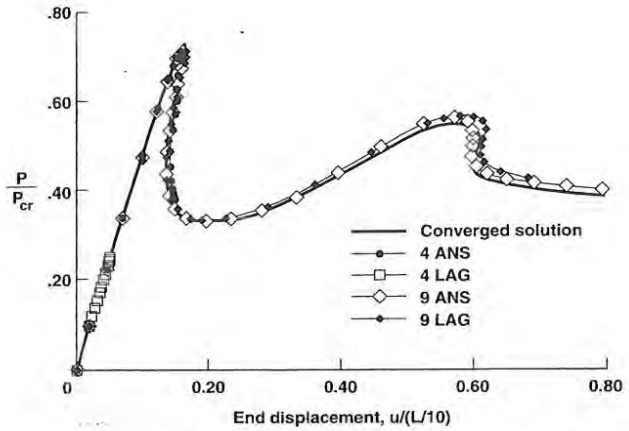

Figure 17. Effect of shell geometry representation using isoparametric elements — 7×7 mesh (from Knight *et al.*, 1995).

strain element type) are shown in Figures 17 and 18 for two different spatial discretizations. Using a 7×7 mesh, the results shown in Figure 17 indicate that models using 4-node elements have difficulty in obtaining the collapse response — the 4-node Lagrangian element with uniformly reduced integration (denoted 4LAG) failed to reach the collapse load due to its inherent rank-deficiency. The results obtained using models with 9-node elements agree well into the postbuckling regime. Using a 9×9 mesh, the results shown in Figure 18 also indicate that all models agree until well into the

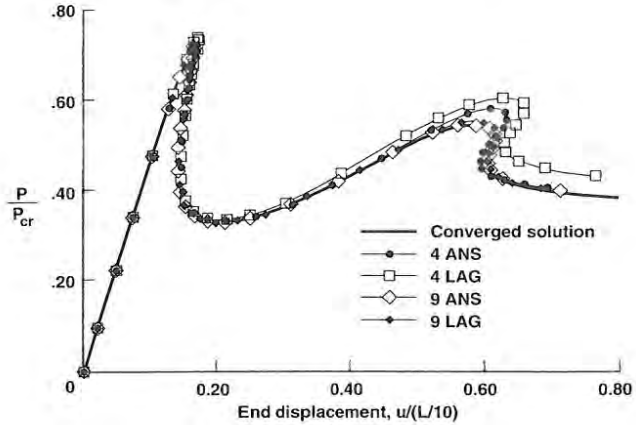

Figure 18. Effect of shell geometry using isoparametric elements — 9×9 mesh.

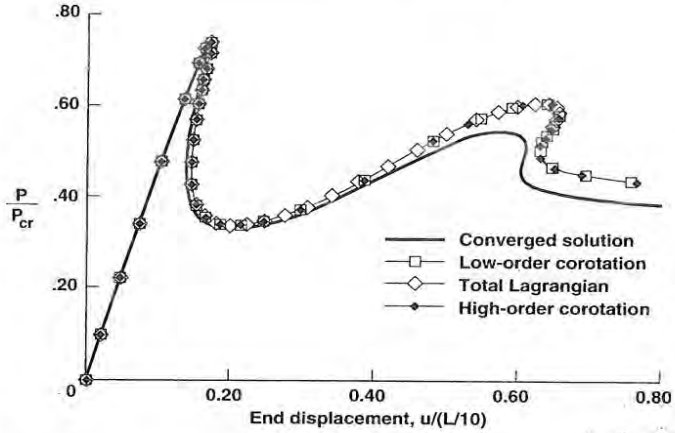

Figure 19. Comparison of different approaches for treating large-deflection, large rotation problems — 9×9 mesh and 4LAG element.

postbuckling regime where large local changes in curvature exist and better representations of both the shell geometry and the shell collapse response are required.

Formulations for treating large deflection, large rotation problems influence the prediction of the postbuckling response. Problems with small or moderate rotations are readily handled by the total Lagrangian approach. As rotations become large, a corotational approach is often used. The interaction between the approach for treating large rotations and the shell element formulation is evident in Figures 19 to 22 for the postbuckling response of a circular cylinder loaded in axial compression. The results obtained using models with 4-node elements use a 9×9 mesh and those for models with 9-node elements use a 9×9 mesh. The postbuckling response shown in Figure 19 obtained using the 4-node Lagrangian element with uniformly-reduced integration (4LAG) indicates little difference between the total Lagrangian approach, the low-order corotational approach, and the high-order corotational approach indicating that this collapse problem does not exhibit large rotations. As shown in Figure 19, the solution obtained using the total Lagrangian approach required smaller load steps than either corotational approach. However, the differences between these solutions with the 4LAG element and the converged solution becomes quite noticeable as the solution progresses well into the postbuckling regime.

The postbuckling response shown in Figure 20 obtained using the 4-node ANS element (4ANS) indicates that the total Lagrangian approach and the high-order corotational approach give the same response with little

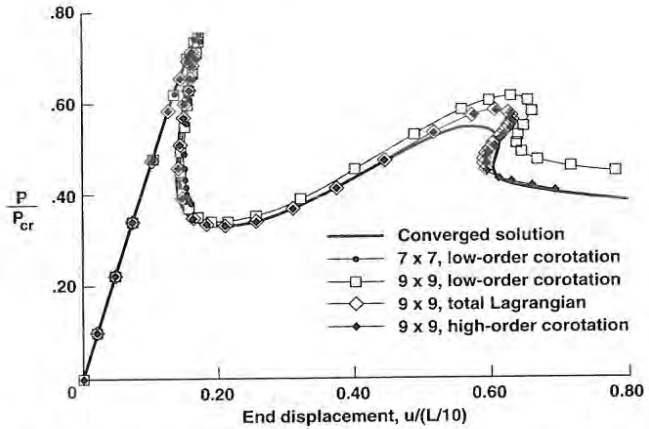

Figure 20. Comparison of different approaches for treating large-deflection, large rotation problems — 9×9 mesh and 4ANS element (from Knight *et al.*, 1995).

difference in either the size of the load steps or the total number of load steps. Using the low-order corotational approach, a slightly stiffer response is predicted indicating that the 4-node ANS element is sensitive to the form of the element strain-displacement relations.

The postbuckling response shown in Figure 21 obtained using the STAGS–410 element (4STG) indicates that this element is very sensitive to the

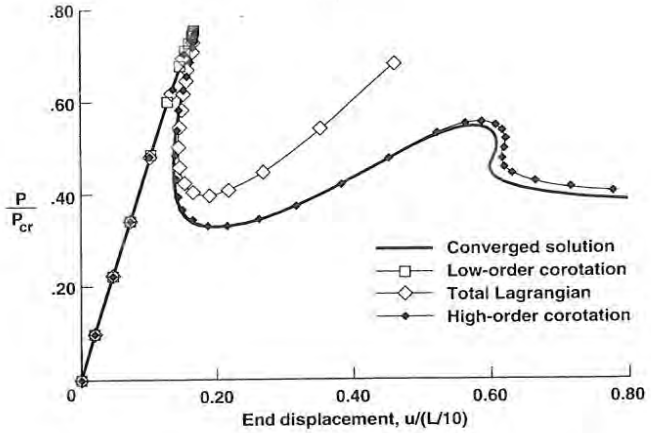

Figure 21. Comparison of different approaches for treating large-deflection, large rotation problems — 9×9 mesh and 4STG element (from Knight *et al.*, 1995).

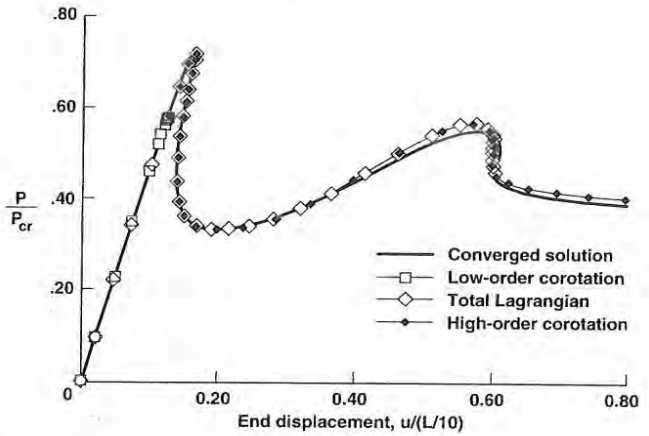

Figure 22. Comparison of different approaches for treating large-deflection, large rotation problems — 9×9 mesh and 9-node elements.

approach used for treating the large deflection, large rotation problem. The low-order corotational approach predicted the collapse load but failed to predict the postbuckling response. The total Lagrangian approach does predict the postbuckling response but predicts a substantially stiffer response. The high-order corotational approach predicts the postbuckling response and agrees with the converged solution. This behavior is due in part to the STAGS-410 element formulation and sensitivity to warping.

The postbuckling response shown in Figure 22 obtained using the 9-node ANS element (9ANS) and the 9-node Lagrangian element with uniformly reduced integration (9LAG) indicates that the total Lagrangian approach and the high-order corotational approach again give the same response with little difference in either the load step sizes or total number of steps. Using the low-order corotational approach, numerical difficulties are encountered for both 9-node models, and a predicted collapse load is not obtained.

1.6.3. Postbuckling Response of Composite Panel

A flat, rectangular, unstiffened, 24-ply graphite-epoxy composite panel loaded in longitudinal compression shown in Figure 23 is considered herein to demonstrate the nonlinear analysis methods. Comparison of the analytically determined postbuckling response with existing experimentally obtained structural response (Panel C4 in Starnes and Rouse, 1981) is presented to aid in the validation of these methods. The panel is fabricated from

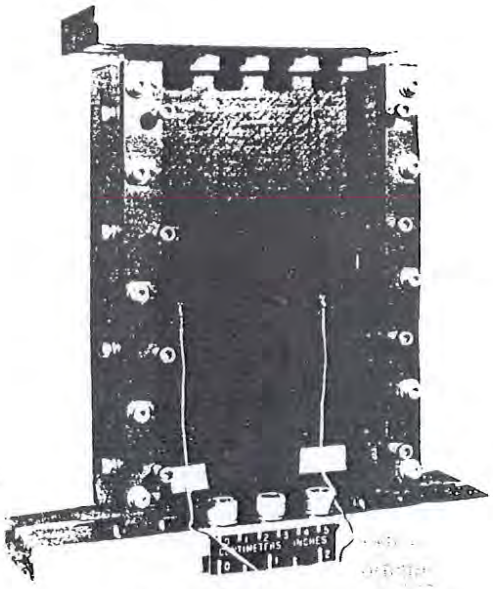

(a) Typical panel with fixture.

(b) Photograph of moire-fringe pattern.

Figure 23. Flat, rectangular composite panel (from Starnes and Rouse, 1981).

commercially available unidirectional Thornel 300 graphite-fiber tapes pre-impregnated with 450 K cure Narmco 5208 thermosetting epoxy resin. Typical lamina properties for this graphite-epoxy system are 131.0 GPa (19,000 ksi) for the longitudinal Young's modulus, 13.0 GPa (1,890 ksi) for the transverse Young's modulus, 6.4 GPa (930 ksi) for the in-plane shear modulus, 0.38 for the major Poisson's ratio, and 0.14 mm (0.0055 in.) for the lamina thickness. Panel C4 is a 24-ply orthotropic laminate with the nominal properties and a length of 50.8 cm (20.0 in.) and width of 17.8 cm (7.0 in.). The laminate stacking sequence is $[\pm 45/0_2/\mp 45/0_2/\pm 45/0/90]_s$. The loaded ends of the panels are clamped by fixtures during testing, and the unloaded edges are simply supported by knife-edge restraints to prevent the panel from buckling as wide columns. A typical panel mounted in the support fixture is shown in Figure 23a.

The postbuckling behavior of this panel is characterized by plotting the end shortening normalized by the analytically predicted critical end shortening at buckling versus the maximum transverse deflection normalized by the thickness of the panel as shown by the solid curve in Figure 24. The transverse deflection pattern corresponds to two longitudinal half waves and one lateral half wave as shown in Figure 23b. Panel failure occurred at nearly four times the end shortening at buckling.

Finite element simulations are performed using the traditional approach and the global function approach. The results for the path derivative approach are reported by Noor and Peters (1981) using a different mathematical model. A refined finite element model is used herein which has twenty 4-node, C^1 flat shell elements per longitudinal half wave and ten elements per lateral half wave or a 40×10 mesh of elements over the entire panel. The model has a total of 2083 active degrees of freedom. Prior to performing the nonlinear postbuckling analysis, a linear stress analysis and a linear bifurcation buckling analysis are performed to aid in understanding the structural response of this class of composite panels. From these analyses, the prebuckling membrane solution and the critical eigenpair are determined which are used to define the initial load level and load step size for the nonlinear analysis. In addition, an initial geometric imperfection is formed based on the buckling mode shape with a maximum amplitude of ten percent of the panel thickness.

The postbuckling response determined using the traditional approach is given by the dashed line in Figure 24 where the filled circles denote converged solutions. This structural response is obtained by starting at a load level below the buckling load and incrementing the load until well into the postbuckling range. An adaptive solution strategy is used to adjust the load step size during the analysis; however, the arc-length control procedure is not used in the present analysis. The size of the initial load step is cut first

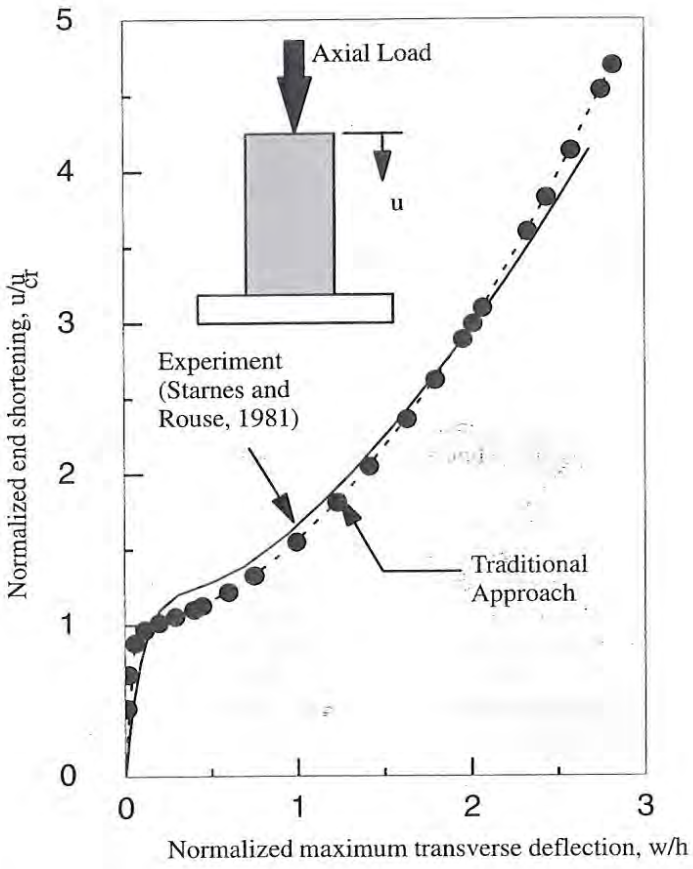

Figure 24. Postbuckling response comparison for experimentally obtained results and numerically determined results based on the traditional approach.

in half and then halved two more times as the load level approaches the buckling load. Beyond the buckling load, the load step size is increased but never regains the original load step size. A convergence tolerance of 10^{-6} on the norm of the iterative change in the displacements (Equation 44) is used. These analytical results, as well as the analytical results of Starnes and Rouse (1981), are in good agreement with the experimentally obtained results.

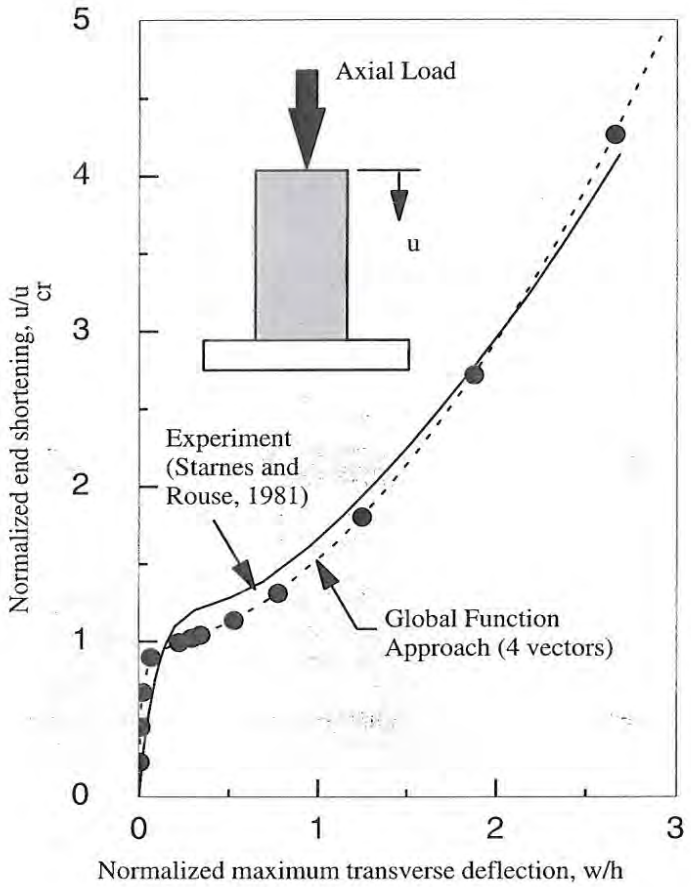

Figure 25. Postbuckling response comparison for experimentally obtained results and numerically determined results based on the global function approach.

The postbuckling response determined using the global function approach is given by the dashed line in Figure 25 where the filled circles denote "corrected" full system solutions. The first four nonlinear solutions are used as the global functions in the transformation matrix. These solutions correspond to load levels just prior to buckling which begin to exhibit the anticipated postbuckling deflection pattern (i.e., one corresponding to the buckling mode shape and consistent with the moire-fringe pattern of

Figure 23b). The number of global functions is restricted to four vectors throughout the nonlinear analysis. After forming the initial transformation matrix using the first four nonlinear solutions (i.e., first four filled circles), the transformation matrix is updated thereafter on each return to the full system of equations (i.e., filled circles beyond the first four). However, the "predicted" solution from the reduced system of equations only required two Newton-Raphson iterations (on an average) to generate each "corrected" solution. Between the filled circles, several solutions using the reduced system of equations are typically determined. Again, the structural response is determined by incrementing the load; however, only the reduced system of equations is solved at each load step. These results are also in good agreement with the experimentally obtained results shown by the solid line on Figure 25.

1.6.4. Postbuckling of Stiffened Composite Panel

The postbuckling behavior of flat stiffened graphite-epoxy panels loaded in axial compression has been studied by several researchers. Starnes, Knight, and Rouse (1985) reported the results of both an experimental and analytical study for composite panels with I-shaped stiffeners (see Figure 26). The configuration considered herein has a panel length of 30.0 inches, panel width of 24.0 inches, and a stiffener spacing of 7.0 inches. The panel skin and stiffener were designed using POSTOP (Dickson and Biggers, 1984) so that skin buckling would occur and postbuckling strength would be exhibited by the structure. The loaded edges of the panel were clamped, and the unloaded edges were free. Details of the panel skin, stiffener, and material properties are given by Starnes *et al.* (1985).

As a starting point in this activity, the modeling fidelity needed for stiffened panels was studied wherein three approaches were considered. The first approach studied was the smeared stiffener model which is by far the simplest. In the smeared theory, the stiffness associated with each stiffener is "averaged" over the panel skin such that even an isotropic skin will exhibit orthotropy due to the smeared stiffeners. The second approach studied was the discrete stiffener model which involves the same computational effort as the smeared approach since there is no increase in the number of equations to be solved. Here each stiffener is represented as a discrete beam element with *EA*, *EI*, and *GJ* stiffnesses and possibly offsets to account for stiffener eccentricity. Lines of stiffness are therefore added to the skin model. The third approach studied was the branched plate model which involves a significant increase in modeling and computational effort. Here each stiffener is represented as an independent assemblage of plate elements that are attached (or connected) to the finite element nodes in the panel skin

(a) Typical panel with fixture.

(b) Photograph of moire-fringe pattern.

Figure 26. Flat, rectangular stiffened composite panel (from Starnes, Knight and Rouse, 1985).

model. The flexibility of the stiffener is accurately modeled in this approach since cross-sectional deformations of the stiffeners are included. Intersecting stiffeners and diagonal stiffeners that do not fall along node lines in the finite element model pose added challenges. When the buckling response is an overall buckling mode shape for the structure, the three modeling approaches predict essentially the same result. When local buckling is present (i.e., the stiffeners contribute to the buckling mode shape of the structure), only the branched plate modeling approach is accurate unless the discrete beam model accounts for cross-sectional deformations. For prismatic structures, PASCO is an excellent tool for analysis and design of axially stiffened panels (see Stroud and Anderson, 1980). Comparisons between finite element buckling solutions and PASCO solutions for a variety of loading conditions and stiffener shapes are given by Stroud, Greene and Anderson (1984). Their results are useful for benchmarking new elements and modeling strategies.

In addition to spatial modeling issues, two approaches for specifying the buckling prestress state can be used. One approach involves the specification of the buckling prestress state *a priori* without the need to compute a linear stress solution. The other approach involves calculating the linear stress solution using a given set of loads and boundary conditions; perhaps using boundary conditions different from those to be used in the buckling analysis. In the first approach, combined inplane load cases are readily solved. However, for the second approach, defining an appropriate load system and boundary condition set is quite complex — especially for the inplane shear loading condition.

Using the first approach for defining the buckling prestress state (i.e., *a priori* specification) introduces errors which may be detrimental to the accuracy of the buckling results in cases where the smeared or discrete stiffener modeling strategy is used. This error is usually introduced because the specified stress state is applied to the panel skin model and not applied to the smeared or discrete stiffeners. For the branched plate modeling approach, specification of a uniform buckling prestress state in each section of the stiffener panel is then readily accomplished and correlation with results from linked plate analyses can be done.

Using the second approach for defining the buckling prestress state (i.e., calculating a linear stress state) introduces different challenges. Often it is desirable to simulate the loading conditions that may be experienced in a testing machine (e.g., uniform end shortening). For an inplane normal prestress state, loads and boundary conditions that perhaps reflect a testing configuration are usually straightforward to define and specify in the finite element model regardless of which modeling approach is used. For branched plate models, two sets of boundary conditions are generally needed if the

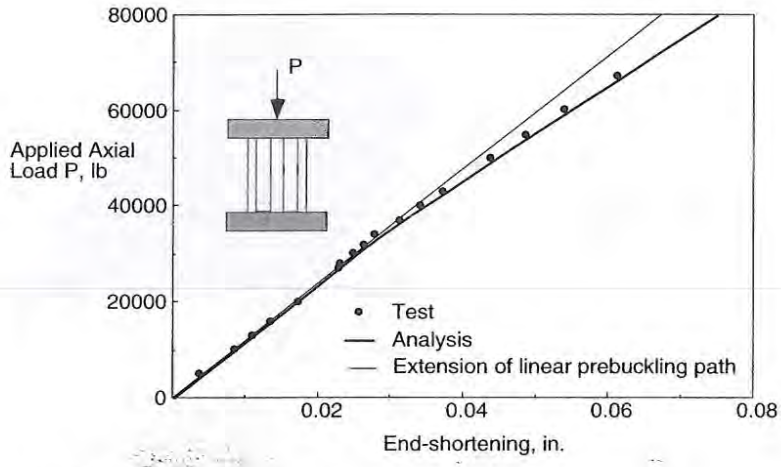

Figure 27. End-shortening results.

intent is to compare with another analytical solution which has a certain inplane stress state. For example, to calculate the buckling load of a panel loaded in uniaxial compression and simply supported on all edges requires a set of pre-buckling boundary conditions which leads to a uniform stress state from the linear solution — uniform end shortening and simple support boundary conditions lead to a combined stress state from the linear solution. However, for the inplane shear loading condition this is not the case.

The postbuckling response is characterized by the end-shortening results as a function of the applied compressive load as shown in Figure 27. The postbuckling analysis was performed using the finite element model shown in Figure 28a which is composed of 612 9-node quadrilateral elements, 2,553 nodes, and 12,079 active degrees of freedom. Experimental and analytical results shown in Figure 27 are in excellent agreement. At load values of the applied load, the structure is in a near membrane state, and the internal load distribution is nearly uniform (see Starnes *et al.*, 1985). After buckling occurs, large out-of-plane deformations occur, and a redistribution of the load from the panel skin towards the stiffeners takes place. This load redistribution continues until skin-stiffener separation occurs, and overall panel failure results as reported by Starnes *et al.* (1985). Deformed geometry plots with exaggerated deflections are shown in Figure 28 indicating large out-of-plane deformations occurring in the panel skin segments between stiffeners and little or no out-of-plane deformation of the stiffeners.

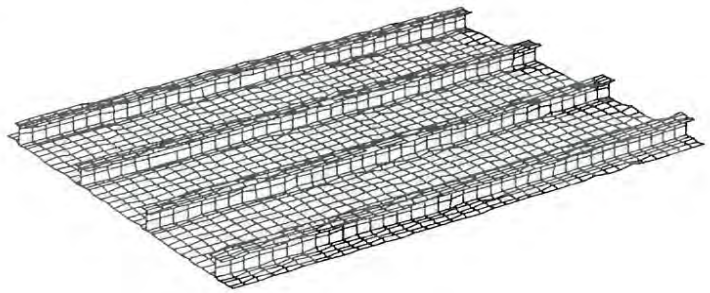

(a) Undeformed geometry.

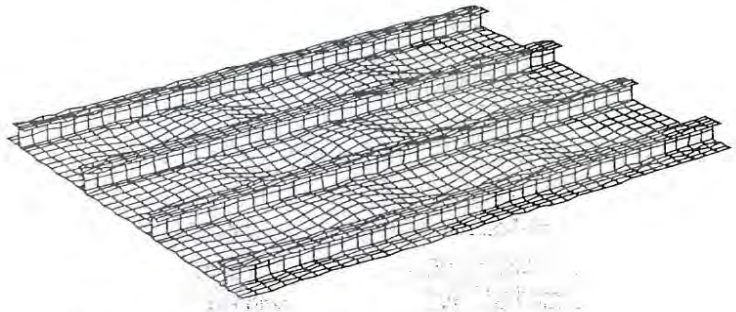

(b) Deformed geometry just after buckling.

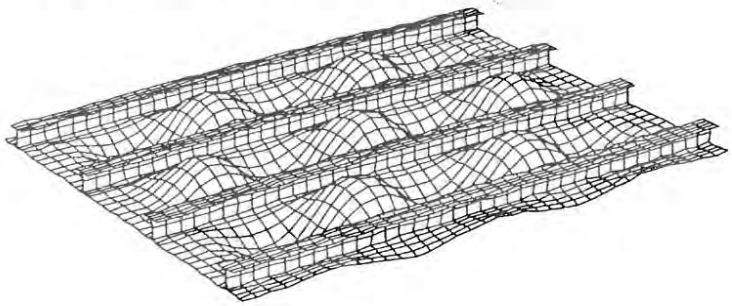

(c) Deformed geometry at maximum load.

Figure 28. Deformed geometries of the I-stiffened panel (from Knight *et al.*, 1990).

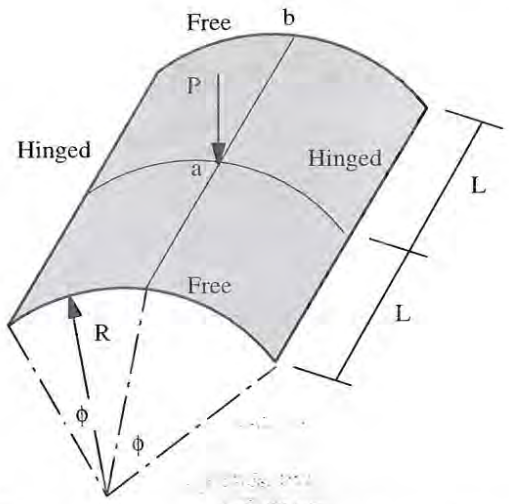

Figure 29. Hinged-free cylinder — geometry, properties and loading.

1.6.5. Collapse of a Hinged-free Cylindrical Panel

The hinged-free cylindrical panel subjected to a center transverse point load is considered to validate the nonlinear aspects of the AQ4 shell element based on the low-order corotational formulation. This structure is shown in Figure 29. The structural response exhibits a limit point, a snap-through behavior, and then a snap-back behavior.

The nonlinear response of the panel is shown in Figure 30 for a midpoint on the free edge (Point b). Two meshes are considered, and the reference solution is taken to be that obtained using a 5×5 mesh of 9ANS elements. The results in Figure 30(a) indicate the response obtained using two meshes of the AQ4 element developed as part of this research. For both meshes, nearly the same nonlinear behavior is obtained. The only difference appears to be after the shell's free edge has snapped through to an inverted position. The results in Figure 30(b) indicate the response obtained using a 5×5 mesh of 4ANS elements with both the low-order and high-order corotational formulation (i.e., NLGEOM = 1 and NLGEOM = 2, respectively). These results appear to bracket the reference solution.

The nonlinear response of the panel is also shown in Figure 31 for the center point (Point a). Two meshes are considered, and the reference solution is taken to be that obtained using a 5×5 mesh of 9ANS elements. The

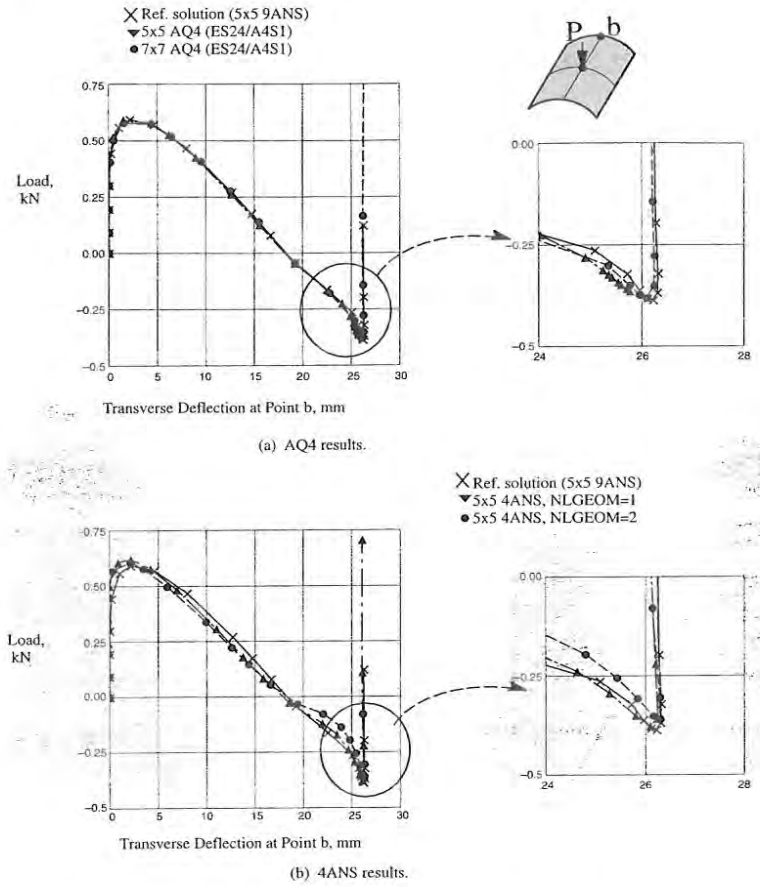

Figure 30. Hinged Cylinder: Load vs. Free Edge Point Deflection.

results in Figure 31(a) indicate the response obtained using two meshes of the AQ4 element. For both meshes, nearly the same nonlinear behavior is obtained. Differences appear after the limit point as the snap-back response occurs. In this region of the nonlinear response, severe local changes in curvature occur and the 5×5 mesh of 4-node elements with the low-order corotation approach is not sufficient to reproduce the reference solution. Adding more elements (i.e., essentially adding more local reference frames) has the effect of refining the solution to obtain the reference solution. As

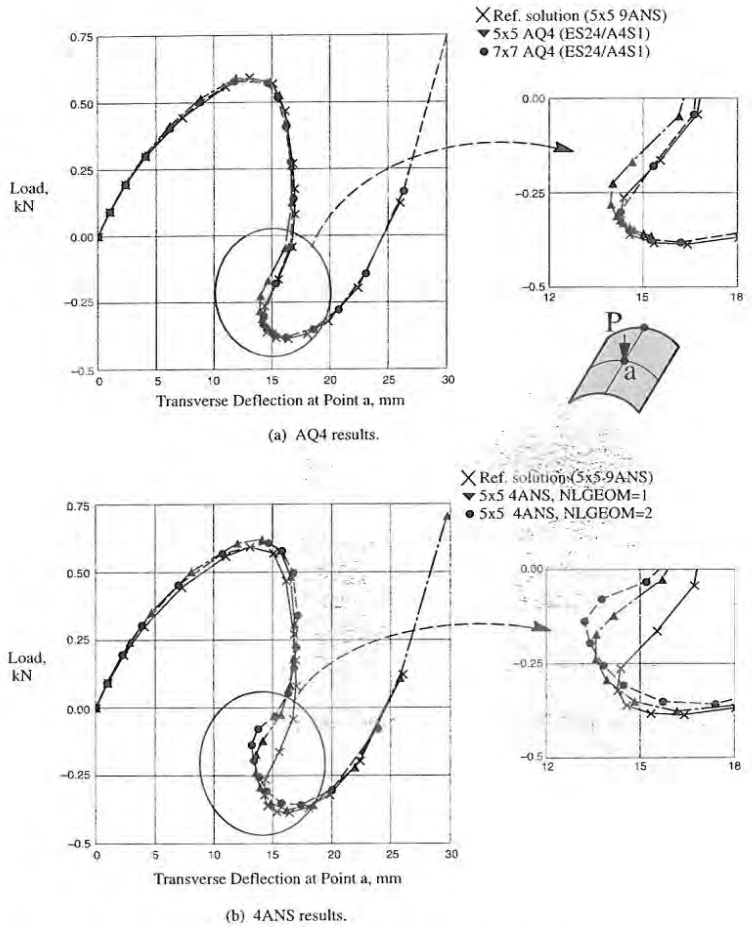

Figure 31. Hinged Cylinder: Load vs. Center Point Deflection.

an alternative, using the high-order corotational approach should have the same effect. The results in Figure 31(b) indicate the response obtained using a 5×5 mesh of 4ANS elements with both the low-order and high-order corotational formulation. These results are similar to the reference solution up until snap-back occurs. The two solutions exhibit a different character than anticipated from previous results.

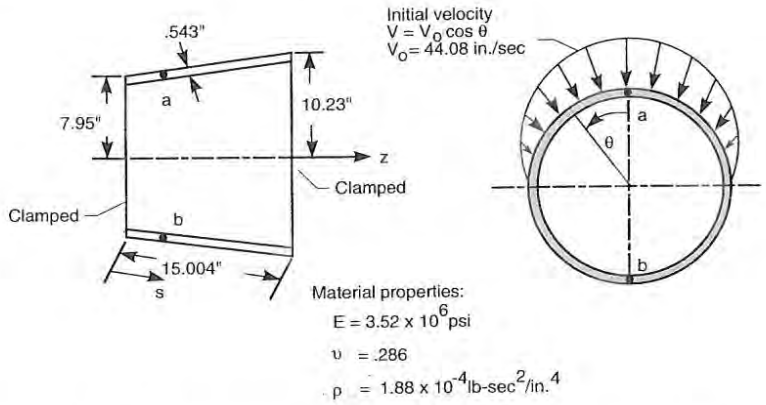

Figure 32. Truncated conical shell — geometry, properties, and loading (from Knight *et al.*, 1989).

1.6.6. Transient Response of a Truncated Conical Shell

This linear elastic transient response of a truncated conical shell subjected to an impulse load (initial velocity) was posed as a benchmark problem by Hartung and Ball (1973). The geometry, material properties, and loading is specified in Figure 32. The finite element model shown in Figure 33 has 540

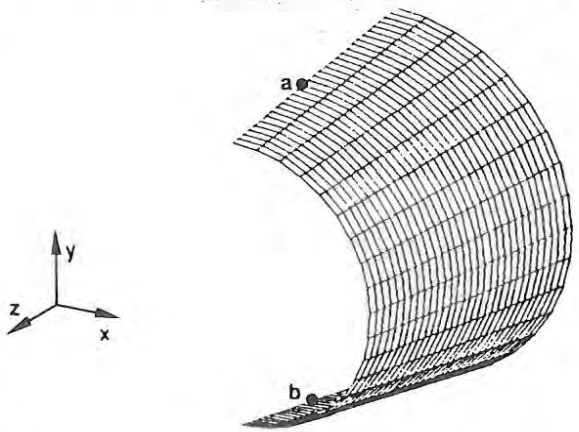

Figure 33. Finite element model of truncated conical shell (from Knight *et al.*, 1989).

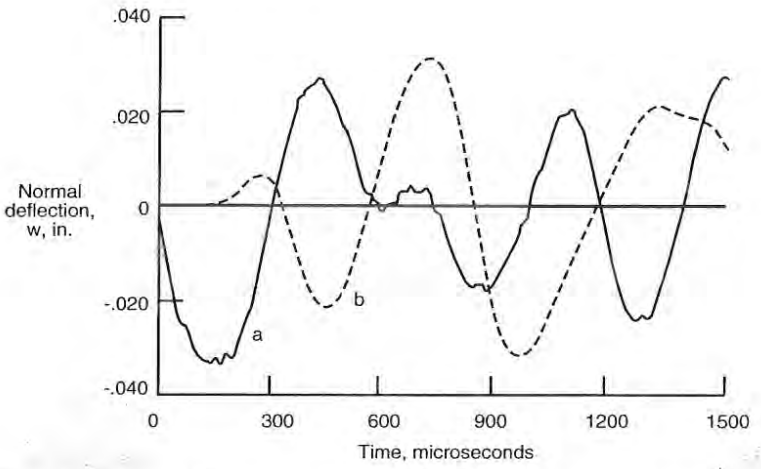

Figure 34. Normal deflections at Points A and B on truncated conical shell (from Knight *et al.*, 1989).

4-node quadrilateral shell elements with 589 nodes and 2569 active degrees-of-freedom. Two points on the symmetric structural model (Points a and b) are monitored during the transient response. Both points are located at 6.5 inches from the clamped, small diameter edge: one at $\theta = 0°$ (Point a) and one at $\theta = 180°$ (Point b). The transient response was computed for an elapsed time of 1,500 microseconds using the Newmark method with a time step of 2 microseconds. The behavior of these two points represented by their normal deflections is indicated in Figure 34.

Oblique views of the deformed shape with exaggerated deflections at various points in time are shown in Figure 35. Contour plots of the hoop stress resultant are superimposed on these deformed shapes. These results indicate the added complexity associated with transient structural response predictions. Linear simulations such as the one presented here are readily performed even though the computational task is significantly higher than a static shell analysis problem whether it is linear or nonlinear. Nonlinear transient simulations still pose computational challenges for the finite element analysts; particularly if plastic collapse, contact, or localized gradients need to be included in the prediction. These results also indicate the role of visualizing the computed solution as an aid to understanding the structural behavior. In the present problem, the shell dynamic problem involves the development of both circumferential and axial waves along with their interaction as shown in Figure 35.

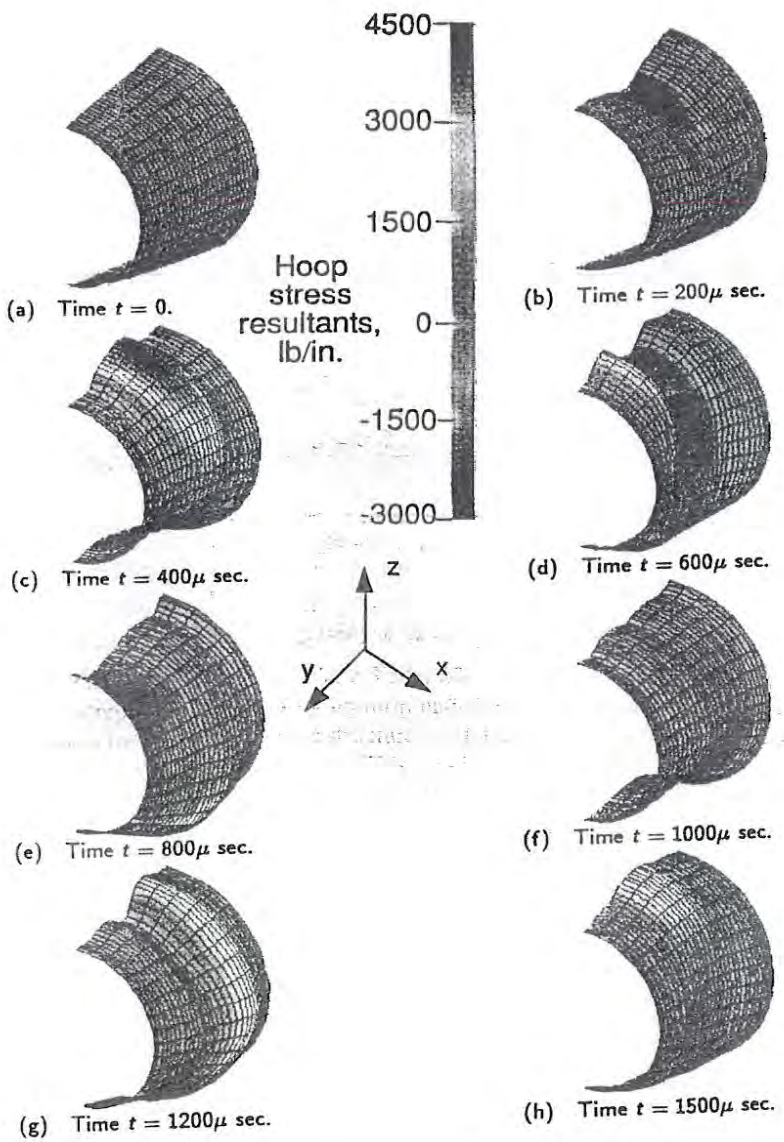

Figure 35. Deformed shapes for truncated conical shell during transient response (from Knight *et al.*, 1989).

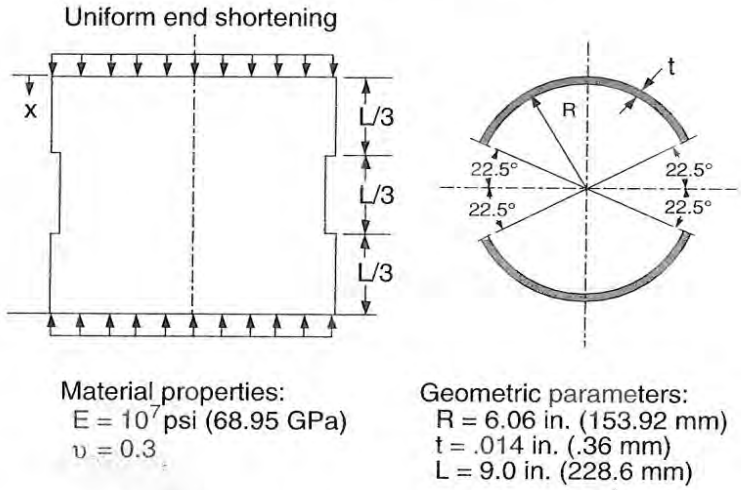

Figure 36. Circular Cylinder with cutouts — geometry, properties, and loading (from Knight *et al.*, 1995).

1.6.7. Collapse of a Circular Cylinder with Cutouts

The circular cylinder (*R/t = 433* and *L/R = 1.5)* with two rectangular cutouts loaded by uniform end shortening shown in Figure 36 is representative of shell-type structures with local discontinuities (e.g., cutouts for access holes or windows). This problem has also been used as a benchmark problem by Hartung and Ball (1973) for shell analysis computer codes and by Almroth and Brogan (1981) for assessing shell elements. These researchers considered only one-eighth of the shell in their analyses. The results reported herein are compared with their results, and hence only one-eighth of the shell is modeled. Symmetry boundary conditions are imposed on three edges and the loaded edge is clamped. Three finite element models were considered as shown by Knight *et al.* (1989). Mesh 1 is composed of 101 9-node curved quadrilateral shell elements, 449 nodes, and 2,012 active degrees-of-freedom. Mesh 2 has the same nodal layout as Mesh 1 but is composed of 404 4-node flat quadrilateral shell elements. Mesh 3 has the same element layout as Mesh 1 but is composed of 101 4-node flat quadrilateral shell elements and has only 124 nodes.

A linear bifurcation buckling analysis was performed prior to the nonlinear elastic collapse analysis. A buckling load of approximately $0.13P_0$ (where $P_0 = 1.2\ \pi E\ t^2$) has been reported by previous investigators, and the buckling mode shape indicates that the vertical edges of the cutout buckle locally.

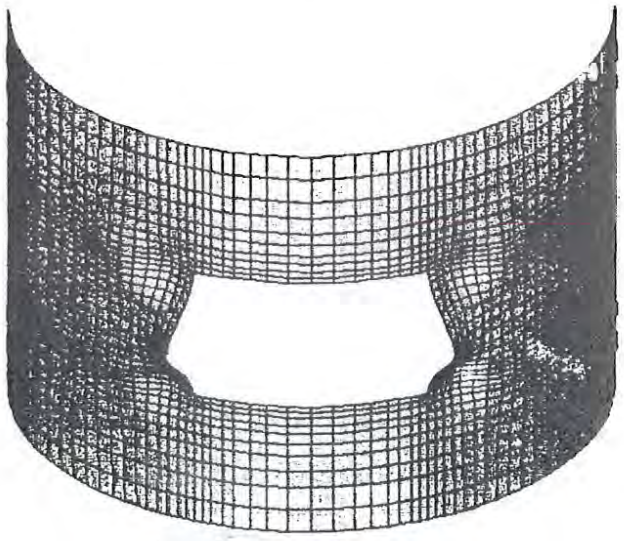

Figure 37. Deformed geometry (from Knight *et al.*, 1995).

The nonlinear response is characterized by large local radial deflections along the straight edges of the cutouts at a load level of approximately $0.43P_0$ followed by overall shell collapse at a load level of approximately $0.40P_0$. The deformed geometry with exaggerated deflections is shown in Figure 37 for the converged solution near the collapse load wherein the one-eighth-model geometry and results have been symmetrically reflected to enhance visualization. As the radial deflections near the vertical edges of the cutouts develop, the compressive axial stresses are redistributed away from the regions above the cutouts, the stress concentration develops along the straight edges of the cutouts, and the load is carried by the remaining portions of the shell.

A nonlinear analysis of the cylinder with cutouts was performed, and the radial deflection, normalized by the cylinder thickness t, for a point at the cylinder midlength at the edge of the cutout (denoted point "a") is shown in Figures 38 and 39 as a function of the applied load normalized by P_0. Results for the three approaches to the large deflection, large rotation problem are shown in Figure 38 for Mesh 1 using the 9ANS element and in Figure 39 for Mesh 2 using the 4ANS element. The solution obtained using Mesh 1 with the 9ANS element and the high-order corotational approach shown in Figure 38 is taken as the converged solution. These results are

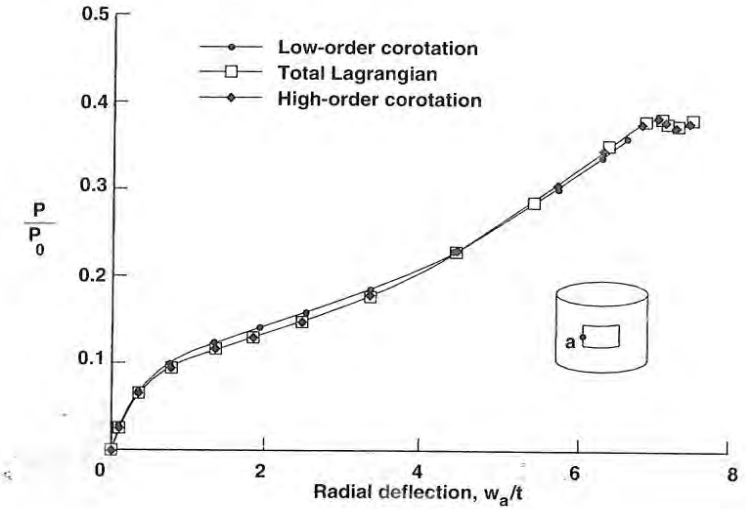

Figure 38. Comparison of different approaches for treating large-deflection, large rotation problems — Mesh 1 using 9ANS elements (from Knight *et al.*, 1995).

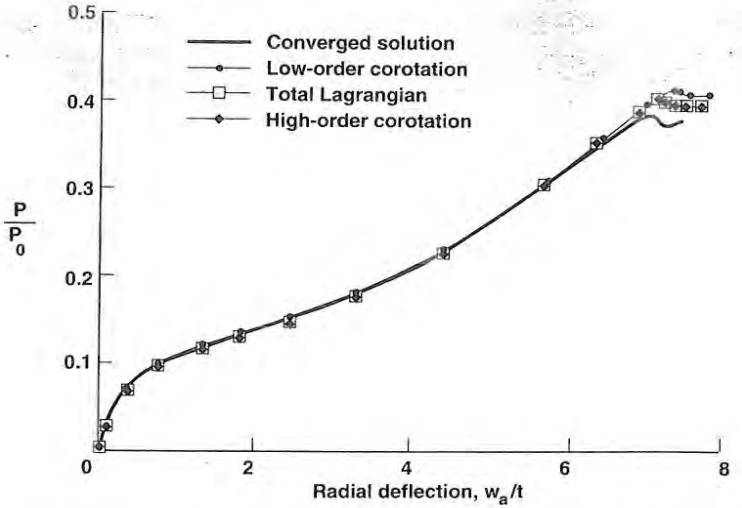

Figure 39. Comparison of different approaches for treating large-deflection, large rotation problems — Mesh 2 using 4ANS elements (from Knight *et al.*, 1995).

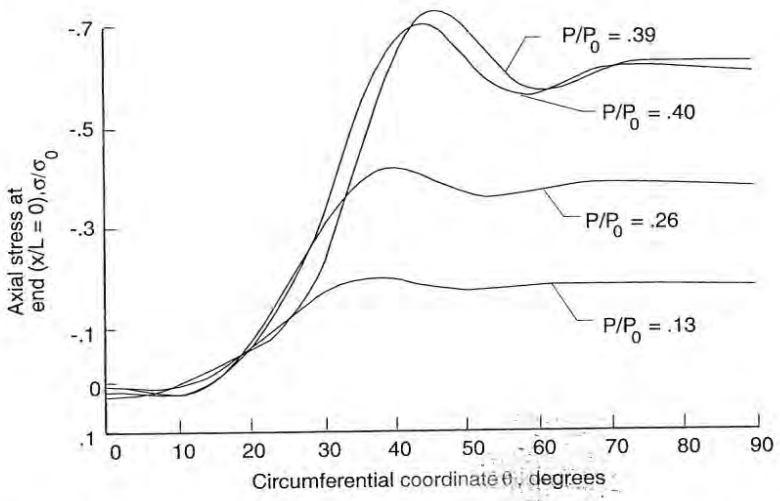

Figure 40. Axial stress at x/L = 0 for various load steps (from Knight *et al.*, 1995).

consistent with the findings for the previous two shell collapse problems; namely, that nonlinear strain-displacement relations at the element level are needed for accurate postbuckling analysis and that the 9ANS element performs best. Hartung and Ball (1973) reported a collapse load of $0.28P_0$ using a finite difference version of STAGS. Later, Almroth and Brogan (1981) using the finite element version of STAGS reported a "nearly" converged collapse load of $0.37P_0$ using the finite element version of STAGS. The collapse load obtained in this study is $0.38P_0$ for the converged solution.

The distribution of the axial stress normalized by σ_0 (where $\sigma_0 = 0.605\ Et/R$) at the midsurface across the end of the cylinder ($x/L = 0$) is shown in Figure 40 for various load levels. These results were obtained using Mesh 2 and the 4ANS element. The distribution of the axial stress at the midsurface across the midplane of the cylinder ($x/L = 1/2$) is shown in Figure 41 for these same load levels. These distributions indicate that substantial redistribution of the axial stress occurs as the collapse load is approached.

A comparison of the postbuckling response of this shell collapse problem for several element types is given in Figure 42. The slightly higher collapse load and different postbuckling response obtained using the 9LAG element is attributed to the inherent weaknesses of elements developed using uniformly-reduced integration. The postbuckling response using the 4ANS element is obtained for both Mesh 2 (same number of nodes as Mesh 1) and

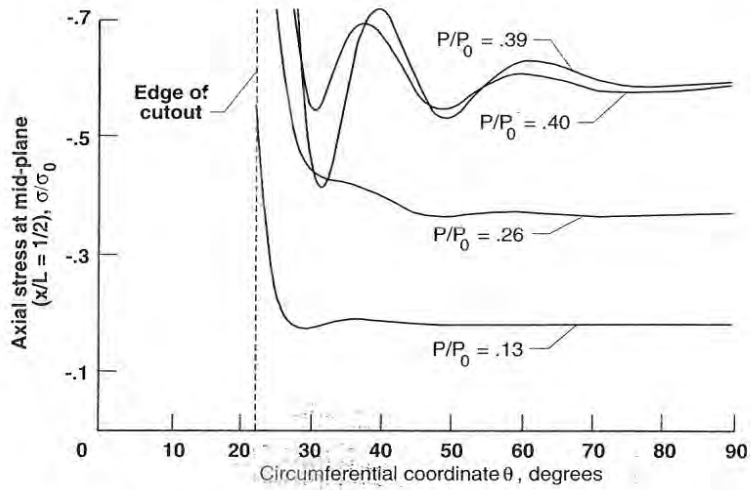

Figure 41. Axial stress at x/L = 1/2 for various load steps (from Knight *et al.*, 1995).

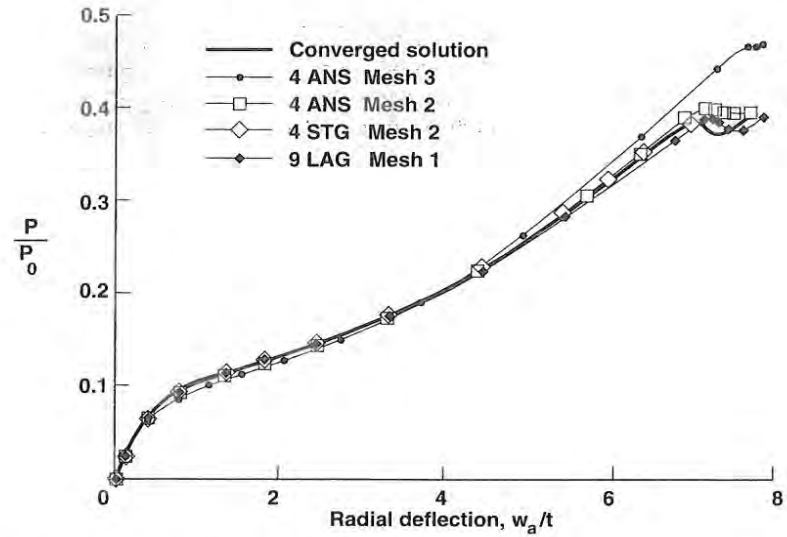

Figure 42. Effect of shell element formulation on postbuckling response and collapse (from Knight *et al.*, 1995).

Mesh 3 (same number of elements as Mesh 1). These results indicate first that the 4ANS models approach the converged solution as the mesh is refined, and second that for the same number of nodes the 9ANS model performs better than 4ANS models. The response obtained using the 4STG element is in excellent agreement with the converged solution up to the collapse load but is unable to proceed beyond the collapse load. These results indicate that the influence of transverse shear deformations on the nonlinear shell response is minimal. However, the use of higher-order shape functions for the bending field approximations (e.g., biquadratic for the 9ANS element and Hermitian for the 4STG element) dramatically affects the solution as indicated by comparing the response obtained using elements with lower-order shape functions (e.g., bilinear for the 4ANS element) for the bending field approximations.

1.6.8. Nonlinear Response of the SRB/ETA Ring Interface

The accident which destroyed the space shuttle Challenger was caused by the failure of a case joint in the right solid rocket motor (SRM) aft attachment segment (Rogers, 1986). The upper end of a lower cylindrical, motor segment (e.g., aft attachment segment) forms a clevis. The lower end of the upper, cylindrical motor segment (e.g., aft center segment) forms a tang which mates with the lower clevis. Around the circumference of both tang and clevis ends are 180 holes into which one-inch-diameter connecting pins are inserted. Three of the pin holes on the tang end are used as alignment slots to facilitate assembly of the SRM segments. The seal between two motor segments is provided by two O-rings in the "inner arm" of the clevis. The O-rings are compressed by a flat sealing surface on the tang.

Several characteristics of the original SRM joint design were identified as potential contributors to the failure (Rogers, 1986). One characteristic was the behavior of the joint under internal pressure load. The motor case expands radially outward due to the pressure. Because the joint has a higher hoop stiffness than the SRM case wall on either side of the joint, its radial expansion is less than that of the case wall. In addition to the nonuniform stiffness in the longitudinal direction due to the presence of the SRM case joints, a nonuniform stiffness in the circumferential direction exists in the aft attachment segment due to the external tank attachment (ETA) ring. Nonuniform radial expansion is the primary cause of the relative motion between the inner clevis arm and the sealing surface on the tang. This relative motion can cause the O-rings to become unseated and therefore lose their sealing capability. These effects were considered in shell analyses performed by Knight (1987) and Knight *et al.* (1988). A summary of the finite element models and results are included here to illustrate the complexities of nonlinear shell response predictions and capabilities of nonlinear shell analysis tools.

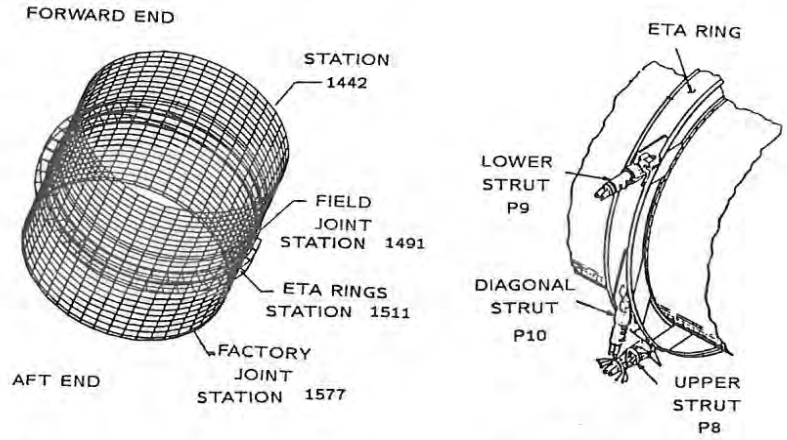

Figure 43. Definition of SRB/ETA ring interface (from Knight, 1987).

The solid rocket booster (SRB) structural subsystem provides the necessary structural support for the shuttle vehicle on the launch pad, transfers thrust loads to the Orbiter and external tank (ET), and provides the housing, structural support and brackets needed for the recovery system, the electrical components, the separation motors, and the thrust vector control system. This subsystem assembly consists of the nose cone assembly, the forward skirt including the forward SRB/ET attach fitting, the aft SRB/ETA ring and struts, the aft skirt including the heat shield, the systems tunnel, and other structure for mounting other SRB subsystem's components. Each SRB is approximately 144 feet long. Nominal dimensions for the SRM case radius and thickness are 72.6 inches and 0.479 inches, respectively. These correspond to a radius-to-thickness ratio of approximately 150. The SRB includes four SRM segments that are assembled at the Kennedy Space Center, and these joints are referred to as the "field joints."

The definition of the SRB/ETA ring interface region considered here and shown in Figure 43 includes both of the ETA rings (ring webs are approximately 12 inches apart), a portion of the SRM aft attachment segment including the factory joint at station 1577 (approximately sixty inches of shell structure), and a portion of the aft center segment including the field joint at station 1491 (approximately 64 inches of shell structure). The total length of the SRB/ETA ring interface region considered is 136 inches (roughly one shell radius on either side of the ETA rings). The center of the

SRB/ETA ring interface region is located at station 1511, approximately 20 inches below the aft attachment segment field joint. The ETA ring assembly is comprised of two tapered, partial rings, H-fittings to attach the ET struts, cover plates, and various other intercostals and brackets. The ETA ring assembly extends only 270-degrees circumferentially around the SRM segment. The ETA rings are bolted every two degrees around the circumference to the stub rings which are integral parts of the SRM aft attachment segment. Three struts attach the aft end of the SRB and the ET. These three attachment struts are designated the lower strut (P9), the diagonal strut (P10), and the upper strut (P8).

Two-dimensional shell finite element analyses were performed by Knight (1987) and Knight, Gillian and Nemeth (1988). The analyses were performed using the STAGS shell finite element code (Rankin, Stehlin and Brogan, 1986), and the finite element models were developed in order to study the overall deflection and stress resultant patterns for the SRB/ETA ring interface. Both the field and factory tang/clevis joints are modeled by using equivalent stiffness joints instead of detailed models of the joints. As such, the effect of local joints on the shell response is included; however, local joint behavior (i.e., O-ring sealing) can not be obtained from these global models. Global shell behavior of the SRB/ETA ring interface can be obtained using an equivalent stiffness joint, and an evaluation of the effects such as shell collapse and ovalization can be performed.

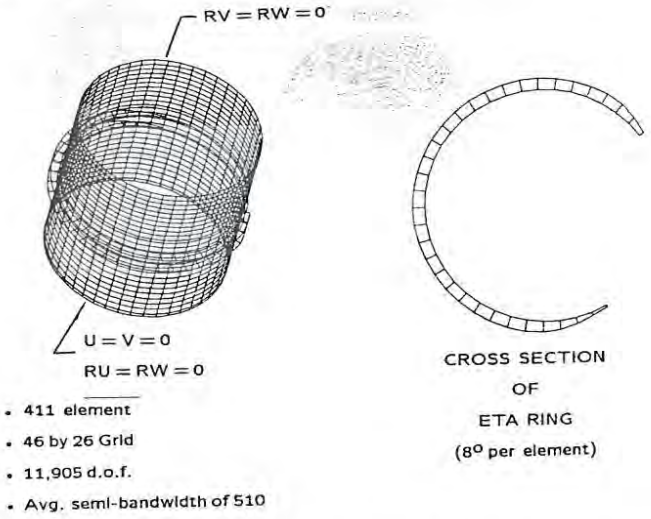

Figure 44. Baseline finite element model of SRB/ETA ring interface (from Knight, 1987).

The baseline finite element model used by Knight (1987) for the SRB/ETA ring interface is shown in Figure 44 and has 45 4-node shell elements uniformly spaced around the shell circumference and 26 elements along its length. Symmetry boundary conditions are imposed at the forward end of the model with the exception that the longitudinal direction is unrestrained. Simple-support boundary conditions are imposed at the aft end of the model with the exception that the radial direction is unrestrained. This set of boundary conditions requires the aft end of the shell to remain circular. The finite element model had approximately 12,000 active degrees of freedom, and the average semi-bandwidth of the global stiffness matrix is 510.

The linear and nonlinear solutions for the baseline finite element model of the SRB/ETA ring interface were obtained when subjected to an internal pressure of 1000 psi. Deformed geometries with exaggerated deflections corresponding to the linear and nonlinear solutions are shown in Figure 45. Deformed geometries of the entire model are shown in the top half of the figure and those of the SRM stub ring alone are shown in the lower half. Both linear and nonlinear solutions exhibit an abrupt change in deflections near the ends of the ETA rings (i.e., the partial rings or C-shaped rings). The radial deflection pattern from the nonlinear analysis indicates a stiffening of the shell response due to the inclusion of geometric nonlinearities. The high local bending causes large tangential shearing and normal forces to develop between the SRM stub rings and the ETA rings.

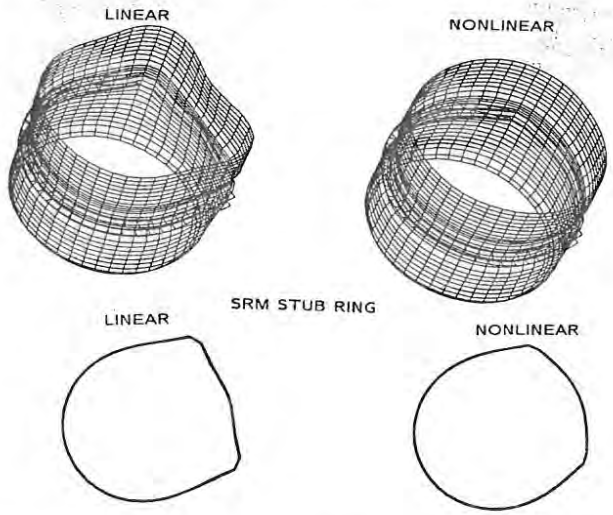

Figure 45. Deformed geometries of the baseline finite element model due to internal pressure only (from Knight, 1987).

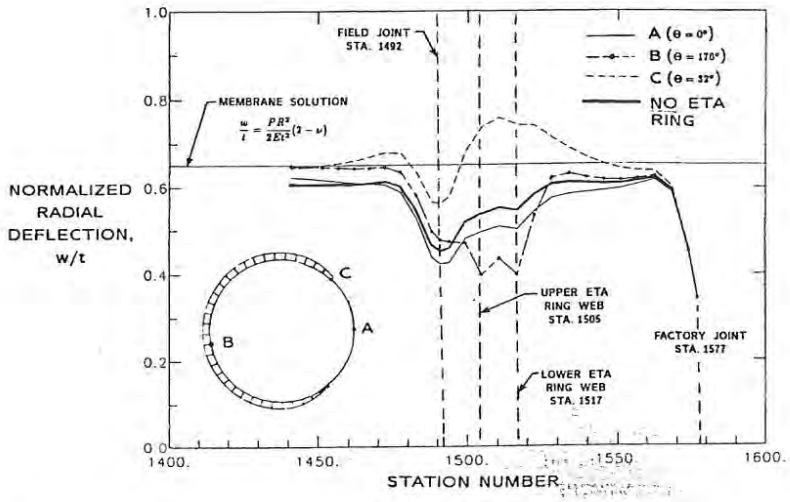

Figure 46. Axial distribution of nonlinear radial deflections (from Knight, 1987).

The axial distribution of the nonlinear radial deflections for the baseline model subjected to 1000 psi internal pressure only is shown in Figure 46 for several circumferential locations. The radial deflections are normalized by the nominal shell thickness and are shown as a function of the SRB station number. Station numbers corresponding to tang-clevis joints (field and factory) and the upper and lower ETA ring webs are also noted in Figure 46. The first circumferential location (Point A) corresponds to midway between the ends of the ETA ring. The radial deflection pattern is denoted as a solid curve. This pattern exhibits a marked change in radial deflections near the field joint at station 1492 and is such that a tang-clevis joint would tend to open. The second location corresponds to Point B which is approximately 180 degrees opposite to Point A. The radial deflection pattern at this location is denoted by a dashed line. The pattern near the field joint is again similar to the patterns at the other locations. However, near the ETA ring webs, the radial deflection pattern is different, and the stiffening influence of the ETA ring on the shell response can be seen. The third location (Point C) corresponds to an end of the ETA ring. The radial deflection at this location is denoted by a line with filled symbols. This pattern is similar to that of Point A except for the increased amplitudes of the radial deflections. For comparison, two additional curves are shown on Figure 46. One curve represents the membrane solution, including the

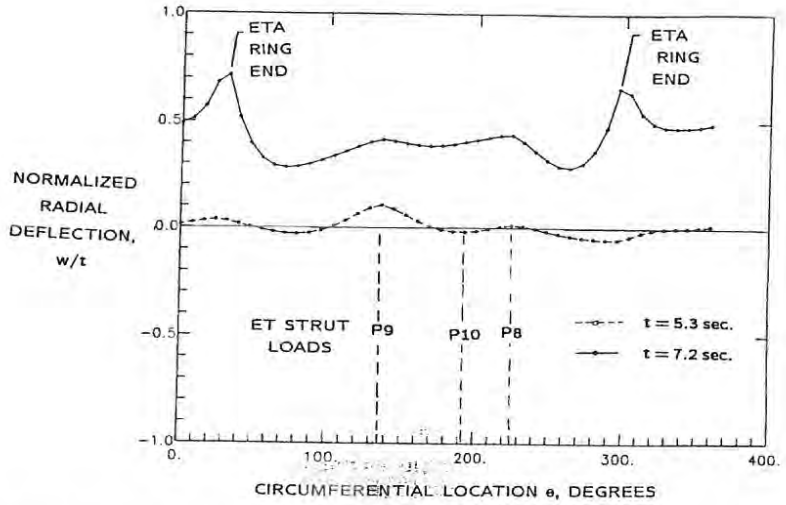

Figure 47. Nonlinear radial deflections of SRM stub ring for pre-liftoff load cases (from Knight, 1987).

biaxial effect, for a uniform thickness (0.479 inches) cylindrical shell with an internal pressure of 1000 psi. The other curve represents the nonlinear solution for the same finite element model used to generate the other results except the partial ETA rings are removed from the model.

Nonlinear analyses of the SRB/ETA ring interface model using the reconstructed flight loads for times 5.3 seconds and 7.2 seconds after space shuttle main engine (SSME) ignition were reported by Knight (1987). Time t = 5.3 seconds corresponds to the time at which maximum bending occurs and has been referred to as "max twang." At this time, the SRM is unpressurized since it has not yet been ignited. Time t = 7.2 seconds corresponds to the time at which the SRM reaches full pressure (approximately 1000 psi) and lift-off occurs. These nonlinear analyses included the asymmetric loads resulting from the aft ET strut loads and the internal pressure. The radial deflection patterns as a function of the circumferential coordinate θ are shown in Figure 47 for these two conditions. The ET strut loads at maximum bending result in an asymmetric radial deflection pattern; however, the amplitudes of these deflections are small compared to either the nominal shell thickness or the radial deflections caused by the internal pressure loading only. Deformed geometries for these two pre-liftoff load cases are

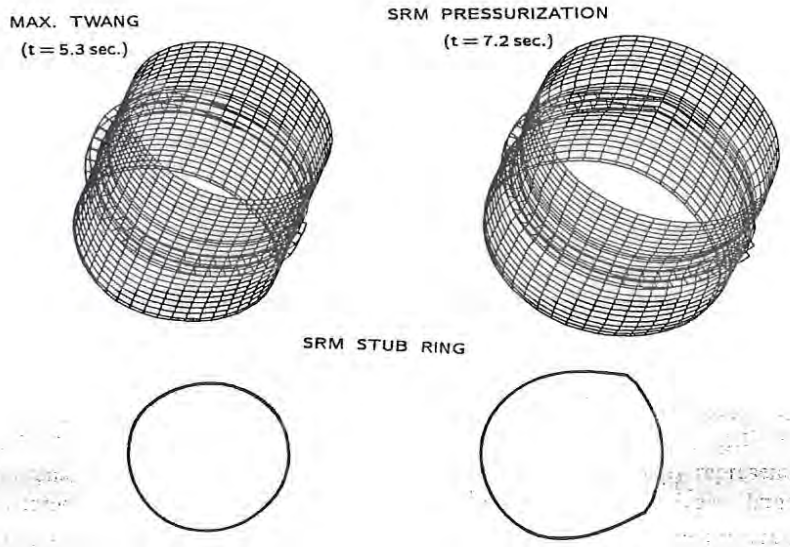

Figure 48. Deformed geometries of baseline model for pre-liftoff load cases (from Knight, 1987).

shown in Figure 48. At SRM pressurization, the overall shell response is dominated by the effects of the internal pressure, and the effect of the ET strut loads appears to be secondary.

1.7. CONCLUSIONS

Various aspects of finite element analysis for predicting postbuckling and collapse of elastic structures have been described in this chapter. Finite element fundamentals have been reviewed to provide a common basis for readers. The basic equations for nonlinear solid mechanics assuming small strain response have been given and different approaches to the formulation identified. Next, the variational formulations commonly used to develop finite elements were presented and discussed. The finite element approximations and assumptions in single-field as well as multi-field models were described and computational aspects mentioned. Details of nonlinear solution algorithms for postbuckling and collapse problems were examined in detail and implementation details provided. The various numerical solutions presented depict different aspects of performing finite element simulations of complex response problems.

While much progress in these areas has been made in the past three decades, much research remains to be done. Problems still remain with element performance and reliability even though production codes are widely used in analysis and design. As the complexity of the finite element models increase, the likelihood of detecting a problem associated with an inherent element deficiency becomes increasingly remote. Some problems continue to overwhelm even the most robust solution algorithms as a result of nonconvergence, mode jumping, and mode interaction. While some analytical work has been done, it may be several more years or even a decade before these "new" methods begin to appear in commercial software systems.

In closing, the finite element analysis tools available today are extremely powerful and able to solve very complex problems. The emergence of advanced high-performance graphics workstations has enabled the development of very large detailed finite element models that "look like" the structural component, and analysts need to step back to ensure that the physics of the simulation are also accurately represented (e.g., see Smith, 1986). As the speed of the computers increase, larger and larger finite element models will be used. The analyst has the responsibility to thoroughly interrogate the computed solution — just because it is three-dimensional with results computed on a supercomputer and displayed in color does not mean that they are correct. Hopefully this chapter has provided some additional insight for solving nonlinear problems.

References

1. Agarwal, T.K., O.O. Storaasli and D.T. Nguyen, 1990, "A Parallel-Vector Algorithm for Rapid Structural Analysis on High-Performance Computers." AIAA Paper No. 90–1149.
2. Allman, D.J., 1984, "A Compatible Triangular Element Including Vertex Rotations for Plane Elasticity Analysis." *Computers and Structures*, **19**(1–2), 1–8.
3. Almroth, B.O. and J.H. Starnes, Jr., 1975, "The Computer in Shell Stability Analysis." *Journal of the Engineering Mechanics Division, ASCE*, **101**(EM6), 873–888.
4. Almroth, B.O. and F.A., Brogan, 1977, "Automatic Choice of Procedures in Computerized Structural Analysis." *Computers and Structures*, **7**, 335–342.
5. Almroth, B.O., P. Stern and F.A., Brogan, 1978, "Automatic Choice of Global Shape Functions in Structural Analysis." *AIAA Journal*, **16**(5), 525–528.
6. Almroth, B.O., P. Stehlin and F.A., Brogan, 1981, "Use of Global Functions for Improvement in Efficiency of Nonlinear Analysis." *AIAA Paper 81–0575*.
7. Almroth, B.O. and F.A., Brogan, 1981, "Computational Efficiency of Shell Elements." In T.J.R. Hughes, A. Pifko and A. Jay, editors, *Nonlinear Finite Element Analysis of Plates and Shells*, pp. 147–165, AMD Vol. 48, ASME.
8. Aminpour, M.A., 1989, "Assessment of SPAR Elements and Formulation of Some Basic 2-D and 3-D Elements for Use with Testbed Generic Element Processor." In N.P. Sykes, editor, *Proceedings of NASA Workshop on Computational Structural Mechanics*, pp. 653–682, NASA CP-10012, Part 2.
9. Anon, 1962, *Collected Papers on Instability of Shell Structures*, NASA TN D-1510.
10. Atluri, S.N., R.H. Gallagher and O.C. Zienkiewicz, editors, 1983, *Hybrid and Mixed Finite Element Methods*, John Wiley and Sons, Inc., Chichester.

11. Barlow, J., 1976, "Optimal Stress Locations in Finite Element Models." *International Journal for Numerical Methods in Engineering*, **10**(2), 243–251. Also see discussion of paper, **11**(3), 604.
12. Bathe, K.J., 1996, *Finite Element Procedures*. Prentice Hall.
13. Bathe, K.J., J. Walczak and H. Zhang, 1993, "Some Recent Advances for Practical Finite Element Analysis." *Computers and Structures*, **45**(4/5), 511–521.
14. Batoz, J.L. and G. Dhatt, 1979, "Incremental Displacement Algorithms for Nonlinear Problems." *International Journal for Numerical Methods in Engineering*, **15**, 1262–1267.
15. Belytschko, T., 1974, "Transient Analysis". In W.D. Pilkey, K. Saczalski and H. Schaeffer, editors, *Structural Mechanics Computer Programs*, pp. 255–276. The University of Virginia Press, Charlottesville.
16. Belytschko, T., 1975, "Nonlinear Analysis Description and Numerical Stability." In Walter and Barbara Pilkey, editors, *Shock and Vibration Computer Programs — Reviews and Summaries*, SVM-10, pp. 537–562.
17. Belytschko, T. and T.J.R. Hughes, editors, 1983, *Computational Methods for Transient Analysis*. Elsevier Science Publishers.
18. Bergan, P.G., 1980, "Solution Algorithms for Nonlinear Structural Problems." *Computers and Structures*, **12**, 497–509.
19. Bergan, P.G. and R.W. Clough, 1972, "Convergence Criteria for Iterative Processes." *AIAA Journal*, **10**(8), 1107–1108.
20. Bert, C.W. and P.H. Francis, 1974, "Composite Material Mechanics: Structural Mechanics." *AIAA Journal*, **12**(9), 1173–1186.
21. Bushnell, D., 1985, "Static Collapse: A Survey of Methods and Modes of Behavior." *Finite Elements in Analysis and Design*, **1**, 165–205.
22. Bushnell, D., 1987, "PANDA2 — Program for Minimum Weight Design of Stiffened, Composite Locally Buckled Panels." *Computers and Structures*, **25**(4), 469–605.
23. Canisius, T.D.G. and R.O. Foschi, 1993, "Some Aspects in the Calculation of Transverse Shear Stresses in Mindlin Plates." *Communications in Numerical Methods in Engineering*, **9**, 681–685.
24. Chen, H., 1995, "Stress Analysis of Laminates with Holes by Special Finite Element." *Composite Structures*, **31**, 99–106.
25. CinQuini, C. and M. Rovati, 1995, "Optimization Methods in (Structural) Engineering." *European Journal of Mechanics. A/Solids*, **14**(3), 413–437.
26. Cook, R.D., 1995, *Finite Element Modeling for Stress Analysis*. John Wiley & Sons, Inc.
27. Cook, R.D., D.S. Malkus and M.E. Plesha, 1989, *Concepts and Applications of Finite Element Analysis*, Third Edition. John Wiley & Sons, Inc.
28. Craig, R.R., Jr., 1981, *Structural Dynamics: An Introduction to Computer Methods*. John Wiley and Sons, Inc., New York.
29. Crisfield, M.A., 1981, "A Fast Incremental/Iterative Solution Procedure that Handles Snap-Through." *Computers and Structures*, **13**, 55–62.
30. Crisfield, M.A., 1982, "An Arc-Length Method Including Line Searches and Acceleration." *International Journal for Numerical Methods in Engineering*, **19**, 1269–1289.
31. Crisfield, M.A., 1992, *Nonlinear Finite Element Analysis of Solids and Structures — Volume 1: Essentials*. John Wiley and Sons, Inc., Chichester.
32. Dennis, J.E. and J. Moore, 1977, "Quasi-Newton Methods, Motivation and Theory." *SIAM Review*, **19**, 46–89.
33. Dickson, J.N. and S.B. Biggers, 1984, "*POSTOP: Postbuckled Open-Stiffener Optimum Panels — Theory and Capability*.." NASA CR–172259.
34. Donnell, L.H. and C.C. Wan, 1950, "Effect of Imperfections on Buckling of Thin Cylinders and Columns Under Axial Compression." *ASME Journal of Applied Mechanics*, **17**(1), 73–83.

35. Engblom, J.J. and O.O. Ochoa, 1985, "Through-the-Thickness Stress Predictions for Laminated Plates of Advanced Composite Materials." *International Journal for Numerical Methods in Engineering*, **21**, 1759–1776.
36. Engelstad, S.P., J.N. Reddy and N.F. Knight, Jr., 1992, "Postbuckling Response and Failure Prediction of Graphite-Epoxy Plates Loaded in Compression." *AIAA Journal*, **30**(8), 2106–2112.
37. Felippa, C.A., 1976, "Procedures for Computer Analysis of Large Nonlinear Structural Systems". In A. Wexler, editor, *Large Engineering Systems*, pp. 60–101. Pergamon Press, Oxford.
38. Fujii, F., B.C. Perez and K.K. Choong, 1992, "Selection of Control Parameter in Displacement Incrementation." *Computers and Structures*, **42**(2), 167–174.
39. Garnet, H. and A. Pifko, 1983, "An Efficient Triangular Plate Bending Finite Element for Crash Simulation." *Computers and Structures*, **16**, 371–379.
40. Govindarajan, R., A.V. Krisha Murthy, K. Vuayakumar and P.V. Raghuram, 1993, "Finite Element Estimation of Elastic Interlaminar Stresses in Laminates." *Composites Engineering*, **3**(5), 451–466.
41. Hartung, R.F., editor, 1971, *Computer Oriented Analysis of Shell Structures*, AFFDL TR-71-79.
42. Hartung, R.F., 1973, *Numerical Solution of Nonlinear Structural Problems*, AMD-Vol. 6, ASME.
43. Hartung, R.F. and R.E. Ball, 1973, *A Comparison of Several Computer Solutions to Three Structural Shell Problems*, AFFDL TR-73-15.
44. Hibbitt, H.D., 1986, "Practical Aspects of Finite Element Computations in Solid Mechanics." *Applied Mechanics Review*, **39**(11), 1678–1681.
45. Hibbitt, H.D., 1993, "Nonlinear Solid Mechanics from the Commercial Software Viewpoint." *Finite Elements in Analysis and Design*, **5**(1), 3–10.
46. Hilber, H.M., T.J.R. Hughes and R.L. Taylor, 1977, "Improved Numerical Dissipation for Time Integration Algorithms in Structural Dynamics." *International Journal for Earthquake Engineering and Structural Dynamics*, **5**(3), 283–292.
47. Hinton, E., D.R.J. Owen and C. Taylor, editors, 1982, *Recent Advances in Nonlinear Computational Mechanics*. Pineridge Press, Swansea.
48. Hoff, N.J., 1966, "The Perplexing Behavior of Thin Circular Cylindrical Shells in Axial Compression." *Israel Journal of Technology*, **4**(1), 1–28.
49. Hurlbut, B.J. and B.P. Stehlin, 1991, *Computationa l Mechanics Testbed (COMET) Generic Constitutive Processor Manual*. Lockheed Contract Report F38484.
50. Johnsen, T.L., 1972, "Note on Symmetric Decomposition of Some Special Symmetric Matrices." *Computer Methods in Applied Mechanics and Engineering*, **1**, 301–306.
51. Jones, R.M., 1975, *Mechanics of Composite Materials*. Scripta Book Company.
52. Kardestuncer, H. and D.H. Norrie, editors, 1987, *Fi nite Element Handbook*. McGraw-Hill Book Company.
53. Kaya, A.C. and H.F. Nied, 1993, "Interface Fracture Analysis of Bonded Ceramic Layers Using Enriched Finite Elements." In K. Kokini, editor,*Ceramic Coatings*, pp. 47–71. ASME Book No. H00853, MD-Vol. 44.
54. Kim, D. and R. Chaudhuri, 1995, "Full and von Karman Geometrically Nonlinear Analyses of Laminated Cylindrical Panels." *AIAA Journal*, **33**(11), 2173–2181.
55. Knight, N.F., Jr., 1987, *Nonlinear Shell Analyses of the SRB/ETA Ring Interface*. NASA TM-89164.
56. Knight, N.F., Jr., R.E. Gillian and M.P. Nemeth, 1988, *Preliminary 2-D Shell Analysis of the Space Shuttle Solid Rocket Boosters*. NASA TM-100515.
57. Knight, N.F., Jr., 1994, "Factors Influencing Nonlinear Static Response Prediction and Test-Analysis Correlation for Composite Panels." *Composite Structures*, **29**, 13–25.
58. Knight, N.F., Jr., S.L. McCleary, S.C. Macy and M.A. Aminpour, 1989, *Large-Scale Structural Analysis: The Structural Analyst, The CSM Testbed and The NAS System*. NASA TM-100643.

59. Knight, N.F., Jr., C.G. Lotts and R.E. Gillian, 1990, "Computational Structural Mechanics Methods Research Using an Evolving Framework." AIAA Paper No. 90–1145.
60. Knight, N.F., Jr., S.C. Macy and S.L. McCleary, 1995, "Assessment of Structural Analysis Technology for Static Collapse of Elastic Cylindrical Shells." *Finite Elements in Analysis and Design*, **18**, 403–431.
61. Korncoff, A.R. and S.J. Fenves, 1979, "Symbolic Generation of Finite Element Stiffness Matrices." *Computers and Structures*, **10**, 119–124.
62. Krawczuk, M., 1994, "Rectangular Shell Finite Element with an Open Crack." *Finite Elements in Analysis and Design*, **15**(3), 233–253.
63. Lee, Sang-Ho and T. Belytschko, 1995, "H-Adaptive Methods for Nonlinear Dynamic Analysis of Shell Structures." *Shock and Vibration*, **2**(3), 193–204.
64. MacNeal, R., 1994, *Finite Elements: Their Design and Performance*. Marcel Dekker, Inc.
65. Matthies, H. and G. Strang, 1979, "The Solution of Nonlinear Finite Element Equations,'" *International Journal for Numerical Methods in Engineering*, **14**, 1613–1626.
66. Melosh, R.J., 1963, "Basis for Derivation of Matrices for the Direct Stiffness Method." *AIAA Journal*, **1**(7), 1631–1637. Also discussion of paper in *AIAA Journal*, **2**(2), 403, 1964; **2**(6), 1161, 1964; **3**(6), 1215–1216, 1965.
67. Noor, A.K., 1980, "Mixed Methods of Analysis — Status and Projections." In N. Perrone and W.D. Pilkey, editors, *Structural Mechanics Software Series — Volume III*, pp. 263–305. The University of Virginia Press, Charlottesville.
68. Noor, A.K., 1992, "Mechanics of Anisotropic Plates and Shells — A New Look at an Old Subject." *Computers and Structures*, **44**(3), 499–514.
69. Noor, A. K. and C.M. Andersen, 1979, "Computerized Symbolic Manipulation in Structural Mechanics — Progress and Potential." *Computers and Structures*, **10**, 95–118.
70. Noor, A.K. and C.M. Andersen, 1981, "Computerized Symbolic Manipulation in Nonlinear Finite Element Analysis." *Computers and Structures*, **13**, 379–403.
71. Noor, A.K., C.M. Andersen and J.M. Peters, 1979, "Global-Local Approach for Nonlinear Shell Analysis." In *Proceedings of the Seventh ASCE Conference on Electronic Computation*, pp. 634–657. Washington University, St. Louis, Missouri.
72. Noor, A.K., J.M. Peters and C.M. Andersen, 1980, "Two-Stage Rayleigh-Ritz Technique for Nonlinear Analysis of Structures." In R. Shaw, W. Pilkey, B. Pilkey, R. Wilson, A. Lakis, A. Chaudouet and C. Marina, editors, *Innovative Numerical Analysis for the Engineering Sciences*, pp. 743–753. The University of Virginia Press, Charlottesville.
73. Noor, A.K. and J.M. Peters, 1980, "Reduced Basis Technique for Nonlinear Analysis of Structures." *AIAA Journal*, **18**(4), 455–462.
74. Noor, A.K. and J.M. Peters, 1990, "Potential of Mixed Formulations for Advanced Analysis Systems." *Computers and Structures*, **35**(4), 369–380.
75. Noor, A.K. and J.M. Peters, 1981, "Bifurcation and Post-Buckling Analysis of Laminated Composite Plates via Reduced Basis Technique." In Hughes, Gartling and Spilker, editors, *New Concepts in Finite Element Analysis*, pp. 107–131. ASME, AMD-Vol. 44.
76. Noor, A.K., T. Belytschko and J.C. Simo, editors, 1989, *Analytical and Computational Models of Shells*. ASME, CED-Vol. 3.
77. Noor, A.K. and W.S. Burton, 1989, "Assessment of Shear Deformation Theories for Multilayered Composite Plates." *Applied Mechanics Review*, **42**(1), 1–12.
78. Noor, A.K. and W.S. Burton, 1990, "Assessment of Computational Models for Multilayered Anisotropic Plates." *Computers and Structures*, **14**, 233–265.
79. Palazotto, A.N. and S.T. Dennis, 1992, *Nonlin ear Analysis of Shell Structures*. AIAA Educational Series, AIAA, Washington, D.C.
80. Park, K.C. and G.M. Stanley, 1986, "A Curved C^0 Shell Element Based on Assumed Natural-Coordinate Strains." *ASME Journal of Applied Mechanics*, **108**, 278–290.
81. Pian, T.H.H., 1964, "Derivation of Element Stiffness Matrices by Assumed Stress Functions." *AIAA Journal*, **2**(7), 1333–1336. Also discussion of paper in *AIAA Journal*, **3**(1), 186–187, 1965.

82. Pian, T.H.H., 1973, "Finite Element Methods by Variational Principles with Relaxed Continuity Requirement." In C.A. Brebbia and H. Tottenham, editors, *Variational Methods in Engineering*, Vol. 1, pp. 3/1–3/24. Southampton University Press.
83. Pian, T.H.H. and P. Tong, 1969, "Basis of Finite Element Methods for Solid Continua." *International Journal for Numerical Methods in Engineering*, **1**, 3–28.
84. Poole, E.L., 1991, "Comparing Direct and Iterative Equation Solvers in a Large Structural Analysis Software System." *Computing Systems in Engineering*, **2**(4), 397–408.
85. Poole, E.L., N.F. Knight Jr. and D.D. Davis Jr., 1992, "High-Performance Equation Solvers and their Impact on Finite Element Analysis." *International Journal for Numerical Methods in Engineering*, **33**(4), 855–868.
86. Ramm, E., 1981, "Strategies for Tracing the Nonlinear Response Near Limit-Points." In Wunderlich, editor, *Nonlinear Finite Element Analysis in Structural Mechanics*, pp. 63–89. Springer-Verlag, Berlin.
87. Ramm, E., 1982, "The Riks-Wempner Approach — An Extension of the Displacement Control Method in Nonlinear Analysis." In Hinton, Owen and Taylor, editors, *Recent Advances in Nonlinear Computational Mechanics*, pp. 63–86. Pineridge Press, Swansea.
88. Rankin, C.C., P. Stehlin and F.A. Brogan, 1986, *Enhancements to the STAGS Computer Code*. NASA CR-4000.
89. Rankin, C.C. and F.A. Brogan, 1986, "An Element-Independent Corotational Procedure for the Treatment of Large Rotations." *ASME Journal of Pressure Vessel Technology*, **108**, 165–174.
90. Rankin, C.C. and B. Nour-Omid, 1988, "The Use of Projectors to Improve Finite Element Performance." *Computers and Structures*, **30**(1/2), 257–267.
91. Rankin, C.C. and F.A. Brogan, 1991, *The Computational Structural Mechanics Testbed Structural Element Processor ES5: STAGS Shell Element*. NASA CR-4358.
92. Reddy, J.N., 1989, "On Refined Computational Models of Composite Laminates." *International Journal for Numerical Methods in Engineering*, **27**, 361–382.
93. Reddy, J.N., 1993, *An Introduction to the Finite Element Method*, Second Edition. McGraw-Hill Book Company, Inc.
94. Reddy, J.N. and D.H. Robbins, Jr., 1994, "Theories and Computational Models for Composite Laminates." *Applied Mechanics Review*, **47**(1), Part 1, 147–169.
95. Reissner, E., 1944, "Note on the Theorem of the Symmetry of the Stress Tensor." *Journal of Mathematics and Physics*, **23**, 192–194.
96. Rengarajan, G., N.F. Knight Jr. and M.A. Aminpour, 1995, "Comparison of Symbolic and Numerical Integration Methods for an Assumed-Stress Hybrid Shell Element." *Communications in Numerical Methods in Engineering*, **11**, 307–316.
97. Rengarajan, G., M.A. Aminpour and N.F. Knight Jr., 1995, "Improved Assumed-Stress Hybrid Shell Element with Drilling Degrees of Freedom for Linear Stress, Buckling and Free Vibration Analyses." *International Journal for Numerical Methods in Engineering*, **38**, 1917–1943.
98. Riks, E., 1970, *On the Numerical Solution of Snapping Problems in the Theory of Elastic Stability*, Stanford University, Report SUDAAR No. 401. (Also available as AFOSR 70-2258TR).
99. Riks, E., 1987, "Progress in Collapse Analysis." *ASME Journal of Pressure Vessel Technology*, **109**, 33–41.
100. Riks, E., 1992, "On Formulations of Path-following Techniques for Structural Stability Analysis." In P. Ladeveze and O. C. Zienkiewicz, editors, *New Advances in Computational Structural Mechanics*, pp. 65–79. Elsevier Science Publishers, Amsterdam.
101. Riks, E., C.C. Rankin and F.A. Brogan, 1996, "On the Solution of Mode Jumping Phenomena in Thin Walled Shell Structures." *Computer Methods in Applied Mechanics and Engineering*, to appear.
102. Rogers, W., 1986, *Report of the Presidential Commission on the Space Shuttle Challenger Accident*, Washington, D.C.

103. Smith, G.E., 1986, "The Dangers of CAD." *Mechanical Engineering*, February, pp. 58–64.
104. Stanley, G.M. and S. Nour-Omid, 1990, *The Computational Structural Mechanics Testbed Generic Structural Element Processor Manual*. NASA CR-181728.
105. Stanley, G.M., K.C. Park and T. Hughes J.R., 1986, "Continuum-Based Resultant Shell Elements." In T.J.R. Hughes and E. Hinton, editors, *Finite Element Methods for Plate and Shell Structures, Volume 1: Element Technology*, pp. 1–45. Pineridge Press International, Swansea, U.K.
106. Stanley, G.M. and C.A. Felippa, 1986, "Computational Procedures for Postbuckling of Composite Shells." In P.G. Bergan, K.J. Bathe and W. Wunderlich, editors, *Proceedings of US-Europe Symposium on Finite Element Methods for Nonlinear Problems*, pp. 359–385. University of Trondheim, Norway.
107. Stanley, G.M, 1991, *The Computational Structural Mechanics Testbed Structural Element Processor ES1: Basic SRI and ANS Elements*, NASA CR-4357.
108. Starnes, J.H. Jr., N.F. Knight Jr. and M. Rouse, 1985, "Postbuckling Behavior of Selected Flat Rectangular Graphite-Epoxy Panels Loaded in Compression." *AIA A Journal*, **25**(8), 1236–1246.
109. Starnes, J.H. Jr. and M. Rouse, 1981, "Postbuckling and Failure Characteristics of Selected Flat Stiffened Graphite-Epoxy Plates Loaded in Compression." AIAA Paper No. 81–0543.
110. Stehlin, P. and F.A. Brogan, 1984, "Analysis of Structural Collapse by the Reduced Basis Technique." In Sobel and Thomas, editors, *Collapse Analysis of Structures*, pp. 69–83. ASME PVP-Vol. 84.
111. Stein, E., W. Wagner and P. Wriggers, P., 1988, "Concepts of Modeling and Discretization of Elastic Shells for Nonlinear Finite Element Analysis." In J.R. Whitman, editor, *The Mathematics of Finite Elements and Applications VI — MAFELAP 1987*, pp. 205–232. Academic Press Limited, London.
112. Stewart, C.B. (compiler), 1990, *The Computational Structural Mechanics Testbed Users' Manual*. NASA TM-100644 (updated).
113. Stewart, C.B. (compiler), 1991, *The Computational Structural Mechanics Testbed Procedures Manual*. NASA TM-100646.
114. Stricklin, J.A. and W.E. Haisler, 1977, "Formulations and Solution Procedures for Nonlinear Structural Analysis." *Computers and Structures*, **7**, 125–136.
115. Stroud, W.J. and M.S. Anderson, 1980, "*PASCO: Structural Panel Analysis and Sizing Code — Capabilities and Analytical Foundations*." NASA TM-80181.
116. Stroud, W.J., 1982, "Optimization of Composite Structures." In Hashin and Herakovich, editors, *IUTAM Proceeding for Mechanics of Composite Materials — Recent Advances*, pp. 307–321. (Also available as NASA TM-84544).
117. Stroud, W.J., W.H. Greene and M.S. Anderson, 1984, *Buckling Loads of Stiffened Panels Subjected to Combined Longitudinal Compression and Shear: Results Obtained with PASCO, EAL and STAGS Computer Programs*. NASA TP-2215.
118. Szabo, B. and I. Babuska, 1991, *Finite Element Analysis*. John Wiley and Sons, Inc., New York.
119. Tan, H.Q., T.Y.P. Chang and D. Zheng, 1991, "On Symbolic Manipulation and Code Generation of a Hybrid Three-Dimensional Solid Element." *Engineering with Computers*, **7**, 47–59.
120. Taylor, R.L., P.J. Beresford and E.L. Wilson, 1976, "A Non-Conforming Element for Stress Analysis." *International Journal for Numerical Methods in Engineering*, **10**(6), 1976, 1211–1219.
121. Tessler, A. and T.J.R. Hughes, 1985, "A Three-Node Mindlin Plate Element with Improved Transverse Shear." *Computer Methods in Applied Mechanics and Engineering*, **50**, 71–101.

122. Thurston, G.A., 1980, "Newton's Method-A Link Between Continuous and Discrete Solutions of Nonlinear Problems." In McComb and Noor, editors, *Research in Nonlinear Structural and Solid Mechanics*, pp. 27–48. NASA CP-2147.
123. Thurston, G.A, F.A. Brogan and P. Stehlin, 1986, "Postbuckling Analysis Using a General-Purpose Code." *AIAA Journal*, **24**(6), 1013–1020.
124. Tillerson, J.R., 1975, "Selecting Solution Procedures for Nonlinear Structural Dynamics." *Shock and Vibration Digest*, **7**(4), 2–13.
125. Tong, P., 1984, "A Hybrid Finite Element Method for Damage Tolerance Analysis." *Computers and Structures*, **19**(1/2), 263–269.
126. Washizu, K., 1968, *Variational Methods in Elasticity and Plasticity*. Pergamon Press, Oxford.
127. Washizu, K., 1972, "Some Considerations of Basic Theory for the Finite Element Method." In J.T. Oden, R.W. Clough and Y. Yamamoto, editors, *Advances in Computational Methods in Structural Mechanics and Design*, pp. 39–53. University of Alabama in Huntsville Press.
128. Weingarten, V.I., P. Seide and J.P. Peterson, 1968, *Buckling of Thin-Walled Circular Cylinders*. NASA SP-8007, revised.
129. Wempner, G.A., 1971, "Discrete Approximations Related to Nonlinear Theories of Solids." *International Journal of Solids and Structures*, **7**, 1581–1599.
130. Wempner, G.A., 1992, "Shells: Mechanics and Approximations — Linear and Nonlinear Aspects." In F.Y. Cheng and F. Zizhi, editors, *Computational Mechanics in Structural Engineering: Recent Developments and Future Trends*, pp. 114–127. Elsevier Science Publishers, Ltd.
131. Wilson, E.L., M.Y. Yuan and J.M. Dickens, 1982, "Dynamic Analysis by Direct Superposition of Ritz Vectors." *International Journal for Earthquake Engineering and Structural Dynamics*, **10**(6), 813–821.
132. Zienkiewicz, O.C., 1970, "The Finite Element Method: From Intuition to Generality." *Applied Mechanics Reviews*, pp. 249–256.
133. Zienkiewicz, O.C., 1971, "Incremental Displacement in Nonlinear Analysis." *International Journal for Numerical Methods in Engineering*, **3**, 587–592.
134. Zienkiewicz, O.C., 1983, "The Generalized Finite Element Method — State of the Art and Future Directions." *ASME Journal of Applied Mechanics*, **50**, 1210–1217.
135. Zienkiewicz, O.C. and R.L. Taylor, 1989, *The Finite Element Method: Volume 1: Basic Formulations and Linear Problems*. Fourth Edition, McGraw-Hill Book Company, London.
136. Zienkiewicz, O.C. and R.L. Taylor, 1991, *The Finite Element Method: Volume 2: Solid and Fluid Mechanics, Dynamics and Nonlinearity*. Fourth Edition, McGraw-Hill Book Company, London.